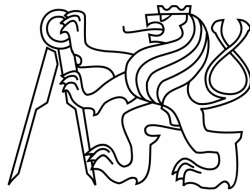


Czech Technical University in Prague  
Faculty of Mechanical Engineering

DISSERTATION THESIS

2008

Mgr. Radka Keslerová



Czech Technical University in Prague  
Faculty of Mechanical Engineering

DISSERTATION THESIS

# **Numerical Solution of Newtonian and Non-Newtonian Flows**

Mgr. Radka Keslerová

Mathematical Engineering  
Study Branch

Prof. RNDr. Karel Kozel, DrSc.  
Supervisor

Copyright © 2008, Radka Keslerová  
All Rights Reserved

# Acknowledgements

I would like to thank my supervisor Prof. RNDr. Karel Kozel, DrSc., Czech Technical University in Prague, Faculty of Mechanical Engineering for the opportunity to do this project, for his help with this work and for his endless patience with me.

I would like to thank my parents that they are always and everywhere with me and for me.



# Abstract

**Key words:** Newtonian fluids, non-Newtonian fluids, finite volume method, incompressible laminar viscous flows, artificial compressibility method, steady and unsteady computations, dual-time stepping method.

This thesis deals with a numerical solution of two and three dimensional laminar flows of incompressible viscous generalized Newtonian fluids in a branching channel. Generalized Newtonian fluids can be divided into three common types. First, Newtonian fluids when the viscosity is constant. Second, the shear thinning non-Newtonian fluids, in this case the shear rate increases with the decreasing viscosity. Third, the shear thickening non-Newtonian fluids, in this case the shear rate increases with the increasing viscosity. This work is concerned on the numerical simulation of Newtonian and non-Newtonian shear thickening fluids flow.

A mathematical model is a generalized system of Navier-Stokes equations where the right hand side is defined by a power-law model for generalized Newtonian fluids. The numerical model is based on the artificial compressibility method. For the spatial discretization the finite volume method is applied. For the time discretization the explicit multistage Runge-Kutta method is used.

Numerical solution is divided into two parts, steady and unsteady. Steady state solution is achieved for  $t \rightarrow \infty$  using steady boundary conditions and followed by steady residual behaviour. For unsteady solution high artificial compressibility coefficient  $\beta^2$  is considered. Two numerical methods for solving unsteady incompressible flows are presented, the artificial compressibility method and dual-time stepping method.

# Anotace

Název disertační práce: **Numerické řešení Newtonského a neNewtonského proudění**

Tato práce se zabývá numerickým řešením dvou a tří dimenzionálního laminárního proudění nestlačitelných vazkých zobecněných Newtonských tekutin ve větveném kanále. Zobecněné Newtonské tekutiny mohou být rozděleny do tří obecných skupin. První, Newtonské tekutiny, když je viskozita konstantní. Druhá, nenewtonské pseudoplastické (shear thinning) tekutiny, v tomto případě s rostoucí rychlostí deformace viskozita klesá. Třetí, nenewtonské dilatační (shear thickening) tekutiny, v tomto případě s klesající rychlostí deformace viskozita roste. Tato práce je zaměřena na numerickou simulaci Newtonského a nenewtonského shear thickening proudění tekutin.

Zobecněný systém Navier-Stokesových rovnic je matematickým modelem. Pravá strana je definována power-law modelem pro zobecněné Newtonské tekutiny. Numerický model je založen na metodě umělé stlačitelnosti. Metoda konečných objemů je aplikována pro prostorovou diskretizaci. Pro časovou diskretizaci je použita explicitní víceúrovňová Runge-Kuttova metoda.

Numerické řešení je rozděleno do dvou částí, stacionární a nestacionární. Stacionární řešení je dosaženo pro  $t \rightarrow \infty$  s užitím stacionárních okrajových podmínek a je kontrolováno chováním stacionárního rezidua. Pro nestacionární řešení vysoká hodnota koeficientu umělé stlačitelnosti  $\beta^2$  je uvažována. Jsou předloženy dvě numerické metody pro řešení nestacionárního nestlačitelného proudění, metoda umělé stlačitelnosti a dual-time stepping metoda.

## State of the Art

Panta rhei (Παντα ρει) - “everything is in a state of flux”, “everything flows” is the philosophy of the greek philosopher Heracleitos of Ephesus. This phrase is the motto of the The Society of Rheology. The rheology is a branch studying laws of viscous fluid flows. The term rheology was coined by Eugene Bingham, a professor at Lafayette College, in 1920. The term was inspired by the quotation attributed to Heracleitos, panta rhei.

The rheology is the mostly applied in engineering, geophysics and physiology. In medicine, hemorrheology deals with blood flow and it has the most important medical significance. In geology, solid Earth materials that exhibit viscous flow over long time scales are known as rheids.

Continuum mechanics	Solid mechanics or strength of materials	Elasticity	Rheology
		Plasticity	
	Fluid mechanics	Non-Newtonian	
		Newtonian	

The rheology contains plastic solid materials and non-Newtonian fluids. One of the tasks of rheology is to establish the relationships between deformations and stresses. Such relationships are adapted to mathematical treatment by established methods of continuum mechanics.

The flow characteristics of fluids are mainly dependent on the viscosity. When the viscosity of the fluids remains constant and is independent of the applied shear stress, such the fluids are termed Newtonian fluids. In the case of the non-Newtonian fluids, viscosity depends on the applied shear force. In this case, when the shear rate is varied, the shear stress does not vary proportionally. In the Figure 1, the dependence of shear stress and viscosity on the shear rate is shown, see e.g. [1].

Generalized Newtonian fluids can be divided into three common types. First, Newtonian fluids, when the viscosity is constant. Second, pseudoplastic fluids, in this case with increasing shear rate the viscosity decreases. Sometimes they are called shear thinning non-Newtonian, see e.g. [2]. Third, dilatant fluids, in this case with increasing shear rate the viscosity increases. They are called shear thickening non-Newtonian.

This work is mainly concerned on the behaviour of Newtonian fluids and non-Newtonian shear thickening fluids flow.

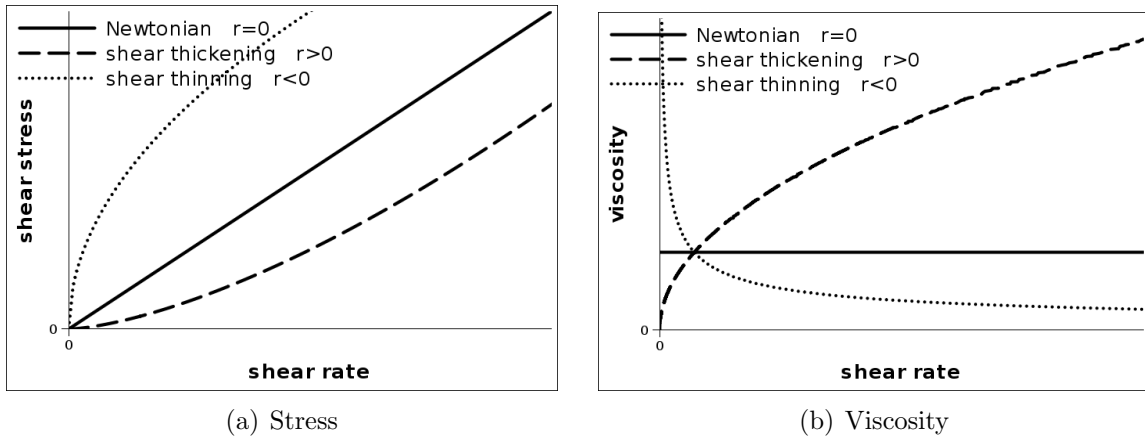


Figure 1: Various types of fluids based on - a) the stress - b) the viscosity

## Research Goals

The main goal of this work is to develop and to implement the numerical method for solving incompressible laminar viscous flows for Newtonian and non-Newtonian shear thickening fluids. The task is to numerically solve two dimensional and three dimensional incompressible flows in the branching channel and to compare numerical solutions for Newtonian and non-Newtonian shear thickening fluids flow. The numerical modelling is divided into a steady and an unsteady numerical simulations.

## Numerical Methods

For the spatial discretization the finite volume method (FVM) is applied. For two and three dimensional steady state numerical modelling multistage Runge-Kutta scheme together with an artificial compressibility method is used. For unsteady numerical computation of two dimensional test cases explicit multistage Runge-Kutta method in conjunction with the artificial compressibility method or a dual-time stepping method is applied.

## Research Results

In this thesis numerical results of steady Newtonian and non-Newtonian fluids flow in two and three dimensional branching channels with different geometry are presented. Numerical results for Newtonian fluids are compared with numerical results for non-Newtonian fluids. In the unsteady case two dimensional numerical results are presented for Newtonian and non-Newtonian fluids flow.

# Contents

<b>Introduction</b>	<b>1</b>
<b>1 Mathematical Models</b>	<b>3</b>
1.1 Generalized Navier-Stokes Equations . . . . .	5
1.2 Incompressible Navier-Stokes Equations for Newtonian Fluids Flow . . . .	7
1.2.1 Dimensional Analysis . . . . .	9
1.2.2 Boundary Conditions . . . . .	10
1.3 Generalized Newtonian Fluids . . . . .	11
<b>2 Numerical Solution</b>	<b>14</b>
2.1 Finite Volume Method . . . . .	14
2.1.1 Finite Volume Method for Generalized Newtonian Fluids Flow . . .	16
2.2 Method of Artificial Compressibility . . . . .	17
2.3 Numerical Scheme . . . . .	19
2.3.1 Multistage Runge-Kutta Method . . . . .	19
2.4 Stability and Convergence . . . . .	23
2.4.1 Time Step . . . . .	29
2.4.2 Convergence . . . . .	30
2.5 Unsteady Computation . . . . .	30
2.5.1 Artificial Compressibility Method . . . . .	30
2.5.2 Dual Time Stepping Method . . . . .	31
2.5.3 Time Step and Convergence . . . . .	32
<b>3 Numerical Results</b>	<b>33</b>
3.1 Two Dimensional Steady Solutions of Newtonian Fluids . . . . .	33
3.2 Three Dimensional Steady Solutions of Newtonian Fluids . . . . .	53
3.3 Two Dimensional Steady Solutions of Non-Newtonian Fluids . . . . .	66
3.4 Three Dimensional Steady Solutions of Non-Newtonian Fluids . . . . .	74
3.5 Two Dimensional Unsteady Numerical Solutions of Newtonian Fluids . . .	82
3.6 Two Dimensional Steady Solutions of Newtonian Fluids - Test of the Meshes	95
<b>Conclusions</b>	<b>100</b>

# List of Symbols

## Latin symbol

Symbol	SI unit	Definition
$f$	Hz	frequency
$n_i$		$i$ -th component of unit normal vector
$\mathbf{n}$		unit normal vector
$\tilde{p}$	Pa	dynamic pressure
$p$	$\text{m}^2\text{s}^{-2}$	kinematic pressure
$r$		power-law index
$t$	s	time
$\Delta t$	s	time step
$\mathbf{u}$	$\text{m s}^{-1}$	velocity vector
$u, v, w$	$\text{m s}^{-1}$	velocity vector components
$x, y, z$	m	cartesian coordinate variables
$A, B, C$		Jacobian matrices
$C_{il}$		edge or surface between $i$ -th and $l$ -th finite volume cell
$\mathbf{D}$		velocity gradient tensor
$D_i$		$i$ -th finite volume cell
$D_{ij}$		$ij$ -th component of velocity gradient
$F$		numerical flux
$F^c, G^c, H^c$		inviscid numerical fluxes
$F^v, G^v, H^v$		viscous numerical fluxes
$\mathcal{F}$		numerical flux function
$H_{ij}$		numerical flux through the edge common to $i$ -th and $l$ -th cell
$\mathcal{I}$		complex unit
$J$		set of indices
$L^*$	m	reference length
$N_i$		index set
$O$	m	reference circumference
$\tilde{\mathbf{R}}$		diagonal matrix
$\tilde{\mathbf{R}}_\beta$		diagonal matrix
Re		Reynolds number
Rez		stationary residual
$\mathbb{R}$		set of real numbers
$\mathbb{R}^+$		set of nonnegative real numbers
$\overline{\text{Rez}}$		unsteady residual
$S$	$\text{m}^2$	reference volume
$U^*$	$\text{m s}^{-1}$	reference velocity value
$W$		vector of conservative variables
$\mathbb{Z}$		set of integer

## Greek Symbol

$\alpha_r$		coefficients of Runge-Kutta method
$\beta$	$\text{m s}^{-1}$	artificial compressibility coefficient
$\delta_{ij}$		Kronecker delta
$\epsilon$		parametr
$\kappa$		dilatational viscosity
$\lambda$		eigenvalue
$\mu$	$\text{Pa s}$	dynamic viscosity
$\nu$	$\text{m}^2\text{s}^{-1}$	kinematic viscosity
$\nu^*$		reference kinematic viscosity
$\pi$		Ludolph's number
$\pi_{ij}$		$ij$ -th normal stress
$\rho$	$\text{kgm}^{-3}$	density
$\boldsymbol{\tau}$		shear stress tensor
$\tau_{ij}$	$\text{Pa}$	$ij$ -th shear stress
$\omega$		angular velocity
$\Omega$		Spatial domain

## Superscript Symbols

*	time level
*	reference value
'	dimensionless value
$c$	convective part
$n$	time index
$v$	viscous part
$\nu$	pseudo-time index
$T$	referring to transposed vector

## Subscript Symbols

$i, j, k, l$	indices
$x, y, z$	derivative over the coordinate variables
$x, y, z$	indices
$t$	derivative over the time
$\tau$	derivative over the pseudo-time

## Abbreviations

CFL	Courant-Friedrichs-Levy number
FVM	Finite volume method
tr	trace of the tensor



# Introduction

The mathematical model of science and engineering mainly take the form of differential or integral equations. Using computer-implemented mathematical model, one can simulate and analyze complicated systems in engineering and science.

This paper deals with numerical solution of two dimensional and three dimensional steady and unsteady laminar incompressible flows for Newtonian and non-Newtonian shear thickening fluids through a branching channel.

The mathematical model used in this work is the generalized system of Navier-Stokes equations. The right hand side of this system is defined by the power-law model [2], [3]. The finite volume method is used as the numerical model for numerical simulations of generalized Newtonian fluids flow. Numerical solutions are divided into two parts, steady and unsteady. Steady numerical results are used as the initial conditions for unsteady numerical simulations.

The work is organized as follows. In the first chapter the governing system of equations is introduced. The system of generalized Navier-Stokes equations and continuity equation is considered as the mathematical model using the power-law model in the definition of the right hand side of the equations of the motion for generalized Newtonian fluids flow.

The second chapter deals with the numerical modelling of the incompressible laminar Newtonian and non-Newtonian shear thickening fluids flow. This chapter is divided into two main parts: steady and unsteady flows. The unsteady system of Navier-Stokes equations is completed by the artificial compressibility method with a term  $\frac{1}{\beta^2} p_t$  in the equation of the continuity. The numerical solutions for Newtonian and non-Newtonian fluids flow are computed by the finite volume method in conjunction with the artificial compressibility method. This method is generally explained for the system of Navier-Stokes equations in generalized Newtonian form. As a numerical scheme the multistage Runge-Kutta method is used. Steady state solution is achieved for  $t \rightarrow \infty$  using steady boundary conditions and followed by steady residual behaviour. The steady simulation is controlled with steady boundary conditions.

For unsteady solution high compressibility coefficient  $\beta^2$  is considered as a first answer. Several approaches of unsteady computations are used for unsteady simulation. First, the artificial compressibility method with a pulsation of the pressure in the outlet boundary is used. Next, the dual-time stepping method with the explicit Runge-Kutta scheme is considered in this section for unsteady computation for Newtonian and non-Newtonian fluids flow.

In the last chapter numerical results for two and three dimensional cases of flows in the branching channel for Newtonian and non-Newtonian shear thickening fluids are presented and compared. This section is divided as previous chapter to the steady and the unsteady parts. The steady numerical results for flows in two and three dimensional branching channel are compared for Newtonian and corresponding non-Newtonian shear thickening fluids flow. The unsteady numerical results are presented for two dimensional branching channel.

## **Acknowledgements**

This work was partly supported by grant GACR No. 201/08/0012, grant GAAVCR No. IAA100190804, Research Plan MSM 684 077 0003 and Research Plan MSM 684 072 0010.

# Chapter 1

## Mathematical Models

This chapter deals with the flows of the viscous fluids. The physical property that characterizes the resistance to flow is the viscosity. In this chapter Newtonian and non-Newtonian shear thickening mathematical model will be discuss.

The one of the main differences between Newtonian and non-Newtonian fluids flow is the validity of Newton's law of the viscosity (see [4], [5])

$$\tau_{yx} = -\mu \frac{du}{dy}, \quad (1.1)$$

where the symbol  $\tau_{yx}$  denotes the force in the  $x$  direction on a unit area perpendicular to the  $y$  direction. This equation states that the shearing force per unit area is proportional to the negative of the velocity gradient. The constant of the proportionality  $\mu$  is a property of the fluid, defined to be the viscosity. The symbol  $u$  denotes the  $x$ -component of a velocity vector and  $y$  is the second coordinate.

The fluids, which are described by eq. (1.1), are referred to as Newtonian fluids. Polymeric liquids, suspensions and other complex fluids are not described by eq. (1.1) and they are referred to as non-Newtonian fluids.

The viscosity  $\mu$  can be expressed from the eq. (1.1) as follows:

$$\mu = -\tau_{yx} \left( \frac{du}{dy} \right)^{-1}, \quad (1.2)$$

the unit of  $\tau_{yx}$  is  $\text{N/m}^2 = \text{Pa}$ , the unit of the velocity  $u$  is  $\text{m/s}$  and the unit of the coordinate  $y$  is  $\text{m}$ . Then the SI unit of the viscosity  $\mu$  is  $\text{Pa s}$ .

In this Newton's law of the viscosity, the viscosity  $\mu$  was defined in terms of a simple steady state shearing flow. Generally, more complicated flows are considered. In this case two (2D case) or three (3D case) velocity components may depend on all two or three resp. coordinates. Therefore the generalization of Newton's law of the viscosity is required.

The velocity components are then given by

$$u = u(x, y), \quad v = v(x, y), \quad (1.3)$$

or

$$u = u(x, y, z), \quad v = v(x, y, z), \quad w = w(x, y, z). \quad (1.4)$$

In such situation, there will be four or nine resp. stress components  $\tau_{ij}$  instead of the component  $\tau_{yx}$  that appears in the eq. (1.1).

Sometimes, the symbol  $\pi_{ij}$  is used as the molecular stresses which include two types of the stresses - the thermodynamical pressure  $p$  and the viscous stresses  $\tau_{ij}$ . (By the stresses the forces per unit area are denoted.) The molecular stresses  $\pi_{ij}$  are defined as follows:

$$\pi_{ij} = p\delta_{ij} + \tau_{ij}, \quad (1.5)$$

where  $i$  and  $j$  may be  $x, y$  or  $z$ . Here  $\delta_{ij}$  is the Kronecker delta, which is 1 if  $i = j$  and 0 if  $i \neq j$ .  $\pi_{ij}$  is the force in the  $j$  direction on the unit area perpendicular to the  $i$  direction.

The stresses  $\pi_{xx} = p + \tau_{xx}$ ,  $\pi_{yy} = p + \tau_{yy}$ ,  $\pi_{zz} = p + \tau_{zz}$  are called normal stresses, whereas the remaining quantities,  $\pi_{xy} = \tau_{xy}$ ,  $\pi_{xz} = \tau_{xz}$ , ... are called shear stresses.

The quantities, which have two subscripts associated with the coordinate directions, are referred to as tensors [6], [7]. The quantities, which have one subscript associated with the coordinate directions, are called vectors. Therefore, the symbol  $\boldsymbol{\tau}$  denotes the viscous stress tensor (with components  $\tau_{ij}$ ) and the symbol  $\boldsymbol{\pi}$  is the molecular stress tensor (with the components  $\pi_{ij}$ ).

The required generalization for Newton's law of the viscosity is the set of four or nine resp. relations (see e.g. [5]):

$$\tau_{ij} = -\mu \left( \frac{\partial v_j}{\partial x_i} + \frac{\partial v_i}{\partial x_j} \right) + \left( \frac{2}{3}\mu - \kappa \right) (\nabla \cdot \mathbf{v}) \delta_{ij}. \quad (1.6)$$

Here  $\tau_{ij} = \tau_{ji}$  and  $i$  and  $j$  can take on the values 1, 2 for two dimensional case or 1, 2, 3 for three dimensional case resp. The quantities  $x_1, x_2, x_3$  in the derivatives denote Cartesian coordinates  $x, y, z$ , and  $v_1, v_2, v_3$  denote the velocity components  $u, v, w$ . The symbol  $\cdot$  denotes the scalar product of two vectors.

These relations rewritten to the set of equations have the form:

- in 2D case

$$\begin{aligned} \tau_{xx} &= -\mu \left[ 2 \frac{\partial u}{\partial x} \right] + \left( \frac{2}{3}\mu - \kappa \right) (\nabla \cdot \mathbf{v}), \\ \tau_{yy} &= -\mu \left[ 2 \frac{\partial v}{\partial y} \right] + \left( \frac{2}{3}\mu - \kappa \right) (\nabla \cdot \mathbf{v}), \\ \tau_{xy} &= \tau_{yx} = -\mu \left[ \frac{\partial v}{\partial x} + \frac{\partial u}{\partial y} \right], \\ (\nabla \cdot \mathbf{v}) &= \frac{\partial u}{\partial x} + \frac{\partial v}{\partial y}, \end{aligned} \quad (1.7)$$

- in 3D case

$$\begin{aligned}
\tau_{xx} &= -\mu \left[ 2 \frac{\partial u}{\partial x} \right] + \left( \frac{2}{3} \mu - \kappa \right) (\nabla \cdot \mathbf{v}), \\
\tau_{yy} &= -\mu \left[ 2 \frac{\partial v}{\partial y} \right] + \left( \frac{2}{3} \mu - \kappa \right) (\nabla \cdot \mathbf{v}), \\
\tau_{zz} &= -\mu \left[ 2 \frac{\partial w}{\partial z} \right] + \left( \frac{2}{3} \mu - \kappa \right) (\nabla \cdot \mathbf{v}), \\
\tau_{xy} = \tau_{yx} &= -\mu \left[ \frac{\partial v}{\partial x} + \frac{\partial u}{\partial y} \right], \\
\tau_{yz} = \tau_{zy} &= -\mu \left[ \frac{\partial w}{\partial y} + \frac{\partial v}{\partial z} \right], \\
\tau_{zx} = \tau_{xz} &= -\mu \left[ \frac{\partial u}{\partial z} + \frac{\partial w}{\partial x} \right], \\
\nabla \cdot \mathbf{v} &= \frac{\partial u}{\partial x} + \frac{\partial v}{\partial y} + \frac{\partial w}{\partial z}.
\end{aligned} \tag{1.8}$$

The important conclusion is that there is the generalization of the eq. (1.1) and this generalization involves two coefficients characterizing the fluid: the dynamical viscosity  $\mu$  and the dilatational viscosity  $\kappa$ . Usually, in solving fluid dynamics problems, it is not necessary to know  $\kappa$ . For incompressible fluids the relation  $(\nabla \cdot \mathbf{v}) = 0$  holds and therefore the term containing  $\kappa$  is discarded anyway.

## 1.1 Generalized Navier-Stokes Equations

The governing system of the equations for Newtonian and non-Newtonian fluids flow is the system of the generalized Navier-Stokes equations and the continuity equation (see [8], [9], [10], [11]). This system for 2D case written in terms of  $\tau_{ij}$  has the conservative form:

$$\tilde{\mathbf{R}} W_t + F_x^c + G_y^c = F_x^v + G_y^v, \tag{1.9}$$

where  $W$  is the vector of unknowns, the pressure  $\tilde{p}$  and the velocity  $u, v$ . The symbols  $F^c$  and  $G^c$  denote convective physical fluxes

$$W = \begin{pmatrix} \tilde{p} \\ \rho u \\ \rho v \end{pmatrix}, \quad F^c = \begin{pmatrix} \rho u \\ \rho u^2 + \tilde{p} \\ \rho uv \end{pmatrix}, \quad G^c = \begin{pmatrix} \rho v \\ \rho uv \\ \rho v^2 + \tilde{p} \end{pmatrix}. \tag{1.10}$$

The symbols  $F^v$  and  $G^v$  denote viscous physical fluxes.

$$F^v = \begin{pmatrix} 0 \\ \tau_{xx} \\ \tau_{xy} \end{pmatrix}, \quad G^v = \begin{pmatrix} 0 \\ \tau_{yx} \\ \tau_{yy} \end{pmatrix}. \tag{1.11}$$

The matrix  $\tilde{\mathbf{R}}$  is the diagonal matrix

$$\tilde{\mathbf{R}} = \begin{pmatrix} 0 & 0 & 0 \\ 0 & 1 & 0 \\ 0 & 0 & 1 \end{pmatrix}. \quad (1.12)$$

This system of the equations can be rewritten to the set of three equations, one equation of the continuity and two equations of the motion.

– the equation of the continuity

$$\frac{\partial u}{\partial x} + \frac{\partial v}{\partial y} = 0, \quad (1.13)$$

– the equations of the motion

$$\begin{aligned} \rho \left( \frac{\partial u}{\partial t} + u \frac{\partial u}{\partial x} + v \frac{\partial u}{\partial y} \right) &= -\frac{\partial \tilde{p}}{\partial x} - \left( \frac{\partial \tau_{xx}}{\partial x} + \frac{\partial \tau_{yx}}{\partial y} \right), \\ \rho \left( \frac{\partial v}{\partial t} + u \frac{\partial v}{\partial x} + v \frac{\partial v}{\partial y} \right) &= -\frac{\partial \tilde{p}}{\partial y} - \left( \frac{\partial \tau_{xy}}{\partial x} + \frac{\partial \tau_{yy}}{\partial y} \right). \end{aligned} \quad (1.14)$$

Similarly for three dimensional case the system of Navier-Stokes equations in the terms of  $\tau_{ij}$  has the conservative form:

$$\tilde{\mathbf{R}} W_t + F_x^c + G_y^c + H_z^c = F_x^v + G_y^v + H_z^v, \quad (1.15)$$

where  $W$  is the vector of unknowns, the pressure  $\tilde{p}$  and three velocity components  $u, v, w$ . The symbols  $F^c$ ,  $G^c$  and  $H^c$  denote the convective physical fluxes.

$$W = \begin{pmatrix} \tilde{p} \\ \rho u \\ \rho v \\ \rho w \end{pmatrix}, \quad F^c = \begin{pmatrix} \rho u \\ \rho u^2 + \tilde{p} \\ \rho uv \\ \rho uw \end{pmatrix}, \quad G^c = \begin{pmatrix} \rho v \\ \rho uv \\ \rho v^2 + \tilde{p} \\ \rho vw \end{pmatrix}, \quad H^c = \begin{pmatrix} \rho w \\ \rho uw \\ \rho vw \\ \rho w^2 + \tilde{p} \end{pmatrix}. \quad (1.16)$$

The symbols  $F^v$ ,  $G^v$  and  $H^v$  denote the viscous physical fluxes.

$$F^v = \begin{pmatrix} 0 \\ \tau_{xx} \\ \tau_{xy} \\ \tau_{xz} \end{pmatrix}, \quad G^v = \begin{pmatrix} 0 \\ \tau_{yx} \\ \tau_{yy} \\ \tau_{yz} \end{pmatrix}, \quad H^v = \begin{pmatrix} 0 \\ \tau_{zx} \\ \tau_{zy} \\ \tau_{zz} \end{pmatrix}. \quad (1.17)$$

The matrix  $\tilde{\mathbf{R}}$  is the diagonal matrix

$$\tilde{\mathbf{R}} = \begin{pmatrix} 0 & 0 & 0 & 0 \\ 0 & 1 & 0 & 0 \\ 0 & 0 & 1 & 0 \\ 0 & 0 & 0 & 1 \end{pmatrix}. \quad (1.18)$$

As for two dimensional case, the system of the equations can be rewritten to the set of four equations, one equation of the continuity and three equations of the motion.

- the equation of the continuity

$$\frac{\partial u}{\partial x} + \frac{\partial v}{\partial y} + \frac{\partial w}{\partial z} = 0, \quad (1.19)$$

- the equations of the motion

$$\begin{aligned} \rho \left( \frac{\partial u}{\partial t} + u \frac{\partial u}{\partial x} + v \frac{\partial u}{\partial y} + w \frac{\partial u}{\partial z} \right) &= -\frac{\partial \tilde{p}}{\partial x} - \left( \frac{\partial \tau_{xx}}{\partial x} + \frac{\partial \tau_{yx}}{\partial y} + \frac{\partial \tau_{zx}}{\partial z} \right), \\ \rho \left( \frac{\partial v}{\partial t} + u \frac{\partial v}{\partial x} + v \frac{\partial v}{\partial y} + w \frac{\partial v}{\partial z} \right) &= -\frac{\partial \tilde{p}}{\partial y} - \left( \frac{\partial \tau_{xy}}{\partial x} + \frac{\partial \tau_{yy}}{\partial y} + \frac{\partial \tau_{zy}}{\partial z} \right), \\ \rho \left( \frac{\partial w}{\partial t} + u \frac{\partial w}{\partial x} + v \frac{\partial w}{\partial y} + w \frac{\partial w}{\partial z} \right) &= -\frac{\partial \tilde{p}}{\partial z} - \left( \frac{\partial \tau_{xz}}{\partial x} + \frac{\partial \tau_{yz}}{\partial y} + \frac{\partial \tau_{zz}}{\partial z} \right). \end{aligned} \quad (1.20)$$

## 1.2 Incompressible Navier-Stokes Equations for Newtonian Fluids Flow

In the incompressible laminar viscous flows the density  $\rho$  is assumed constant. Under this assumption of the incompressible flow, i.e. the density is constant and restriction to the constant viscosity, the equations of the motion (1.14) and (1.20) can be divided by  $\rho$  (see e.g. [8]).

The viscous stresses can be rewritten with using  $(\nabla \cdot \mathbf{v}) = 0$  to the form

$$\begin{aligned} \tau_{xx} &= -\nu 2 \frac{\partial u}{\partial x}, \\ \tau_{yy} &= -\nu 2 \frac{\partial v}{\partial y}, \\ \tau_{zz} &= -\nu 2 \frac{\partial w}{\partial z}, \\ \tau_{xy} &= -\nu \left[ \frac{\partial u}{\partial y} + \frac{\partial v}{\partial x} \right], \\ \tau_{xz} &= -\nu \left[ \frac{\partial u}{\partial z} + \frac{\partial w}{\partial x} \right], \\ \tau_{yz} &= -\nu \left[ \frac{\partial v}{\partial z} + \frac{\partial w}{\partial y} \right]. \end{aligned} \quad (1.21)$$

From the equations of the continuity for 2D or 3D cases the relations for  $u_{xx}$ ,  $v_{yy}$  and  $w_{zz}$  can be expressed as follows:

$$\begin{aligned} u_{xx} &= -v_{yx}, & v_{yy} &= -u_{xy}, \\ u_{xx} &= -v_{yx} - w_{zx}, & v_{yy} &= -u_{xy} - w_{yz}, & w_{zz} &= -u_{xz} - v_{yz}. \end{aligned} \quad (1.22)$$

Therefore the system of Navier-Stokes equations in two dimensional case can be rewritten to the conservative form

$$\tilde{\mathbf{R}} W_t + F_x^c + G_y^c = F_x^v + G_y^v, \quad (1.23)$$

where subscripts  $t, x, y$  denote the partial derivatives under the time and the space. And the vector  $W$  and the convective physical fluxes  $F^c$  and  $G^c$  are defined as follows:

$$W = \begin{pmatrix} p \\ u \\ v \end{pmatrix}, \quad F^c = \begin{pmatrix} u \\ u^2 + p \\ uv \end{pmatrix}, \quad G^c = \begin{pmatrix} v \\ uv \\ v^2 + p \end{pmatrix}, \quad (1.24)$$

where  $u, v$  are the velocity vector components,  $p$  is the kinematic pressure and it is defined by the relation

$$p = \frac{\tilde{p}}{\rho}. \quad (1.25)$$

The viscous physical fluxes  $F^v$  and  $G^v$  are defined by the relations:

$$F^v = \nu \begin{pmatrix} 0 \\ u_x \\ v_x \end{pmatrix}, \quad G^v = \nu \begin{pmatrix} 0 \\ u_y \\ v_y \end{pmatrix}, \quad (1.26)$$

where  $\nu$  is the kinematic viscosity and it is defined by the relation

$$\nu = \frac{\mu}{\rho} \quad (1.27)$$

here  $\rho$  denotes the constant density.

This system can be rewritten to the form of three equations:

$$\begin{aligned} \frac{\partial u}{\partial x} + \frac{\partial v}{\partial y} &= 0, \\ \frac{\partial u}{\partial t} + u \frac{\partial u}{\partial x} + v \frac{\partial u}{\partial y} &= -\frac{\partial p}{\partial x} + \nu \left[ \frac{\partial^2 u}{\partial x^2} + \frac{\partial^2 u}{\partial y^2} \right], \\ \frac{\partial v}{\partial t} + u \frac{\partial v}{\partial x} + v \frac{\partial v}{\partial y} &= -\frac{\partial p}{\partial y} + \nu \left[ \frac{\partial^2 v}{\partial x^2} + \frac{\partial^2 v}{\partial y^2} \right]. \end{aligned} \quad (1.28)$$

Similarly in three dimensional case, the system of Navier-Stokes equations has the conservative form

$$\tilde{\mathbf{R}} W_t + F_x^c + G_y^c + H_z^c = F_x^v + G_y^v + H_z^v, \quad (1.29)$$

where subscripts  $t, x, y, z$  denote the partial derivatives under the time and the space. And the vector  $W$  and the convective physical fluxes  $F^c$ ,  $G^c$  and  $H^c$  are defined as follows:

$$W = \begin{pmatrix} p \\ u \\ v \\ w \end{pmatrix}, \quad F^c = \begin{pmatrix} u \\ u^2 + p \\ uv \\ uw \end{pmatrix}, \quad G^c = \begin{pmatrix} v \\ uv \\ v^2 + p \\ vw \end{pmatrix}, \quad H^c = \begin{pmatrix} w \\ uw \\ vw \\ w^2 + p \end{pmatrix}, \quad (1.30)$$



where  $u, v, w$  are the velocity vector components,  $p$  is the kinematic pressure and it is defined as for 2D case (eq. (1.25)).

The viscous physical fluxes  $F^v$ ,  $G^v$  and  $H^v$  are defined by the relations:

$$F^v = \nu \begin{pmatrix} 0 \\ u_x \\ v_x \\ w_x \end{pmatrix}, \quad G^v = \nu \begin{pmatrix} 0 \\ u_y \\ v_y \\ w_y \end{pmatrix}, \quad H^v = \nu \begin{pmatrix} 0 \\ u_z \\ v_z \\ w_z \end{pmatrix}, \quad (1.31)$$

where  $\nu$  is the kinematic viscosity defined by the eq. (1.27).

As for 2D case this system can be rewritten to the set of four equations as follows:

$$\begin{aligned} \frac{\partial u}{\partial x} + \frac{\partial v}{\partial y} + \frac{\partial w}{\partial z} &= 0, \\ \frac{\partial u}{\partial t} + u \frac{\partial u}{\partial x} + v \frac{\partial u}{\partial y} + w \frac{\partial u}{\partial z} &= -\frac{\partial p}{\partial x} + \nu \left[ \frac{\partial^2 u}{\partial x^2} + \frac{\partial^2 u}{\partial y^2} + \frac{\partial^2 u}{\partial z^2} \right], \\ \frac{\partial v}{\partial t} + u \frac{\partial v}{\partial x} + v \frac{\partial v}{\partial y} + w \frac{\partial v}{\partial z} &= -\frac{\partial p}{\partial y} + \nu \left[ \frac{\partial^2 v}{\partial x^2} + \frac{\partial^2 v}{\partial y^2} + \frac{\partial^2 v}{\partial z^2} \right], \\ \frac{\partial w}{\partial t} + u \frac{\partial w}{\partial x} + v \frac{\partial w}{\partial y} + w \frac{\partial w}{\partial z} &= -\frac{\partial p}{\partial z} + \nu \left[ \frac{\partial^2 w}{\partial x^2} + \frac{\partial^2 w}{\partial y^2} + \frac{\partial^2 w}{\partial z^2} \right]. \end{aligned} \quad (1.32)$$

### 1.2.1 Dimensional Analysis

In most flow systems one can identify the following ‘‘scale factors’’: the reference length  $L^*$ , the reference velocity  $U^*$  and the reference kinematic viscosity  $\nu^*$  ([5], [12]). Then dimensionless variables (denoting by the primes) can be defined as follows:

$$\begin{aligned} x' &= \frac{x}{L^*}, & y' &= \frac{y}{L^*}, & z' &= \frac{z}{L^*}, & t' &= \frac{tU^*}{L^*}, \\ u' &= \frac{u}{U^*}, & v' &= \frac{v}{U^*}, & w' &= \frac{w}{U^*}, & \mathbf{v}' &= \frac{\mathbf{v}}{U^*}, \\ p' &= \frac{p}{U^{*2}}, & \nu' &= \frac{\nu}{\nu^*}. \end{aligned} \quad (1.33)$$

Multiply the continuity equation by  $\frac{L^*}{U^*}$  and the equations of the motion by  $\frac{L^*}{U^{*2}}$  in the eq. (1.28) for 2D case and in the eq. (1.32) for 3D case. Then for Newtonian fluids the system of Navier-Stokes equations and the continuity equation has the form:

- 2D case

$$\begin{aligned} \frac{\partial u'}{\partial x'} + \frac{\partial v'}{\partial y'} &= 0, \\ \left( \frac{\partial u'}{\partial t'} + u' \frac{\partial u'}{\partial x'} + v' \frac{\partial u'}{\partial y'} \right) &= -\frac{\partial p'}{\partial x'} + \frac{\nu^*}{L^*U^*} \left( \frac{\partial^2 u'}{\partial x'^2} + \frac{\partial^2 u'}{\partial y'^2} \right), \\ \left( \frac{\partial v'}{\partial t'} + u' \frac{\partial v'}{\partial x'} + v' \frac{\partial v'}{\partial y'} \right) &= -\frac{\partial p'}{\partial y'} + \frac{\nu^*}{L^*U^*} \left( \frac{\partial^2 v'}{\partial x'^2} + \frac{\partial^2 v'}{\partial y'^2} \right), \end{aligned} \quad (1.34)$$

- 3D case

$$\begin{aligned} \frac{\partial u'}{\partial x'} + \frac{\partial v'}{\partial y'} + \frac{\partial w'}{\partial z'} &= 0, \\ \left( \frac{\partial u'}{\partial t'} + u' \frac{\partial u'}{\partial x'} + v' \frac{\partial u'}{\partial y'} + w' \frac{\partial u'}{\partial z'} \right) &= -\frac{\partial p'}{\partial x'} + \frac{\nu^*}{L^* U^*} \left( \frac{\partial^2 u'}{\partial x'^2} + \frac{\partial^2 u'}{\partial y'^2} + \frac{\partial^2 u'}{\partial z'^2} \right), \\ \left( \frac{\partial v'}{\partial t'} + u' \frac{\partial v'}{\partial x'} + v' \frac{\partial v'}{\partial y'} + w' \frac{\partial v'}{\partial z'} \right) &= -\frac{\partial p'}{\partial y'} + \frac{\nu^*}{L^* U^*} \left( \frac{\partial^2 v'}{\partial x'^2} + \frac{\partial^2 v'}{\partial y'^2} + \frac{\partial^2 v'}{\partial z'^2} \right), \\ \left( \frac{\partial w'}{\partial t'} + u' \frac{\partial w'}{\partial x'} + v' \frac{\partial w'}{\partial y'} + w' \frac{\partial w'}{\partial z'} \right) &= -\frac{\partial p'}{\partial z'} + \frac{\nu^*}{L^* U^*} \left( \frac{\partial^2 w'}{\partial x'^2} + \frac{\partial^2 w'}{\partial y'^2} + \frac{\partial^2 w'}{\partial z'^2} \right). \end{aligned} \quad (1.35)$$

The expression on the right hand side in the equations of the motion is the reverse value of Reynolds number. The definition of Reynolds for two dimensional and three dimensional case can be defined by the expressions

$$\text{Re} = \frac{U^* L^*}{\nu^*}, \quad \text{Re} = \frac{U^* 4S}{\nu^* O}, \quad (1.36)$$

where for 3D  $S$  represents the reference volume of the entrance (for the square entrance  $S = L^* L^*$ ) and  $O$  is the reference circumference of the entrance (for the square entrance  $O = 4L^*$ ).

## 1.2.2 Boundary Conditions

The flow is considered in a bounded domain. The boundaries are solid wall, outlet and inlet. Let us define concrete boundary conditions for two dimensional case.

**Inlet:** At the inlet Dirichlet boundary conditions for the velocity vector  $(u, v)^T$  are used and other values ( $p$ ) are computed by the extrapolation from the domain.

**Outlet:** At the outlet the pressure value is given and the velocity components  $u, v$  are computed by the extrapolation from the domain.

**Wall:** The homogenous Dirichlet boundary conditions for the velocity are used on the wall. For the pressure we used the extrapolation from the computed domain to boundary where normal derivative of the pressure is zero - Prandtl's boundary layer relation.

Similarly, the boundary conditions for three dimensional channel can be defined. In this case the inlet and the outlet boundary conditions are the same as for two dimensional case. And for the wall and the corners of the domain the homogenous Dirichlet boundary conditions are used. For the pressure the extrapolations are used.

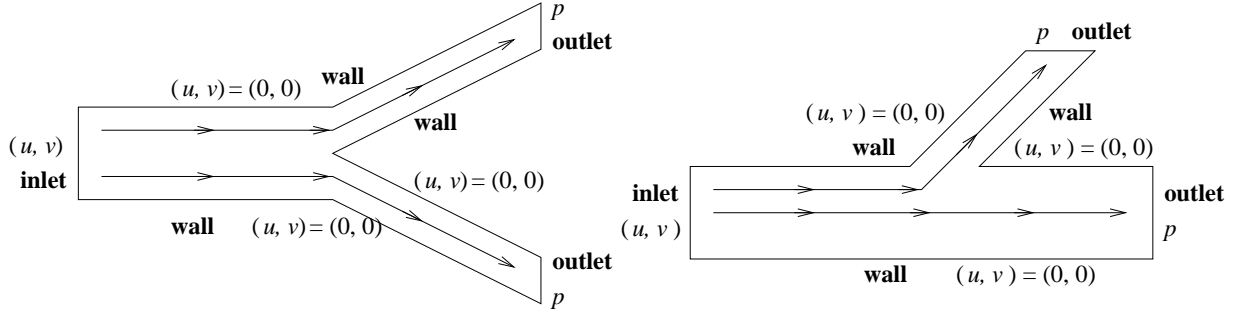


Figure 1.1: Consider domain and boundary conditions

### 1.3 Generalized Newtonian Fluids

Let us consider the generalized Newtonian fluids. The system of Navier-Stokes equations written in the conservative vector form for 2D:

$$\tilde{\mathbf{R}}W_t + F_x^c + G_y^c = \frac{1}{\text{Re}}(F_x^v + G_y^v), \quad (1.37)$$

$$W = \begin{pmatrix} p \\ u \\ v \end{pmatrix}, \quad F^c = \begin{pmatrix} u \\ u^2 + p \\ uv \end{pmatrix}, \quad G^c = \begin{pmatrix} v \\ uv \\ v^2 + p \end{pmatrix}. \quad (1.38)$$

The symbol  $\tilde{\mathbf{R}}$  represents the diagonal matrix ( $\tilde{\mathbf{R}} = \text{diag}(0, 1, 1)$ ),  $p$  is the pressure,  $(u, v)^T$  is the velocity vector (in dimensionless form). The symbols  $t, x, y$  are used for denoting of the partial derivatives under the time and the spatial coordinates.

The vectors  $F^c, G^c$  are the inviscid physical fluxes defined by (1.38) and  $F^v, G^v$  are the viscous physical fluxes defined by

$$F^v = \begin{pmatrix} 0 \\ \tau_{xx} \\ \tau_{xy} \end{pmatrix}, \quad G^v = \begin{pmatrix} 0 \\ \tau_{yx} \\ \tau_{yy} \end{pmatrix}. \quad (1.39)$$

The right hand side of Navier-Stokes equations is given by one of the simple non-Newtonian models, the power-law model. The viscous stress is defined as follows:

$$\boldsymbol{\tau} = 2\eta(\dot{\gamma})\mathbf{D} \quad (1.40)$$

and

$$\boldsymbol{\tau} = \begin{pmatrix} \tau_{xx} & \tau_{xy} \\ \tau_{yx} & \tau_{yy} \end{pmatrix}, \quad (1.41)$$

where viscosity  $\eta(\dot{\gamma})$  is defined by the power-law model as follows:

$$\eta(\dot{\gamma}) = \nu \left( \sqrt{\text{tr}\mathbf{D}^2} \right)^r, \quad (1.42)$$

where  $\nu$  is the kinematic viscosity of Newtonian fluids which belongs to the definition of Reynolds number (eq. (1.36)), symbol  $\text{tr}$  denotes the trace of the tensor. The symmetric tensor  $\mathbf{D}$  is called the velocity gradient and it is defined by the relation

$$\mathbf{D} = (D)_{ij} = \begin{pmatrix} D_{xx} & D_{xy} \\ D_{yx} & D_{yy} \end{pmatrix}. \quad (1.43)$$

where  $i$  and  $j$  maybe  $x$  and  $y$ . The components of the velocity gradient  $D_{ij}$  are defined by the expressions

$$D_{ij} = \frac{1}{2} \left( \frac{\partial v_i}{\partial x_j} + \frac{\partial v_j}{\partial x_i} \right), \quad (1.44)$$

where  $i$  and  $j$  can take on the values 1, 2. The quantities  $x_1$  and  $x_2$  in the derivatives denote Cartesian coordinates  $x, y$ . And  $v_1$  and  $v_2$  denote the velocity vector components  $u, v$ .

Therefore the velocity gradient  $\mathbf{D}$  has the form

$$\mathbf{D} = \begin{pmatrix} u_x & \frac{1}{2}(u_y + v_x) \\ \frac{1}{2}(u_y + v_x) & v_y \end{pmatrix} \quad (1.45)$$

and the trace of the tensor  $\mathbf{D}^2$  is then

$$\text{tr } \mathbf{D}^2 = u_x^2 + \frac{1}{2}(u_y + v_x)^2 + v_y^2. \quad (1.46)$$

The constant  $r$  in the power-law model is called the power-law index. Newtonian fluids are the special case of non-Newtonian fluids with the constant  $r = 0$ . If  $r$  is bigger than 0 then non-Newtonian fluids are called the shear thickening fluids, if  $r$  is less than 0 then non-Newtonian fluids are called the shear thinning fluids. In this work this index is from the closed interval  $[0, 1]$ . It means that this work is concerned on the numerical solution of Newtonian fluids ( $r = 0$ ) and on the numerical solutions of the shear thickening non-Newtonian fluids ( $r > 0$ ).

Similarly for three dimensional case, the system of Navier-Stokes equations and the continuity equation for the generalized Newtonian fluids can be written in the conservative form

$$\tilde{\mathbf{R}}\mathbf{W}_t + F_x^c + G_y^c + H_z^c = \frac{1}{\text{Re}}(F_x^v + G_y^v + H_z^v), \quad (1.47)$$

$$\begin{aligned} \mathbf{W} &= \begin{pmatrix} p \\ u \\ v \\ w \end{pmatrix}, & \mathbf{F}^c &= \begin{pmatrix} u \\ u^2 + p \\ uv \\ uw \end{pmatrix}, \\ \mathbf{G}^c &= \begin{pmatrix} v \\ uv \\ v^2 + p \\ vw \end{pmatrix}, & \mathbf{H}^c &= \begin{pmatrix} w \\ uw \\ vw \\ w^2 + p \end{pmatrix}. \end{aligned} \quad (1.48)$$

The symbol  $\tilde{\mathbf{R}}$  is the diagonal matrix ( $\tilde{\mathbf{R}} = \text{diag}(0, 1, 1, 1)$ ),  $p$  is the pressure,  $u$ ,  $v$  and  $w$  are the velocity vector components. The subscripts  $t$ ,  $x$ ,  $y$  and  $z$  are used for the partial derivatives under the time and the space.

The vector  $W$  is the vector of the unknowns and the vectors  $F^c, G^c, H^c$  are the inviscid physical fluxes. The definition of the viscous physical fluxes  $F^v, G^v, H^v$  are defined as follows:

$$F^v = \begin{pmatrix} 0 \\ \tau_{xx} \\ \tau_{xy} \\ \tau_{xz} \end{pmatrix}, \quad G^v = \begin{pmatrix} 0 \\ \tau_{yx} \\ \tau_{yy} \\ \tau_{yz} \end{pmatrix}, \quad H^v = \begin{pmatrix} 0 \\ \tau_{zx} \\ \tau_{zy} \\ \tau_{zz} \end{pmatrix}. \quad (1.49)$$

In 3D case the same power-law model is used as for 2D case, eq. (1.40). The viscous stress tensor  $\boldsymbol{\tau}$  is given by the matrix

$$\boldsymbol{\tau} = \begin{pmatrix} \tau_{xx} & \tau_{xy} & \tau_{xz} \\ \tau_{yx} & \tau_{yy} & \tau_{yz} \\ \tau_{zx} & \tau_{zy} & \tau_{zz} \end{pmatrix}, \quad (1.50)$$

where the viscosity  $\eta(\dot{\gamma})$  is defined by the power-law model (1.42), where  $\nu$  is the kinematic viscosity of Newtonian fluids which belongs to the definition of Reynolds number (eq. (1.36)), the symbol  $\text{tr}$  denotes the trace of the tensor. The symmetric tensor  $\mathbf{D}$  is called the velocity gradient and it is defined by the relation

$$\mathbf{D} = (D)_{ij} = \begin{pmatrix} D_{xx} & D_{xy} & D_{xz} \\ D_{yx} & D_{yy} & D_{yz} \\ D_{zx} & D_{zy} & D_{zz} \end{pmatrix}, \quad (1.51)$$

where  $i$  and  $j$  maybe  $x$ ,  $y$  and  $z$ . The components of the velocity gradient  $D_{ij}$  are defined by the equation

$$D_{ij} = \frac{1}{2} \left( \frac{\partial v_i}{\partial x_j} + \frac{\partial v_j}{\partial x_i} \right), \quad (1.52)$$

where  $i$  and  $j$  can take on the values 1, 2, 3. The quantities  $x_1$ ,  $x_2$  and  $x_3$  in the derivatives denote Cartesian coordinates  $x, y, z$ . And  $v_1$ ,  $v_2$  and  $v_3$  denote the velocity vector components  $u, v, w$ .

Therefore the velocity gradient  $\mathbf{D}$  has the form

$$\mathbf{D} = \begin{pmatrix} u_x & \frac{1}{2}(u_y + v_x) & \frac{1}{2}(u_z + w_x) \\ \frac{1}{2}(u_y + v_x) & v_y & \frac{1}{2}(v_z + w_y) \\ \frac{1}{2}(u_z + w_x) & \frac{1}{2}(v_z + w_y) & w_z \end{pmatrix} \quad (1.53)$$

and the trace of the tensor  $\mathbf{D}^2$  is then

$$\text{tr } \mathbf{D}^2 = u_x^2 + \frac{1}{2}(u_y + v_x)^2 + v_y^2 + \frac{1}{2}(u_z + w_x)^2 + \frac{1}{2}(v_z + w_y)^2 + w_z^2. \quad (1.54)$$

The constant  $r$  in the power-law model is the power-law index. If  $r = 0$  then fluids are Newtonian. If  $r > 0$  then non-Newtonian fluids are shear thickening fluids, if  $r < 0$  then non-Newtonian fluids are shear thinning fluids. This work is concerned on the numerical solution of Newtonian fluids ( $r = 0$ ) and the shear thickening non-Newtonian fluids ( $r > 0$ ).

# Chapter 2

## Numerical Solution

### 2.1 Finite Volume Method

The finite volume method (FVM) is the discretization method for conservation laws (see [13], [14]). Let consider general hyperbolic system of the equations

$$W_t + \nabla \cdot F(W) = 0 \quad (2.1)$$

at each point  $x$  and at each time  $t$  where the conservation of  $W$  is to be written. In the eq. (2.1) the symbol  $W$  represents the state vector  $W = (w_1, \dots, w_m)^T \in \mathbb{R}^m$  and the vector  $F = (F_1(W), \dots, F_n(W))^T$  represents the corresponding flux vector,  $(\cdot)_t$  denotes partial derivative over the time and  $\nabla$  operator is the vector of the partial derivatives over space coordinates,  $\nabla = (\frac{\partial}{\partial x_1}, \dots, \frac{\partial}{\partial x_n})^T$ . The flux  $F$  can be in general decomposed into a convective and a diffusive part. The diffusive part is proportional to the gradient of the quantity considered.

Let  $\Omega$  is the closed bounded domain ( $\Omega \subset \mathbb{R}^n$ ). This domain is divided to the finite subdomains  $D_i$ ,  $i \in J$  ( $J \subset \mathbb{Z}$ ) with properties:

1.  $\bigcup_{i \in J} D_i = \overline{\Omega}$ ,
2. for  $\forall i, j \in J$ ;  $i \neq j$ :  $D_i \cap D_j = \emptyset$ .

The finite volume method is based on an integral form of the system of conservation laws (eq. (2.1)). Denote us by the symbol  $D_i$  the  $i$ -th grid cell in general case.

The value  $W_i^n$  will approximate the average value over the finite volume cell  $D_i$  at time  $t_n$ :

$$W_i^n \approx \frac{1}{\mu_i} \int_{D_i} W(x_1, \dots, x_n, t^n) d\Omega, \quad (2.2)$$

where  $\mu_i$  is the volume of the finite volume cell  $D_i$  and the superscript  $n$  denotes the time level.

Integrating (2.1) over the cell  $D_i$  and in the time from  $t^n$  to  $t^{n+1}$  yields

$$\int_{t^n}^{t^{n+1}} \int_{D_i} \frac{\partial W}{\partial t}(x_1, \dots, x_n, t) \, d\Omega \, dt + \int_{t^n}^{t^{n+1}} \int_{D_i} \nabla \cdot F(W(x_1, \dots, x_n, t)) \, d\Omega \, dt = 0. \quad (2.3)$$

Since, the domain  $\Omega$  (therefore all of subdomains  $D_i$ ) is independent on the time we can rewrite eq. (2.3) to the integral form of the conservation laws

$$\int_{t^n}^{t^{n+1}} \frac{d}{dt} \int_{D_i} W(x_1, \dots, x_n, t) \, d\Omega \, dt + \int_{t^n}^{t^{n+1}} \int_{D_i} \nabla \cdot F(W(x_1, \dots, x_n, t)) \, d\Omega \, dt = 0. \quad (2.4)$$

Given  $W_i^n$ , the cell averages at time  $t^n$ , we can approximate  $W_i^{n+1}$ , the cell averages at time  $t^{n+1}$  after a time step  $\Delta t = t^{n+1} - t^n$ . It gives

$$(W_i^{n+1} - W_i^n) \mu_i + \int_{t^n}^{t^{n+1}} \int_{D_i} \nabla \cdot F(W(x_1, \dots, x_n, t)) \, d\Omega \, dt = 0. \quad (2.5)$$

Applying Green's theorem on the integral in the left hand side of the equation (2.5) it results in

$$(W_i^{n+1} - W_i^n) \mu_i + \int_{t^n}^{t^{n+1}} \oint_{\partial D_i} F(W(x_1, \dots, x_n, t)) \cdot \mathbf{n}_i \, dS_i \, dt = 0, \quad (2.6)$$

where  $\partial D_i$  is the boundary of the finite cell  $D_i$  and  $\mathbf{n}_i$  is the unit normal vector to  $\partial D_i$ . In two dimensional case, the finite volume cell  $D_i$  is a polygon (denoting by symbol  $D_{ij}$ ) and in three dimensional case, the finite volume cell  $D_i$  is a polyhedron (denoting by symbol  $D_{ijk}$ ). Therefore the eq. (2.6) can be rewritten to the form

$$(W_i^{n+1} - W_i^n) \mu_i + \sum_{l=1}^{N_i} \int_{t^n}^{t^{n+1}} \oint_{\partial C_{il}} F(W(x_1, \dots, x_n, t)) \cdot \mathbf{n}_{il} \, dS_{il} \, dt = 0, \quad (2.7)$$

where  $N_i$  is the number of all neighbouring finite cells  $D_l$  of the finite cell  $D_i$ . The symbol  $C_{il}$  represents the  $l$ -th boundary between the cell  $D_i$  and the cell  $D_l$ , in 2D  $D_{il}$  corresponds to the edge of polygon and in 3D  $D_{il}$  is the surface of the polyhedron. Symbol  $\mathbf{n}_{il}$  denotes the outward unit normal to the boundary  $D_{il}$  (see figure (2.1)).

In general, the time integral in the left hand side of eq. (2.7) cannot be evaluated exactly, since  $W(x_1, \dots, x_n, t)$  varies with the time along each edge of the cell, and therefore there is no exact solution to work with. Finally, the finite volume scheme is defined as follows:

$$(W_i^{n+1} - W_i^n) \mu_i + \Delta t \sum_{l=1}^{N_i} H_{il}^n \psi_{il} = 0, \quad (2.8)$$

where  $\psi_{il}$  is the volume of the boundary  $C_{il}$  and  $H_{il}^n$  is approximation to the average flux called "numerical flux"

$$H_{il}^n \approx \frac{1}{\Delta t \psi_{il}} \int_{t^n}^{t^{n+1}} \oint_{\partial C_{il}} F(W(x_1, \dots, x_n, t)) \cdot dS_{il} dt. \quad (2.9)$$

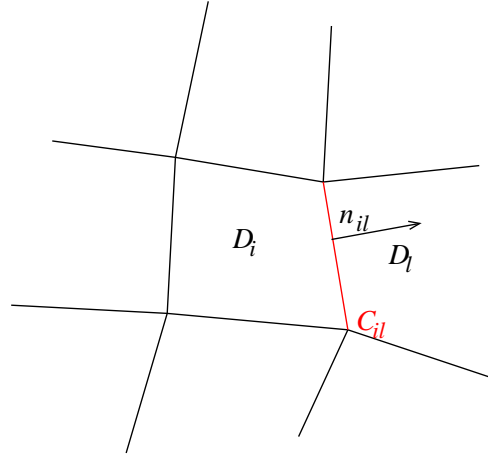


Figure 2.1: Structured finite volume mesh in 2D form

For a hyperbolic problem the information propagates with the finite speed therefore the numerical flux  $H_{il}^n$  is based only on the values  $W_i^n$  and  $W_l^n$ , the cell averages on either side of the interface. Then following expression can be used

$$H_{il}^n = \mathcal{F}(W_i^n, W_l^n), \quad (2.10)$$

where  $\mathcal{F}$  is the some numerical flux function. Then the method (2.8) can be rewritten to the form

$$W_i^{n+1} = W_i^n - \frac{\Delta t}{\mu_i} \sum_{l=1}^{N_i} \mathcal{F}(W_i^n, W_l^n) \psi_{il}. \quad (2.11)$$

The method obtained depends on how the numerical flux function  $\mathcal{F}$  is chosen. In general, any method of this type is an explicit method, and the value  $W_i^{n+1}$  depends on three values  $W_{i-1}^n, W_i^n$  and  $W_{i+1}^n$ .

### 2.1.1 Finite Volume Method for Generalized Newtonian Fluids Flow

Let us consider two dimensional generalized Newtonian fluids flow (eq. (1.37) - (1.46)) written in the vector form ([16], [17], [18])

$$\tilde{\mathbf{R}}W_t = - \left( \tilde{F}_x + \tilde{G}_y \right), \quad (2.12)$$

where the physical fluxes are defined as follows:

$$\tilde{F} = F^c - \frac{1}{\text{Re}} F^v, \quad \tilde{G} = G^c - \frac{1}{\text{Re}} G^v, \quad (2.13)$$



where  $F^c, G^c$  are the inviscid physical fluxes defined by (1.38) and  $F^v, G^v$  are the viscous fluxes defined by (1.39) - (1.46).

The eq. (2.12) is integrated over  $D_{ij}$  ( $D_{ij}$  is the finite volume cell in two dimensional case, i.e. it is the polygon, see figure (2.2), with the volume of the cell  $D_{ij}, \mu_{ij} = \iint_{D_{ij}} dx dy$ )

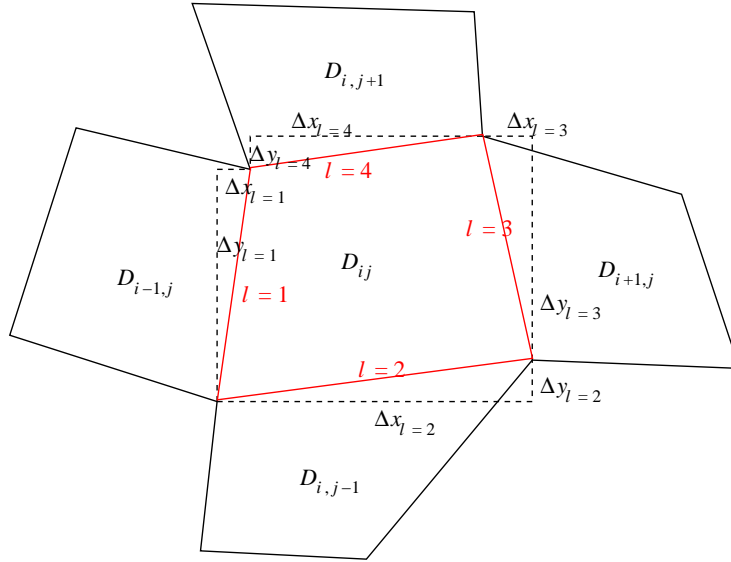


Figure 2.2: Finite volume cell for two dimensional case

$$\tilde{\mathbf{R}} \iint_{D_{ij}} W_t dx dy = - \iint_{D_{ij}} (\tilde{F}_x + \tilde{G}_y) dx dy, \quad (2.14)$$

the mean value theorem is applied to the left-hand side of (2.12), and Green's theorem is applied on the right-hand side of (2.12) hence

$$\tilde{\mathbf{R}} W_t |_{ij} = - \frac{1}{\mu_{ij}} \oint_{\partial D_{ij}} \tilde{F} dy - \tilde{G} dx. \quad (2.15)$$

## 2.2 Method of Artificial Compressibility

In this part, the steady state solution is considered. In such a case an artificial compressibility method can be applied. This method was first introduced by Chorin (see [19], [20]). The basic idea is to complete the equation of the continuity by the term  $\frac{1}{\beta^2} p_t$ , i.e. to the form

- 2D

$$\frac{1}{\beta^2} p_t + u_x + v_y = 0, \quad (2.16)$$

- 3D

$$\frac{1}{\beta^2} p_t + u_x + v_y + w_z = 0, \quad (2.17)$$

where  $\beta \in \mathbb{R}^+$  is called the artificial compressibility coefficient. Therefore the systems of the equations (1.37) - (1.46) in 2D case or the systems of the equations (1.47) - (1.54) in 3D case resp. can be rewritten with new matrices  $\tilde{\mathbf{R}}_\beta$

$$\tilde{\mathbf{R}}_\beta = \begin{pmatrix} \frac{1}{\beta^2} & 0 & 0 \\ 0 & 1 & 0 \\ 0 & 0 & 1 \end{pmatrix}, \quad \tilde{\mathbf{R}}_\beta = \begin{pmatrix} \frac{1}{\beta^2} & 0 & 0 & 0 \\ 0 & 1 & 0 & 0 \\ 0 & 0 & 1 & 0 \\ 0 & 0 & 0 & 1 \end{pmatrix}. \quad (2.18)$$

The system of Navier-Stokes equations and the continuity equation for generalized Newtonian fluids flow for 2D or 3D case with the new matrices  $\tilde{\mathbf{R}}_\beta$  (2.18) is now hyperbolic therefore the standard numerical methods can be used.

For the solving of these hyperbolic systems a knowledge of eigenvalues of the matrices  $A = \partial F^c / \partial(\tilde{\mathbf{R}}_\beta W)$  and  $B = \partial G^c / \partial(\tilde{\mathbf{R}}_\beta W)$  for 2D case and the eigenvalues of the matrices  $A = \partial F^c / \partial(\tilde{\mathbf{R}}_\beta W)$ ,  $B = \partial G^c / \partial(\tilde{\mathbf{R}}_\beta W)$  and  $C = \partial H^c / \partial(\tilde{\mathbf{R}}_\beta W)$  for 3D case is needed. These matrices have the form

$$A = \begin{pmatrix} 0 & \beta^2 & 0 \\ 1 & u & 0 \\ 0 & 0 & u \end{pmatrix}, \quad B = \begin{pmatrix} 0 & 0 & \beta^2 \\ 0 & v & 0 \\ 1 & 0 & v \end{pmatrix}, \quad (2.19)$$

$$A = \begin{pmatrix} 0 & \beta^2 & 0 & 0 \\ 1 & u & 0 & 0 \\ 0 & 0 & u & 0 \\ 0 & 0 & 0 & u \end{pmatrix}, \quad B = \begin{pmatrix} 0 & 0 & \beta^2 & 0 \\ 0 & v & 0 & 0 \\ 1 & 0 & v & 0 \\ 0 & 0 & 0 & v \end{pmatrix}, \quad C = \begin{pmatrix} 0 & 0 & 0 & \beta^2 \\ 0 & w & 0 & 0 \\ 0 & 0 & w & 0 \\ 1 & 0 & 0 & w \end{pmatrix}. \quad (2.20)$$

Then the eigenvalues for 2D case are:  $u, \frac{u}{2} \pm \sqrt{\frac{u^2}{4} + \beta^2}$  from the matrix  $A$  and  $v, \frac{v}{2} \pm \sqrt{\frac{v^2}{4} + \beta^2}$  from the matrix  $B$  respectively. And for 3D case eigenvalues are:  $u, u, \frac{u}{2} \pm \sqrt{\frac{u^2}{4} + \beta^2}$  from  $A$ ,  $v, v, \frac{v}{2} \pm \sqrt{\frac{v^2}{4} + \beta^2}$  from  $B$  or  $w, w, \frac{w}{2} \pm \sqrt{\frac{w^2}{4} + \beta^2}$  from  $C$  respectively.

Let us consider the system of the equations with the new matrices  $\tilde{\mathbf{R}}_\beta$  eq. (2.18)

- 2D case

$$\tilde{\mathbf{R}}_\beta W_t + F_x^c + G_y^c = \frac{1}{\text{Re}} (F_x^v + G_y^v), \quad (2.21)$$

- 3D case

$$\tilde{\mathbf{R}}_\beta W_t + F_x^c + G_y^c + H_z^c = \frac{1}{\text{Re}} (F_x^v + G_y^v + H_z^v), \quad (2.22)$$

with the definitions of the different right hand side for Newtonian and non-Newtonian shear thickening fluids.

The artificial compressibility coefficient  $\beta$  has dimension of the velocity. The optimal choice of the value  $\beta$  is

$$\beta \approx \max_{D_i, n_{ij}}(u_{ij}), i \in I, j \in N_i, \quad (2.23)$$

where  $I$  represents the set of the indices of all cells from the domain  $\Omega$  and  $N_i$  is the set of the indices of all cells neighbouring with the cell  $D_i$ . For dimensionless value the artificial compressibility coefficients is divided by reference velocity  $U^*$ . For steady computation, the artificial compressibility coefficient is equal  $\beta = 1$ , for unsteady computations, the different values of  $\beta$  is chosen ( $\beta$  is high positive value or ideally  $\beta \rightarrow \infty$ ).

## 2.3 Numerical Scheme

The multistage Runge-Kutta method is used as the numerical model for the numerical solutions of Newtonian and shear thickening non-Newtonian fluids flow for 2D and 3D case. The numerical scheme is implemented in cell-centered form. It means that average values of conservative variables are situated to the centres of gravity of the finite volume cells.

### 2.3.1 Multistage Runge-Kutta Method

The general system of ordinary differential equations (2.11) is solved by multistage Runge-Kutta method, see [21], [22], [23].

$$\begin{aligned} W_i^{(0)} &= W_i^n, \\ W_i^{(r)} &= W_i^{(0)} - \alpha_{r-1} \Delta t \text{Res}(W)_i^{(r-1)}, \\ W_i^{n+1} &= W_i^{(m)} \quad r = 1, \dots, m, \end{aligned} \quad (2.24)$$

where a stationary residual  $\text{Res}(W)_i$  is defined as follows:

$$\text{Res}(W)_i = \frac{1}{\mu_i} \sum_{l=1}^4 \left[ \tilde{F}_{il} \Delta y_{il} - \tilde{G}_{il} \Delta x_{il} \right], \quad (2.25)$$

where  $\mu_i$  is the volume of the finite volume cell,  $\Delta x_{il}$  and  $\Delta y_{il}$  represent lengths of the  $l$ -th edge between the finite cell  $D_i$  and the neighbouring finite cell  $D_l$  in  $x$  and  $y$  directions. Index  $l$  stands for indices 1, 2, 3 and 4 as is shown in the figures 2.3 and 2.4. In the figure 2.4 the definition of the lengths  $\Delta x_{il}$  and  $\Delta y_{il}$  is shown.

In this work the structured mesh is considered. Under this assumption the finite volume cells are quadrilateral in 2D case and hexahedrons in 3D case. Figure 2.3 shows ideal orthogonal form of the finite volume cell  $D_i$  with its four neighbouring finite volume cells. By red color the dual finite volume cells corresponding to the finite volume cell  $D_i$  are shown.

Numerical fluxes  $\tilde{F}_{il}^*$  and  $\tilde{G}_{il}^*$  are defined as follows:

$$\tilde{F}_{il}^* = \tilde{\mathbf{R}}_{\beta}^{-1} F^c|_{il}^* - \frac{1}{\text{Re}} F^v|_{il}^*, \quad \tilde{G}_{il}^* = \tilde{\mathbf{R}}_{\beta}^{-1} G^c|_{il}^* - \frac{1}{\text{Re}} G^v|_{il}^*, \quad (2.26)$$

where  $F^c|_{il}^*$  and  $G^c|_{il}^*$  are the inviscid numerical fluxes and  $F^v|_{il}^*$  and  $G^v|_{il}^*$  are the numerical approximations of the viscous fluxes given by (1.39) - (1.46). The symbol \* denotes corresponding time level at which the numerical fluxes are evaluated. The matrix  $\tilde{\mathbf{R}}_{\beta}$  is given by (2.18).

**Inviscid fluxes**

The inviscid numerical fluxes are computed as an arithmetic average of the inviscid numerical fluxes of two neighbouring finite volume cells

$$F^c|_{il}^* = F^c \left( \frac{W_i^* + W_l^*}{2} \right), \quad G^c|_{il}^* = G^c \left( \frac{W_i^* + W_l^*}{2} \right), \quad (2.27)$$

where  $F^c$ ,  $G^c$  are given by (1.38).

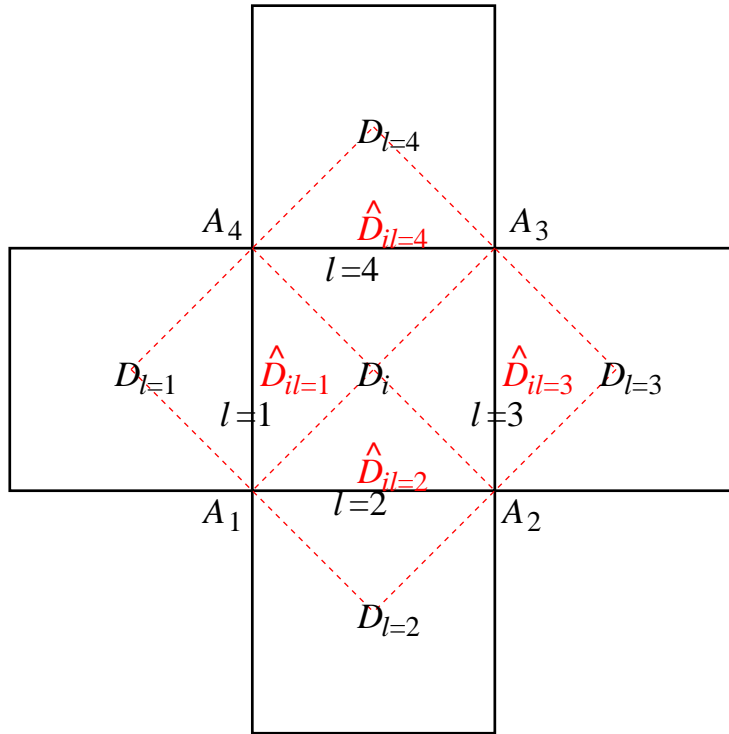
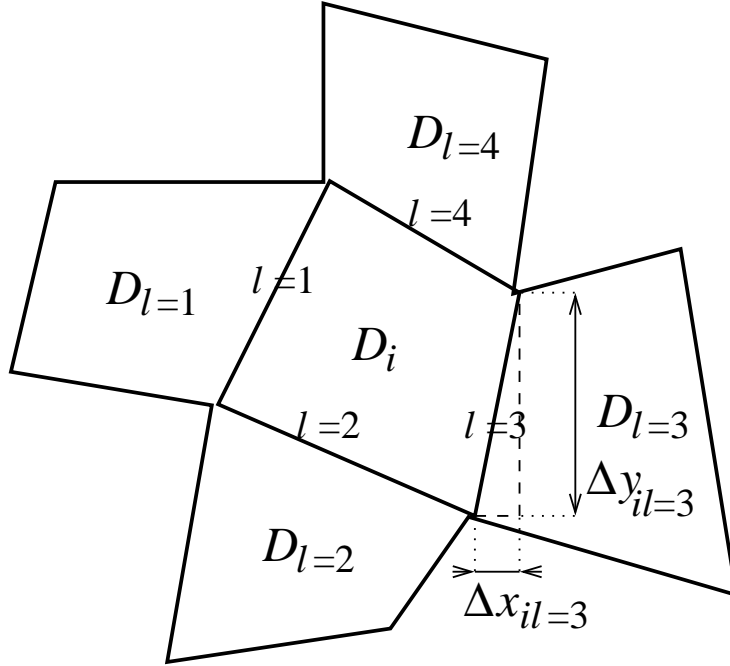


Figure 2.3: Finite volume cell and neighbouring finite cells (by red dashed lines)

**Viscous fluxes**

Now let us define the viscous part of the equation (2.26). In the definition of the viscous fluxes there are the partial derivatives of velocity vector components  $u, v$  with respect to

Figure 2.4: Finite volume cell with definition of  $\Delta x_{ij|k}$  and  $\Delta y_{ij|k}$ 

the spatial coordinates  $x, y$ . And these derivatives  $u_x, u_y, v_x$  and  $v_y$  need to be discretized. Denote us the approximations of  $u_x, u_y, v_x, v_y$  at the edge between cells  $D_i$  and  $D_l$  by  $u_x|_{il}^*, u_y|_{il}^*, v_x|_{il}^*, v_y|_{il}^*$ . Integrate velocity derivatives over a dual volume cell  $\hat{D}_{il}$  and using mean value theorem and Green's theorem, results in

$$u_x|_{il}^* = \frac{1}{\hat{\mu}_{il}} \int_{\hat{D}_{il}} u_x^* d\Omega = \frac{1}{\hat{\mu}_{il}} \oint_{\partial \hat{D}_{il}} u^* dy \approx \frac{1}{\hat{\mu}_{il}} \sum_{m=1}^4 u_{il|m}^* \Delta y_{il|m}. \quad (2.28)$$

Hence,

$$u_x|_{il}^* = \frac{1}{\hat{\mu}_{il}} \sum_{m=1}^4 u_{il|m}^* \Delta y_{il|m}, \quad (2.29)$$

where  $\hat{\mu}_{il}$  is the volume of the  $l$ -th dual cell (see figure 2.5). Similarly approximations of  $u_y, v_x$  and  $v_y$  are defined as follows

$$\begin{aligned} u_y|_{il}^* &= -\frac{1}{\hat{\mu}_{il}} \sum_{m=1}^4 u_{il|m}^* \Delta x_{il|m}, \\ v_x|_{il}^* &= \frac{1}{\hat{\mu}_{il}} \sum_{m=1}^4 v_{il|m}^* \Delta y_{il|m}, \\ v_y|_{il}^* &= -\frac{1}{\hat{\mu}_{il}} \sum_{m=1}^4 v_{il|m}^* \Delta x_{il|m} \end{aligned} \quad (2.30)$$

and

$$\begin{aligned}
 u_{il|m}^* &= \frac{1}{2}(u_{il|m}^* + u_{il|m+1}^*), & m = 1, 2, 3, 4, & & u_{il|m=5}^* &= u_{il|m=1}^*, \\
 v_{il|m}^* &= \frac{1}{2}(v_{il|m}^* + v_{il|m+1}^*), & m = 1, 2, 3, 4, & & v_{il|m=5}^* &= v_{il|m=1}^*, \\
 \Delta x_{il|m} &= x_{il|m+1} - x_{il|m}, & m = 1, 2, 3, 4, & & x_{il|m=5} &= x_{il|m=1}, \\
 \Delta y_{il|m} &= y_{il|m+1} - y_{il|m}, & m = 1, 2, 3, 4, & & y_{il|m=5} &= y_{il|m=1}.
 \end{aligned} \tag{2.31}$$

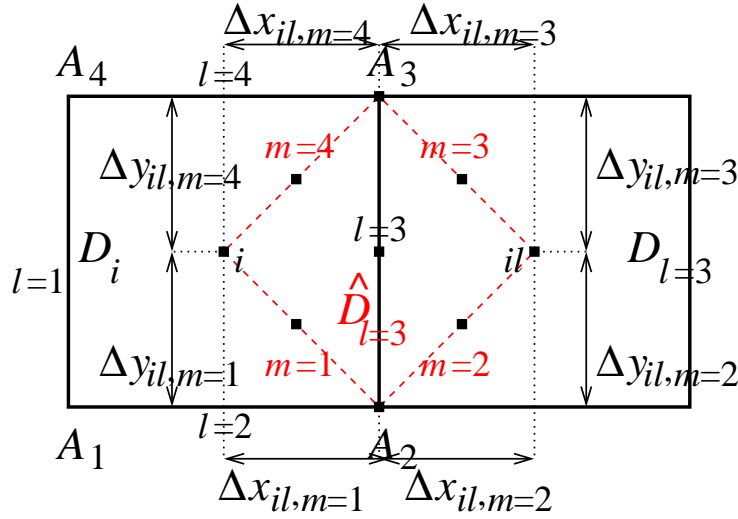


Figure 2.5: Dual volume cell -  $\hat{D}_{l=3}$

The values of conservative variables (vector  $W$ ) in the centre of the gravity of the finite volume cell are computed by multistage Runge-Kutta method. The values of the vector  $W$  in the centre of four edges of the finite cell are computed as the average of two values in the centres of the gravity of two neighbouring finite volume cells, i.e. computation of the inviscid numerical fluxes. The values in the grid nodes ( $A_1, A_2, A_3$  and  $A_4$ , and the coordinates of the grid node are  $A_k = [x_k, y_k]$ , where  $k = 1, 2, 3, 4$ ) (fig. 2.6) are computed as the average of four values in corresponding centres of gravity, e.g. for grid node  $A_1$ :

$$\begin{aligned}
 u_{A_1} &= \frac{1}{4}(u_i + u_1 + u_2 + u_3), \\
 v_{A_1} &= \frac{1}{4}(v_i + v_1 + v_2 + v_3).
 \end{aligned} \tag{2.32}$$

The values of the velocity components in the center of the edges of the dual volume cells are computed as the average of values in the nodes of the edges, e.g. the dual volume cell  $\hat{D}_{l=3}$  and the edge for  $m = 2$  see figure 2.5:

$$u_{l=3,m=2} = \frac{1}{2}(u_{A_2} + u_{i,l=3}), \quad v_{l=3,m=2} = \frac{1}{2}(v_{A_2} + v_{i,l=3}). \tag{2.33}$$

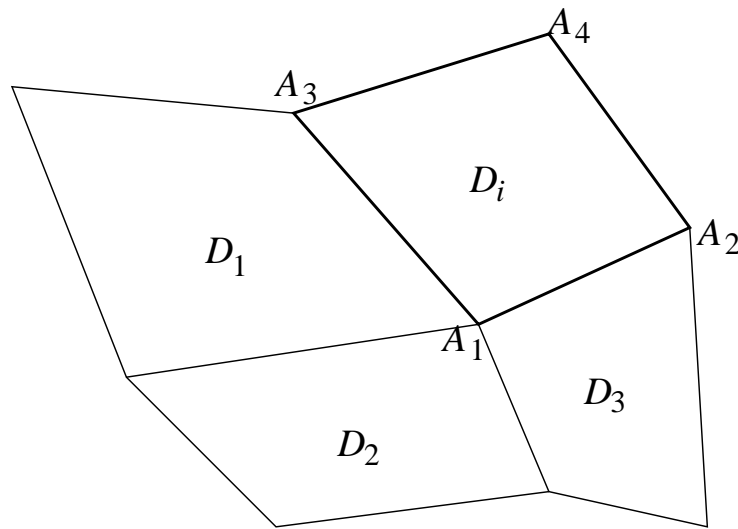


Figure 2.6: Structure of the finite volume cells for computation of velocity components in the grid node  $A_1$

In the figure 2.7, the structure of the finite volume cell and all corresponding dual volume cells are shown, with denoting of all edges in the finite volume cell and in the dual volume cells.

In this work, the three-stage Runge-Kutta method of second order accuracy in the time and in the space is used with three coefficients  $\alpha_1 = \alpha_2 = \frac{1}{2}$ ,  $\alpha_3 = 1$ .

## 2.4 Stability and Convergence

An investigation of the stability of the schemes can be obtained by the different ways. In this chapter a spectral analysis will be shown. In the case of the linear schemes it leads to necessary and sufficient condition of stability (see [24], [25]). In the case of nonlinear schemes only the sufficient condition of stability can be found.

The application of the spectral analysis will be shown in the case of the three-stage Runge-Kutta method for linear scalar equation

$$u_t + au_x = 0, \quad (2.34)$$

with the initial condition

$$u(x, 0) = u_0(x). \quad (2.35)$$

Let us rewrite three-stage Runge-Kutta method for this linear one dimensional scalar

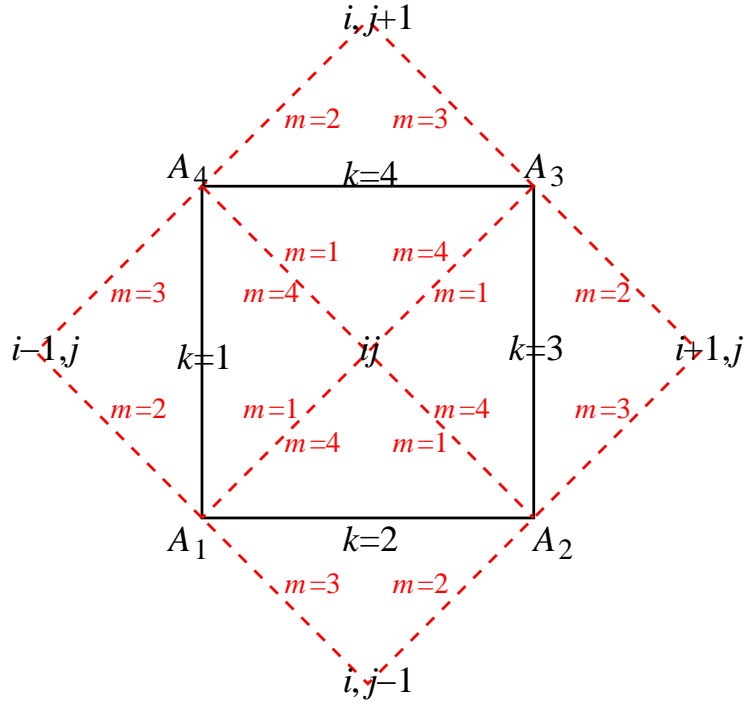


Figure 2.7: Structure of finite volume cell and dual volume cells, denoting of all edges of finite and dual cells

equation

$$\begin{aligned}
 u_i^{(0)} &= u_i^n, \\
 u_i^{(1)} &= u_i^{(0)} - \alpha_0 \frac{\sigma}{2} (u_{i+1}^{(0)} - u_{i-1}^{(0)}), \\
 u_i^{(2)} &= u_i^{(0)} - \alpha_1 \frac{\sigma}{2} (u_{i+1}^{(1)} - u_{i-1}^{(1)}), \\
 u_i^{(3)} &= u_i^{(0)} - \alpha_2 \frac{\sigma}{2} (u_{i+1}^{(2)} - u_{i-1}^{(2)}), \\
 u_i^{n+1} &= u_i^{(3)},
 \end{aligned} \tag{2.36}$$

where  $\sigma = \frac{\alpha \Delta t}{\Delta x}$ . After substituting it leads

$$\begin{aligned}
 u_i^{n+1} &= u_i^n - \alpha_2 \frac{\sigma}{2} (u_{i+1}^n - u_{i-1}^n) + \alpha_1 \alpha_2 \left(\frac{\sigma}{2}\right)^2 (u_{i+2}^n - 2u_i^n + u_{i-2}^n) \\
 &\quad - \alpha_0 \alpha_1 \alpha_2 \left(\frac{\sigma}{2}\right)^3 (u_{i+3}^n - 3u_{i+1}^n + 3u_{i-1}^n - u_{i-3}^n).
 \end{aligned} \tag{2.37}$$

It is obvious that from the reason of the approximation (of the consistency) the constant



$\alpha_2$  must be equal to 1. Therefore

$$u_i^{n+1} = u_i^n - \frac{\sigma}{2} (u_{i+1}^n - u_{i-1}^n) + \alpha_1 \left(\frac{\sigma}{2}\right)^2 (u_{i+2}^n - 2u_i^n + u_{i-2}^n) - \alpha_0 \alpha_1 \left(\frac{\sigma}{2}\right)^3 (u_{i+3}^n - 3u_{i+1}^n + 3u_{i-1}^n - u_{i-3}^n). \quad (2.38)$$

In this equation it can be shown that this scheme contains the convective term, an artificial dissipation with the coefficient  $\alpha_1$  and the term of dispersion with the coefficient  $\alpha_1 \alpha_0$  which is the approximation of the third derivative  $u_{xxx}$ .

If  $\alpha_1 = \frac{1}{2}$  then the scheme is of the second order of accuracy in the time. It follows from Taylor serie or from the comparison with Lax-Wendroff scheme.

Let us consider the scheme of Lax-Wendroff type. The principle of the schemes of Lax-Wendroff type is to expand the solution to Taylor serie in the time and to replace the time derivatives by the space derivatives. Let us consider the sufficient smooth solution of Cauchy problem eq. (2.34) and (2.35). Taylor serie in the point  $x_i, t_n$  gives

$$u(x_i, t_{n+1}) = u(x_i, t_n) + \Delta t u_t(x_i, t_n) + \frac{1}{2} \Delta t^2 u_{tt}(x_i, t_n) + \frac{1}{6} \Delta t^3 u_{ttt}(x_i, t_n) + O(\Delta t^4). \quad (2.39)$$

From the linear equation can be expressed

$$u_t = -a u_x \quad (2.40)$$

and therefore second and third derivatives in the time  $u_{tt}$  and  $u_{ttt}$  can be expressed as follows:

$$\begin{aligned} u_{tt} &= -a u_{xt} = -a u_{tx} = a^2 u_{xx}, \\ u_{ttt} &= a^2 u_{xxt} = a^2 u_{txx} = -a^3 u_{xxx}. \end{aligned} \quad (2.41)$$

Let us substitute the time derivatives to Taylor serie and therefore it results in

$$\begin{aligned} u(x_i, t_{n+1}) &= u(x_i, t_n) - \Delta t a u_x(x_i, t_n) + \frac{1}{2} a^2 \Delta t^2 u_{xx}(x_i, t_n) \\ &\quad - \frac{1}{6} a^3 \Delta t^3 u_{xxx}(x_i, t_n) + O(\Delta t^4). \end{aligned} \quad (2.42)$$

The space derivatives will be expressed by the centered differences of the second order of accuracy

$$\begin{aligned} u_x &= \frac{1}{2\Delta x} (u_{i+1} - u_{i-1}) + O(\Delta x^2), \\ u_{xx} &= \frac{1}{4\Delta x^2} (u_{i+2} - 2u_i + u_{i-2}) + O(\Delta x^2), \\ u_{xxx} &= \frac{1}{9\Delta x^3} (u_{i+3} - 3u_{i-1} + 3u_{i-1} - u_{i-3}) + O(\Delta x^2). \end{aligned} \quad (2.43)$$

Substituting these expressions to Taylor serie gives

$$u_i^{n+1} = u_i^n - \frac{\sigma}{2} (u_{i+1}^n - u_{i-1}^n) + \frac{\sigma^2}{8} (u_{i+2}^n - u_i^n + u_{i-2}^n) - \frac{\sigma^3}{54} (u_{i+3}^n - 3u_{i+1}^n + 3u_{i-1}^n - u_{i-3}^n). \quad (2.44)$$

Next three-stage Runge-Kutta scheme (2.38) will be compared with this last scheme of Lax-Wendroff type (2.44). From this comparing coefficient  $\alpha_1$  can be chosen as  $\frac{1}{2}$  then the scheme of second order of accuracy in the time will be obtained.

The stability of three-stage Runge-Kutta by the spectral analysis will be investigate. Let us set

$$u_i^n = \lambda^n e^{\mathcal{I}k\alpha}, \quad (2.45)$$

where symbol ( $\mathcal{I} = \sqrt{-1}$ ) is the complex unit,  $\alpha \in (0, 2\pi)$  is a frequency. Let us substitute (2.45) to the eq. (2.38) therefore

$$\begin{aligned} \lambda^{n+1} e^{\mathcal{I}i\alpha} &= \lambda^n e^{\mathcal{I}i\alpha} - \frac{\sigma}{2} (\lambda^n e^{\mathcal{I}(i+1)\alpha} - \lambda^n e^{\mathcal{I}(i-1)\alpha}) \\ &\quad + \alpha_1 \left(\frac{\sigma}{2}\right)^2 (\lambda^n e^{\mathcal{I}(i+2)\alpha} - 2\lambda^n e^{\mathcal{I}i\alpha} + \lambda^n e^{\mathcal{I}(i-2)\alpha}) \\ &\quad - \alpha_0 \alpha_1 \left(\frac{\sigma}{2}\right)^3 (\lambda^n e^{\mathcal{I}(i+3)\alpha} - 3\lambda^n e^{\mathcal{I}(i+1)\alpha} + 3\lambda^n e^{\mathcal{I}(i-1)\alpha} - \lambda^n e^{\mathcal{I}(i-3)\alpha}). \end{aligned} \quad (2.46)$$

Dividing (2.46) by  $\lambda^n e^{\mathcal{I}i\alpha}$  and using two expressions

$$\cos \alpha = \frac{e^{\mathcal{I}\alpha} + e^{-\mathcal{I}\alpha}}{2}, \quad \sin \alpha = \frac{e^{\mathcal{I}\alpha} - e^{-\mathcal{I}\alpha}}{2\mathcal{I}}, \quad (2.47)$$

it results in

$$\begin{aligned} \lambda &= 1 - \sigma \mathcal{I} \sin \alpha - 2\alpha_1 \left(\frac{\sigma}{2}\right)^2 (1 - \cos 2\alpha) - \alpha_0 \alpha_1 \left(\frac{\sigma}{2}\right)^3 (2\mathcal{I} \sin 3\alpha - 6\mathcal{I} \sin \alpha) \\ &= 1 - \sigma \mathcal{I} \sin \alpha - 4\alpha_1 \left(\frac{\sigma}{2}\right)^2 \sin^2 \alpha + 8\alpha_0 \alpha_1 \left(\frac{\sigma}{2}\right)^3 \mathcal{I} \sin^3 \alpha \\ &= 1 - 4\alpha_1 \left(\frac{\sigma}{2}\right)^2 \sin^2 \alpha - \mathcal{I} \sigma \sin \alpha (1 - \sigma^2 \alpha_0 \alpha_1 \sin^2 \alpha). \end{aligned} \quad (2.48)$$

From the condition  $|\lambda| \leq 1$  can be obtained

$$2\alpha_1 - 1 \geq \sigma^2 \sin^2 \alpha (\alpha_1^2 - 2\alpha_0 \alpha_1 + \alpha_0^2 \alpha_1^2 \sigma^2 \sin^2 \alpha). \quad (2.49)$$

If the coefficient  $\alpha_1$  is chosen as  $\frac{1}{2}$  the scheme is of the second order of accuracy in the time. Hence

$$0 \geq \sigma^2 \sin^2 \alpha \left(\frac{1}{4} - \alpha_0 + \frac{1}{4} \alpha_0^2 \sigma^2 \sin^2 \alpha\right). \quad (2.50)$$

The maximal value of sinus function will be taken then

$$0 \geq \frac{1}{4} - \alpha_0 + \frac{1}{4} \alpha_0^2 \sigma^2. \quad (2.51)$$

If the coefficient  $\alpha_0$  is equal to  $\frac{1}{2}$  then  $|\sigma| \leq 2$  and from the definition of the value  $\sigma$  it follows

$$\Delta t \leq 2 \frac{\Delta x}{|a|} \quad (2.52)$$

and the result of this analysis is that three-stage Runge-Kutta method is of second order of accuracy in the time and of second order of accuracy in the space.

By the analogous way can be proofed by the same analysis that the condition of stability for the equation with two space variables

$$u_t + au_x + bu_y = 0, \quad (2.53)$$

is defined by the expression

$$\Delta t \leq \frac{2}{\frac{|a|}{\Delta x} + \frac{|b|}{\Delta y}}. \quad (2.54)$$

For the equation with the convection and the dissipation

$$u_t + au_x = \nu u_{xx}, \quad (2.55)$$

the stability condition has the form

$$\Delta t \leq \frac{2}{\frac{|a|}{\Delta x} + \frac{2\nu}{\Delta x^2}}. \quad (2.56)$$

Let us consider the system of one dimensional Euler equation

$$W_t + F_x^c = 0, \quad (2.57)$$

where  $W$  is the vector of the unknown variables and  $F(W)$  is the numerical flux

$$W = \begin{pmatrix} p \\ u \end{pmatrix}, \quad F^c = \begin{pmatrix} u \\ u^2 + p \end{pmatrix}. \quad (2.58)$$

For the spectral analysis the kvasilinear form of the system will be used

$$W_t + A(W)W_x = 0, \quad (2.59)$$

where  $A(W) = \partial F^c / \partial W$ . It can be proofed that the eigenvalues of the matrix  $A$  (matrix 2x2) are  $\frac{u}{2} \pm \sqrt{\frac{u^2}{4} + 1}$ . It's possible to transformate the matrix  $A$  to the diagonal form  $A = R\Lambda R^{-1}$ , where  $\Lambda = \text{diag}(\lambda_1, \lambda_2)$ . Hence,

$$W_t + R\Lambda R^{-1}W_x = 0. \quad (2.60)$$

This is the system of the scalar equations and therefore this system can be numerically solve by the applying the numerical scheme on the every equation.

In this work three-stage Runge-Kutta scheme is used. For the system of Euler equations (2.57) with (2.58) it has the form

$$\begin{aligned} W_i^{(0)} &= W_i^n, \\ W_i^{(r)} &= W_i^{(0)} - \alpha_{r-1} \frac{\Delta t}{2\Delta x} \left[ F(W_{i+1}^{(r-1)}) - F(W_{i-1}^{(r-1)}) \right], \\ W_i^{n+1} &= W_i^{(m)} \quad r = 1, \dots, 3. \end{aligned} \quad (2.61)$$

The stability condition of this system will be investigated as for scalar case. Therefore let us rewrite the eq. (2.48) to the matrix form ( $\sigma = \frac{\Delta t}{\Delta x}$ )

$$\begin{aligned} G(\alpha, \sigma) &= I - A\mathcal{I}\sigma \sin \alpha - \frac{1}{2}A^2\sigma^2 \sin^2 \alpha + \frac{1}{4}A^3\mathcal{I}\sigma^3 \sin^3 \alpha = \\ &= R \left[ I - \Lambda\mathcal{I}\sigma \sin \alpha - \frac{1}{2}\Lambda^2\sigma^2 \sin^2 \alpha + \frac{1}{4}\Lambda^3\mathcal{I}\sigma^3 \sin^3 \alpha \right] R^{-1}, \end{aligned} \quad (2.62)$$

where matrix  $G$  is the matrix 2x2. The eigenvalues of the matrix  $G$  are

$$\begin{aligned} \beta_1 &= 1 - \lambda_1\mathcal{I} \sin \alpha - \frac{1}{2}\lambda_1^2 \sin^2 \alpha + \frac{1}{4}\lambda_1^3\mathcal{I} \sin^3 \alpha, \\ \beta_2 &= 1 - \lambda_2\mathcal{I} \sin \alpha - \frac{1}{2}\lambda_2^2 \sin^2 \alpha + \frac{1}{4}\lambda_2^3\mathcal{I} \sin^3 \alpha, \end{aligned} \quad (2.63)$$

where  $\lambda_1, \lambda_2$  are the eigenvalues of the system of Euler equations. Therefore the spectral radius of the matrix  $G$  is

$$\rho_G^2 = I + \rho_A^2\sigma^2 \sin^2 \alpha + \frac{1}{4}\rho_A^4\sigma^4 \sin^4 \alpha + \frac{1}{16}\rho_A^6\sigma^6 \sin^6 \alpha - \rho_A^2\sigma^2 \sin^2 \alpha - \frac{1}{2}\rho_A^4\sigma^4 \sin^4 \alpha. \quad (2.64)$$

The scheme is stable if the norm  $\|G(\alpha, \sigma)\| \leq 1$ . The spectral norm will be used and therefore the stability condition for the system of Euler equations (2.57) with (2.58) will be obtained in the form

$$\sigma|\rho_A| \leq 2, \quad (2.65)$$

therefore the similar condition as for the case of the scalar equation

$$\Delta t \leq \frac{\text{CFL}}{\frac{\rho_A}{\Delta x}}. \quad (2.66)$$

As for the scalar equation three-stage Runge-Kutta scheme with the coefficients  $\alpha_0 = \frac{1}{2}$ ,  $\alpha_1 = \frac{1}{2}$ ,  $\alpha_2 = 1$  is of second order of accuracy in the time and in the space. And this method is stable for  $\text{CFL} = 2$ .

If the system of Navier-Stokes equations in one dimensional is considered the condition of stability is obtained in the form

$$\Delta t \leq \frac{\text{CFL}}{\frac{\rho_A}{\Delta x} + \frac{2}{\text{Re}} \frac{1}{\Delta x^2}}. \quad (2.67)$$

The stability conditions can be expanded into two and three dimensional case for the system of Navier-Stokes equations (1.23) - (1.26) for 2D case and (1.29) - (1.31) for 3D case resp. Hence, the time step for the linearized system of Navier-Stokes equations in 2D case is expressed in the form

$$\Delta t \leq \frac{\text{CFL}}{\frac{\rho_A}{\Delta x} + \frac{\rho_B}{\Delta y} + \frac{2}{\text{Re}} \left( \frac{1}{\Delta x^2} + \frac{1}{\Delta y^2} \right)} \quad (2.68)$$

and for 3D case resp.

$$\Delta t \leq \frac{\text{CFL}}{\frac{\rho_A}{\Delta x} + \frac{\rho_B}{\Delta y} + \frac{\rho_C}{\Delta z} + \frac{2}{\text{Re}} \left( \frac{1}{\Delta x^2} + \frac{1}{\Delta y^2} + \frac{1}{\Delta z^2} \right)}, \quad (2.69)$$

where  $\rho_A$ ,  $\rho_B$  and  $\rho_C$  resp. are the spectral radii of Jacobi matrices  $A = \partial F^c / \partial(\tilde{\mathbf{R}}_\beta W)$ ,  $B = \partial G^c / \partial(\tilde{\mathbf{R}}_\beta W)$  or  $C = \partial H^c / \partial(\tilde{\mathbf{R}}_\beta W)$  resp. in the space directions  $x, y$  or  $z$  resp. The symbol CFL is Courant-Friedrichs-Levy number and for three stage Runge-Kutta scheme with used coefficients is equal to 2.

### 2.4.1 Time Step

The system of Navier-Stokes equations for the generalized Newtonian fluids in two dimensional case (1.37) - (1.46) and three dimensional case (1.47) - (1.54) resp. is considered in this work. The multistage Runge-Kutta scheme is used as the explicit scheme. This scheme is conditionally stable, it means that the time step is limited.

In the previous section the time step was evaluated for the system of Navier-Stokes equations for two and three dimensional Newtonian fluids flow. These two expressions are for the uniform orthogonal mesh used for 2D or 3D cases. (And also these expressions valid for the method of the finite differences.) These time evaluations for the finite volume method and for the non-uniform non-orthogonal mesh can be expanded.

Therefore for two dimensional case of the viscous generalized Newtonian fluids flow the time step is

$$\Delta t = \min_{i,l} \frac{\text{CFL } \mu_i}{\rho_A \Delta y_l + \rho_B \Delta x_l + \frac{2\sqrt{\text{tr}\mathbf{D}^2}^r}{\text{Re}} \left( \frac{(\Delta x_l)^2 + (\Delta y_l)^2}{\mu_i} \right)}, \quad (2.70)$$

index  $i$  represents the position of the finite volume cell, index  $l$  symbolizes the index of one of the edges corresponds to the finite volume cell  $D_i$ . The volume of this cell is denoted by the symbol  $\mu_i$ . Re is Reynolds number defined as  $\text{Re} = \frac{U^* L^*}{\nu^*}$  and CFL is Courant-Friedrichs-Levy number and for three-stage Runge-Kutta scheme is equal to 2.  $\Delta x_l$  and  $\Delta y_l$  are the lengths of the  $l$ th-edge of the cell  $D_i$  in the  $x$  and  $y$  direction. The term  $\sqrt{\text{tr}\mathbf{D}^2}^r$  is non-Newtonian viscosity, eq. (1.42).

In 3D case the time step is evaluated by the expression

$$\Delta t = \min_{i,l} \frac{\text{CFL } \mu_i}{\rho_A \Delta y_l z_l + \rho_B \Delta x_l z_l + \rho_C \Delta x_l y_l + \frac{2\sqrt{\text{tr}\mathbf{D}^2}^r}{\text{Re}} \left( \frac{(\Delta y_l z_l)^2 + (\Delta x_l z_l)^2 + (\Delta x_l y_l)^2}{\mu_i} \right)}, \quad (2.71)$$

index  $i$  denotes the position of the finite volume cell in 3D domain. Index  $l$  presents the index of the wall between two neighbouring cells for the finite volume cell  $D_i$  its volume is denoted by the symbol  $\mu_i$ . Reynolds number for three dimensional case is defined by the formula  $Re = \frac{U^*4S}{\nu^*O}$ , the CFL number is the same as for 2D case. The term  $\sqrt{\text{tr}\mathbf{D}^2}$  is non-Newtonian viscosity, eq. (1.42).

$\Delta xy_l$  is the volume of the  $l$ -edge in the  $xy$  plain,  $\Delta xz_l$  is the volume of the  $l$ -edge in the  $xz$  plain,  $\Delta yz_l$  is the volume of the  $l$ -edge in the  $yz$  plain.

### 2.4.2 Convergence

An iteration process is controled by the change of the residual. The global behaviour of the solution during the computational process is followed by the  $L^2$  norm of the steady residual. It is given by

$$\| \text{Res}(W^n) \|_{L^2} = \sqrt{\frac{1}{MN} \sum_i \left( \frac{W_i^{n+1} - W_i^n}{\Delta t} \right)^2} \quad (2.72)$$

All the operations carried out with the vector of conservative variables  $W$  are considered componentwise. The computation is performed until the value of the  $L^2$ -norm of residual satisfy  $\text{Res}(W_i^n) \leq \epsilon$  with  $\epsilon$  small enough ( $MN$  denotes the number of grid cells in the computational domain)

The decadic logarithm of  $\| \text{Res}(W^n) \|_{L^2}$  is plotted in graphs presenting convergence history of simulations.

## 2.5 Unsteady Computation

This section deals with the numerical solution of laminar incompressible viscous flow through the branching channel. Two approaches are used for the numerical solution of unsteady governing Navier-Stokes equations. First, the artificial compressibility method is applied. Second the dual-time stepping method are used in this section.

### 2.5.1 Artificial Compressibility Method

The principe of this method is to complete the continuity equation by the term  $\frac{1}{\beta^2} p_t$  as for steady solution. The systems of equations (1.37) - (1.46) for generalized Newtonian fluid in two dimensional case represent the mathematical model of unsteady flows. The definition of the matrix  $\tilde{\mathbf{R}}_\beta$  for 2D case were defined in (2.18). The artificial compressibility coefficient  $\beta$  is chosen as big positive value, ideally  $\beta \rightarrow \infty$ .

The boundary conditions are changed to the unsteady boundary conditions (see Fig. 2.8). In the inlet and in the wall the same boundary conditions are used as for steady case.

In the outlet in one of the branch the constant pressure value is set. In the second branch the pressure value is prescribed by the periodic function

$$p_{01} = \frac{1}{4} \left( 1 + \frac{1}{2} \sin(\omega t) \right), \quad (2.73)$$

where  $\omega$  is the angular velocity and it's defined as  $\omega = 2\pi f$ , where  $f$  is the frequency.

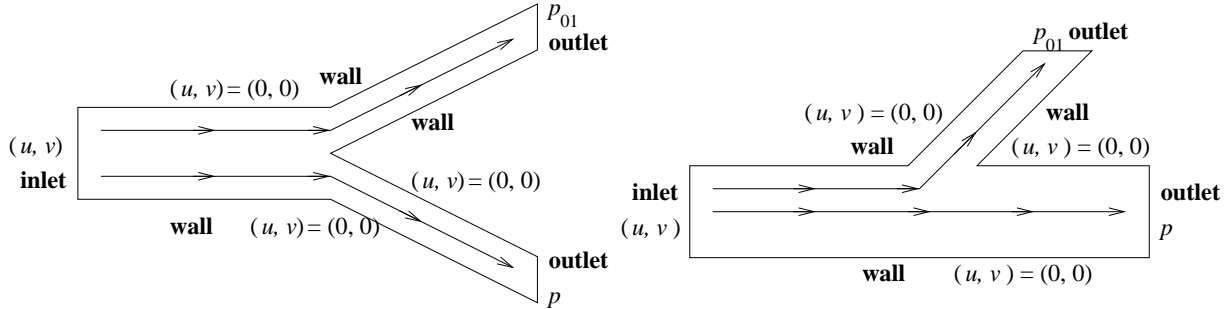


Figure 2.8: Consider domain and unsteady boundary conditions

## 2.5.2 Dual Time Stepping Method

Other possibility to obtain unsteady solution is to introduce artificial time  $\tau$  and to apply the artificial compressibility method in the artificial time. The dual time stepping approach is known to be the pseudo-compressibility method to the calculation of unsteady incompressible flows (see [26], [8], [27], [28]). The system of Navier-Stokes equations (1.37) - (1.46) is used as the mathematical model for the dual time stepping method for generalized Newtonian fluids. These systems can be extended to unsteady flows by adding artificial time derivatives  $\partial W / \partial \tau$  to all equations. Applying the artificial compressibility approach only to the pseudo-time  $\tau$ , then the physical time behaviour is not influenced as long as the solution converges in the pseudo-time to a “steady state” for each physical time  $t$ . The new system of Navier-Stokes equations now reads

$$\tilde{\mathbf{R}}_{\beta} W_{\tau} + \tilde{\mathbf{R}} W_t + F_x^c + G_y^c = \frac{1}{\text{Re}} (F_x^v + G_y^v), \quad (2.74)$$

with

$$\tilde{\mathbf{R}} = \begin{pmatrix} 0 & 0 & 0 \\ 0 & 1 & 0 \\ 0 & 0 & 1 \end{pmatrix}, \quad \tilde{\mathbf{R}}_{\beta} = \begin{pmatrix} \frac{1}{\beta^2} & 0 & 0 \\ 0 & 1 & 0 \\ 0 & 0 & 1 \end{pmatrix} \quad (2.75)$$

and  $\beta \in \mathcal{R}^+$  is a constant. The vector  $W$  and the inviscid fluxes  $F^c, G^c$  are given by (1.38) and the viscous fluxes  $F^v, G^v$  by (1.39) - (1.46) for generalized Newtonian fluids. If the term  $W_{\tau}$  converges to zero ( $\partial p / \partial \tau, \partial u / \partial \tau, \partial v / \partial \tau \rightarrow 0$ ), the original system of the equations (1.37) is solved. Setting  $\tilde{\mathbf{R}} = \mathbf{0}$  provides a system of differential equations appropriate for solving steady state problems.

If derivatives with respect to the real time  $t$  are discretized using a three-point backward formula, it results in the explicit scheme

$$\tilde{\mathbf{R}}_\beta \frac{W_i^{\nu+1} - W_i^\nu}{\Delta\tau} + \tilde{\mathbf{R}} \frac{3W_i^\nu - 4W_i^n + W_i^{n-1}}{2\Delta t} + \text{Res}(W)_i^\nu = 0, \quad (2.76)$$

where  $\Delta t = t^{n+1} - t^n$  and  $\text{Res}(W)_i$  is the steady residual where the steady residual

$$\text{Res}(W)_i = \left( F_i^c - \frac{1}{\text{Re}} F_i^v \right)_x + \left( G_i^c - \frac{1}{\text{Re}} G_i^v \right)_y. \quad (2.77)$$

This backward differencing scheme is strongly stable and dissipative. We can express  $W_i^{\nu+1}$  from the eq. (2.76)

$$\tilde{\mathbf{R}}_\beta \frac{W_i^{\nu+1} - W_i^\nu}{\Delta\tau} = -\tilde{\mathbf{R}} \frac{3W_i^\nu - 4W_i^n + W_i^{n-1}}{2\Delta t} - \text{Res}(W)_i^\nu \equiv -\overline{\text{Res}}(W)_i^\nu. \quad (2.78)$$

This method is of the second order of accuracy in the time.  $\overline{\text{Res}}(W)_i^\nu$  is the unsteady residual. The superscript  $n$  denotes the real time and the index  $\nu$  is associated with the pseudo-time.

The integration in pseudo-time can be carried out by explicit multistage Runge-Kutta scheme. If the index  $\nu$  is the index associated with pseudo-time, this scheme can be written in the form

$$\begin{aligned} W_i^{(0)} &= W_i^\nu, \\ W_i^{(r)} &= W_i^{(0)} - \alpha_{r-1} \Delta\tau \text{Res}(W)_i^{(r-1)}, \\ W_i^{\nu+1} &= W_i^{(m)} \quad r = 1, \dots, m, \end{aligned} \quad (2.79)$$

here the coefficients are chosen as for steady case:  $\alpha_0 = \alpha_1 = \frac{1}{2}$  and  $\alpha_2 = 1$ . The real-time step  $\Delta t$  is chosen to ensure the adequate time accuracy.

### 2.5.3 Time Step and Convergence

The dual-time step  $\Delta\tau$  is estimated using formula 2.70. Furthermore, to prevent stability problems when the dual-time step  $\Delta\tau$  is large compared to the real one  $\Delta t$ , the dual-time step is limited so that  $\Delta\tau \leq 2\Delta t/3$ .

We assume that the numerical solution at the real-time  $t^n$  is known. We set  $W_i^{\nu=0} = W_i^n$  then the iterations using Runge-Kutta scheme (2.79) are performed until the condition

$$\|\text{Res}(W)^\nu\|_{L^2} = \sqrt{\frac{1}{MN} \sum_i \left( \frac{W_i^{\nu+1} - W_i^\nu}{\Delta\tau} \right)^2} \leq \epsilon \quad (2.80)$$

is satisfied for the small positive constant  $\epsilon$ .

When the condition (2.80) is satisfied for particular dual time  $\nu$  then  $W_i^{\nu+1} = W_i^{\nu+1}$ . Then we shift the index  $\nu$  one up, i.e.  $n = n + 1$  then the new iteration process at the new time level  $t^{n+1} = t^n + \Delta t$  with new values  $W_i^{n-1} = W_i^n$ ,  $W_i^n = W_i^{n+1}$  can be started.



# Chapter 3

## Numerical Results

In all case upstream velocity is  $\frac{U}{U_\infty} = \frac{U_\infty}{U_\infty} = 1$  there isolines of velocity in the field are compared to  $q = \sqrt{u_\infty^2 + v_\infty^2} = 1$ , similarly for pressure, where  $p = \frac{\tilde{p}}{\rho}|_\infty = 0.5$ . One can also see very good convergence in the logarithmic norm, there all steady computations are really steady.

Comparisons are considered in the following form:

a) 2D Newtonian fluids flow with increasing Reynolds number (Re) (increasing upstream physical velocity  $U_\infty$ ) - steady solutions in the same geometry.

b) 2D non-Newtonian fluids flow with increasing Re - steady solutions in the same geometry.

c) 2D comparison of the flows in the same geometry, same Re but for Newtonian and non-Newtonian fluids flow.

d) 3D similar comparison.

Then one can see smaller or higher changes flow field characteristics (pressure, velocity, separation region, ...)

### 3.1 Two Dimensional Steady Solutions of Newtonian Fluids

In this section, two dimensional numerical results of incompressible laminar viscous flows for Newtonian fluids are presented and compared. Numerical simulations were performed for two dimensional branching channels with one entrance and two exit parts. The steady boundary conditions are used for the steady state solutions.

The numerical results are shown for several shapes of the domain. The different values of Reynolds number were used for comparing pressure and velocity isolines for used domain.

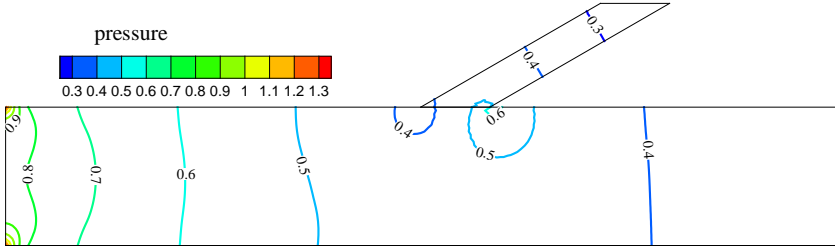
Several shapes of the domain were tested. First shape of the domain is the branching channel in the shape T with the angle 30 degrees. Second domain is the channel with the angle 90 degrees. Third used domain is symmetric branching channel (shape Y) with the angle 20 degrees. Last domain is the nonsymmetric channel with two angles 20 and 30 degrees.

For all shapes of the domain pressure and velocity isolines are compared for the different values of Reynolds number. Three values of Reynolds number are used:  $Re = 200$ ,  $Re = 400$  and  $Re = 600$ .

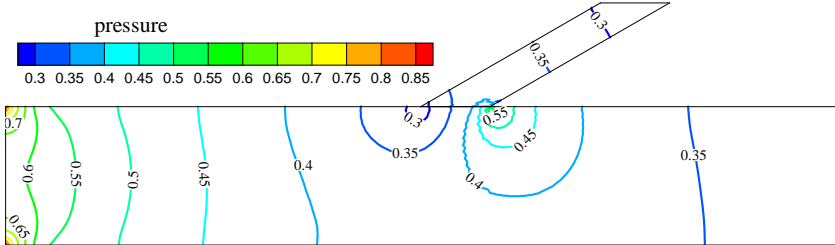
The figures are organized as follows: first, series of three figures in the form of the pressure isolines are presented (figures 3.1, 3.6, 3.11 and 3.15), next series of the figures in the form of the velocity isolines are shown (figures 3.2, 3.7, 3.12 and 3.16), third series of the figures show the graphs of the convergence history of the numerical simulations (figures 3.3, 3.8, 3.13 and 3.17). Last series of the figures shows the nondimensional velocity profile of velocity component  $u$  as the function of  $y$  (for T geometry also the velocity profile of  $v$  velocity component as the function of  $x$ ) (figures 3.5, 3.10, 3.14 and 3.18).

In the figures 3.4 and 3.9 the details of the separation regions in the vector form are presented. The considered domain is the branching channel in the T geometry with the angle 30 and 90 degrees.

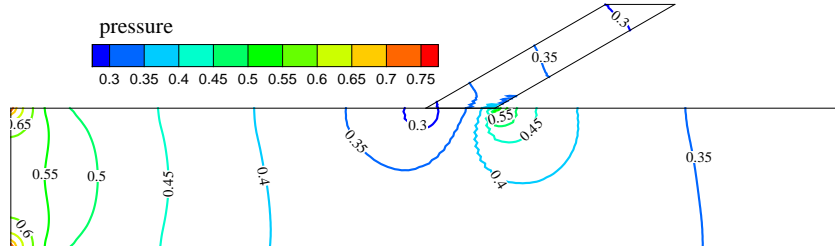
In this section, numerical results for higher Reynolds number ( $Re = 400$ ,  $Re = 600$ ) are nearly identical while numerical result for small Reynolds number ( $Re = 200$ ) differs from these results. It is obvious from all series of the figures. For  $Re = 200$  the maximal values of the pressure are higher (almost 1.5 times) while for  $Re = 400$  and for  $Re = 600$  these maximal pressure values are the same. Also from the history of the convergence and from the nondimensional velocity profiles it can be seen the differences between small Reynolds number ( $Re = 200$ ) and higher values ( $Re = 400$  and  $Re = 600$ ).



(a)  $Re = 200$

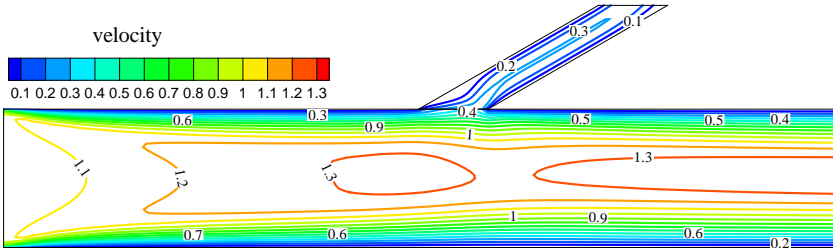


(b)  $Re = 400$

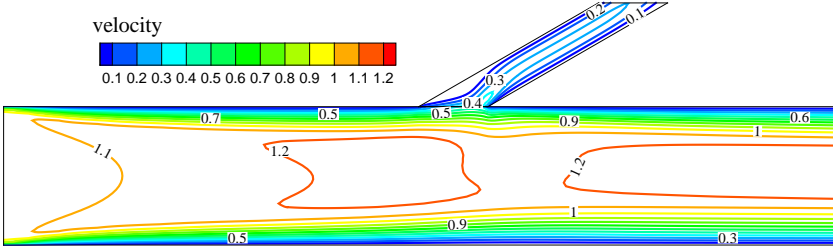


(c)  $Re = 600$

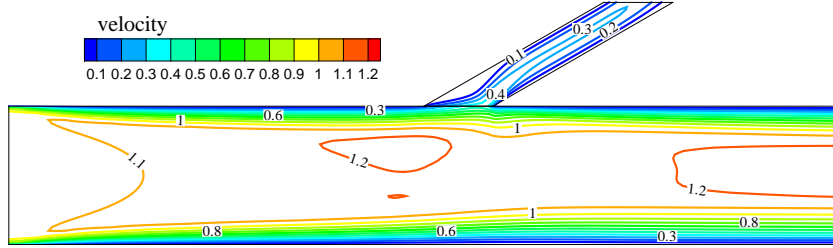
Figure 3.1: Pressure isolines of Newtonian fluids flow in 2D branching channel with the angle 30 degrees - a)  $Re = 200$  - b)  $Re = 400$  - c)  $Re = 600$



(a)  $Re = 200$



(b)  $Re = 400$



(c)  $Re = 600$

Figure 3.2: Velocity isolines of Newtonian fluids flow in 2D branching channel with the angle 30 degrees - a)  $Re = 200$  - b)  $Re = 400$  - c)  $Re = 600$

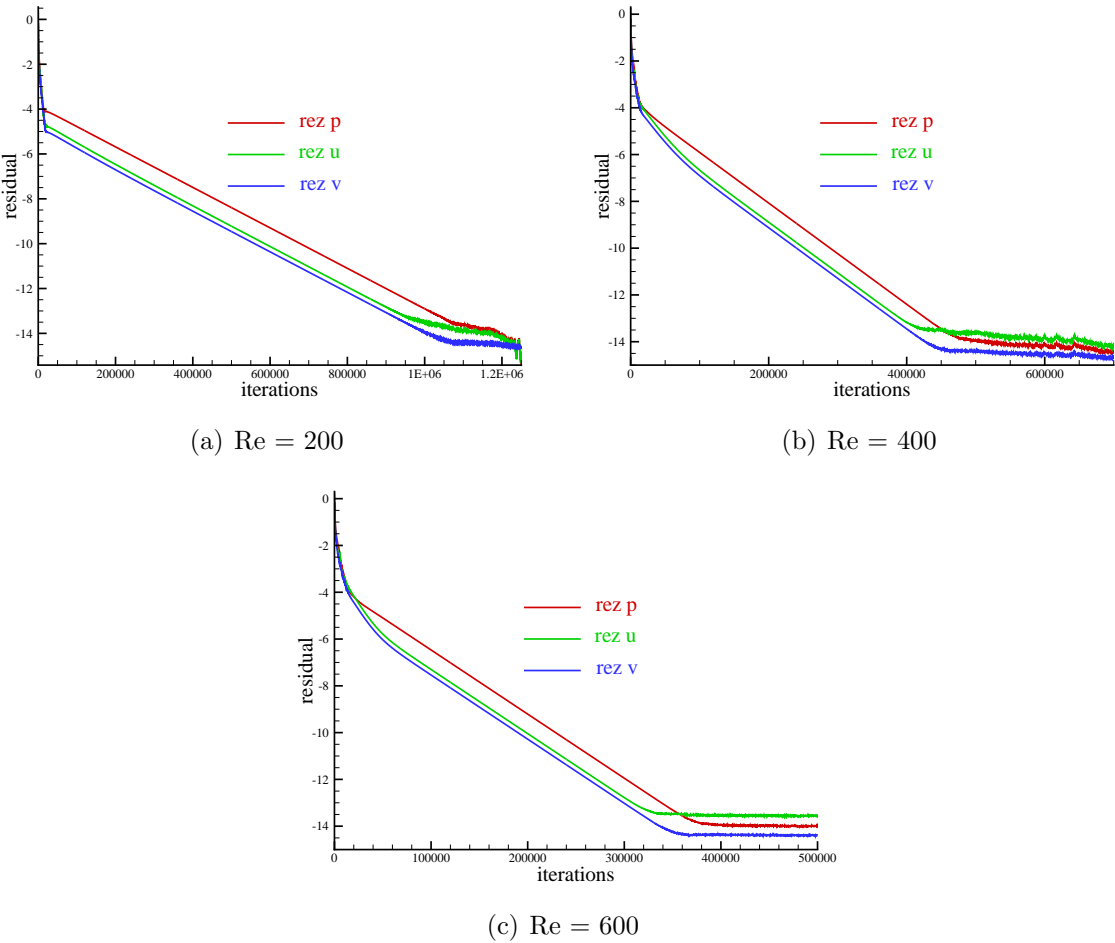


Figure 3.3: The convergence history of Newtonian fluids flow in 2D branching channel with the angle 30 degrees - a)  $Re = 200$  - b)  $Re = 400$  - c)  $Re = 600$

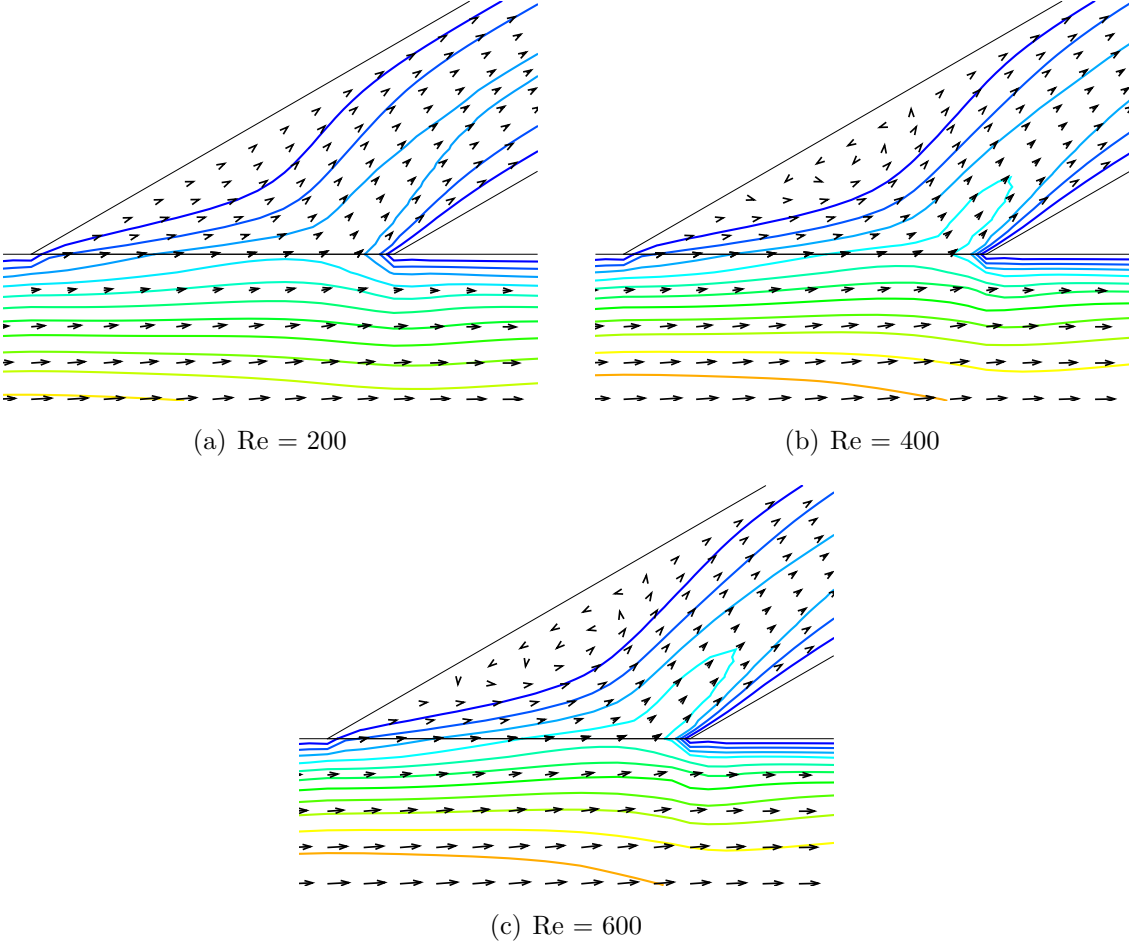


Figure 3.4: The details of separation in the vector form for Newtonian fluids flow in 2D branching channel with the angle 30 degrees - a)  $Re = 200$  - b)  $Re = 400$  - c)  $Re = 600$

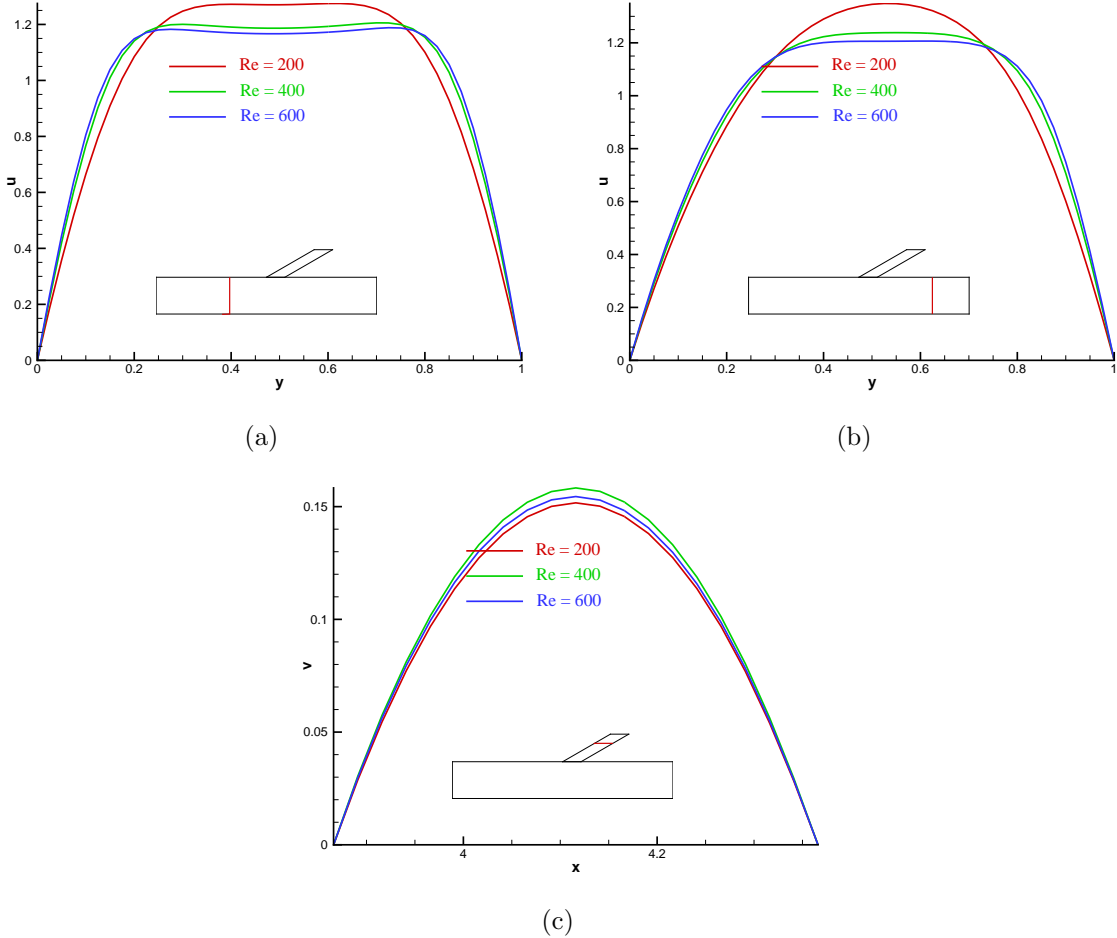
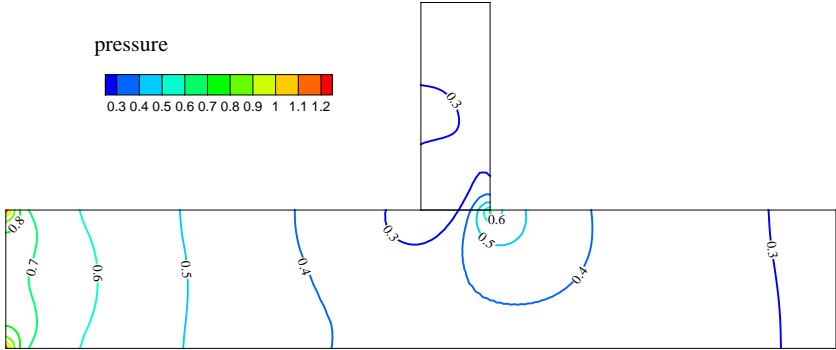
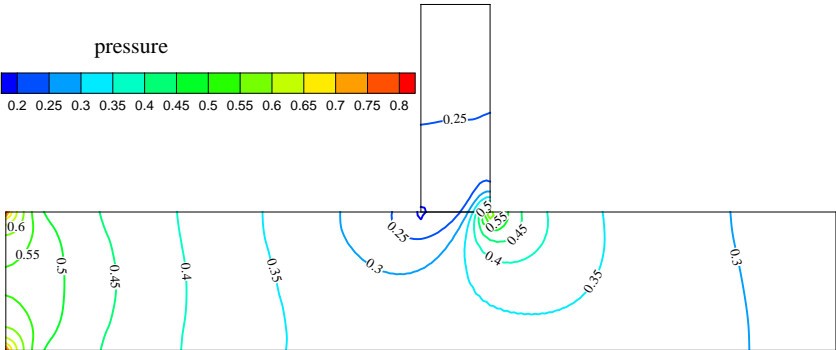


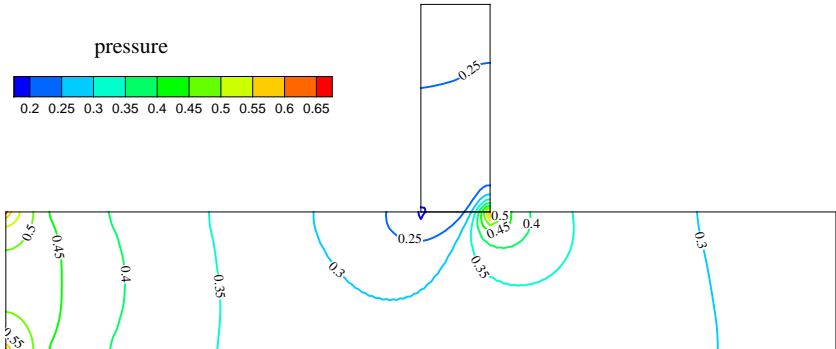
Figure 3.5: Nondimensional velocity profile of velocity component  $u$  as the function of  $y$  in the main channel and the velocity profile of velocity  $v$  as the function of  $x$  in the small branch of 2D branching channel with the angle 30 degrees



(a)  $Re = 200$



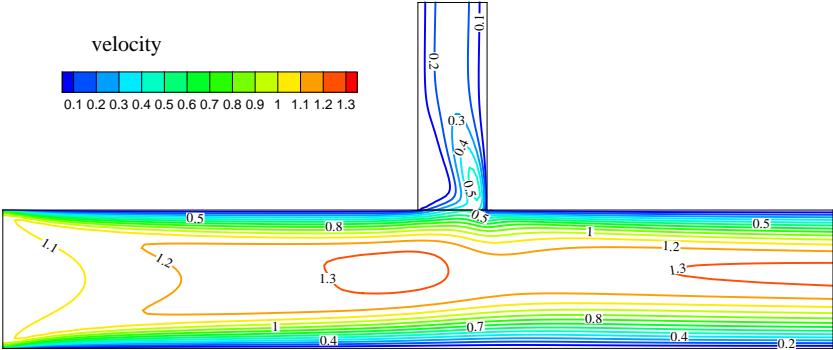
(b)  $Re = 400$



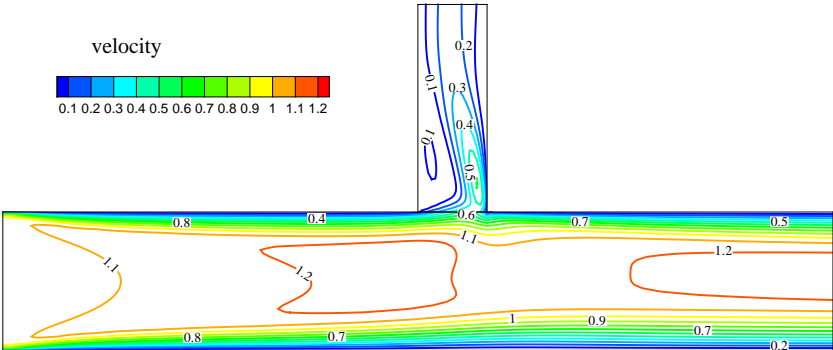
(c)  $Re = 600$

Figure 3.6: Pressure isolines of Newtonian fluids flow in 2D branching channel with the angle 90 degrees - a)  $Re = 200$  - b)  $Re = 400$  - c)  $Re = 600$

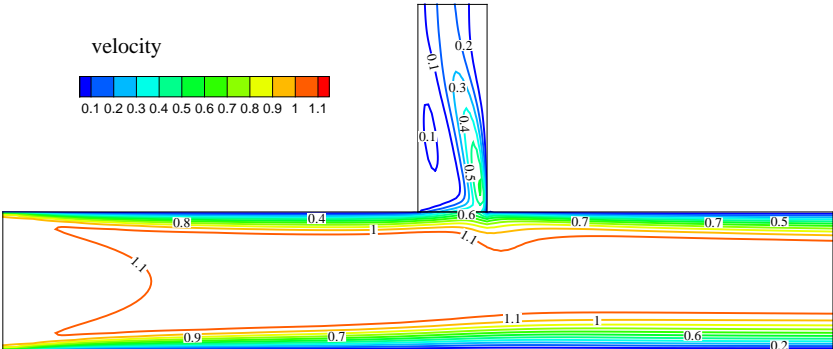




(a)  $Re = 200$



(b)  $Re = 400$



(c)  $Re = 600$

Figure 3.7: Velocity isolines of Newtonian fluids flow in 2D branching channel with the angle 90 degrees - a)  $Re = 200$  - b)  $Re = 400$  - c)  $Re = 600$

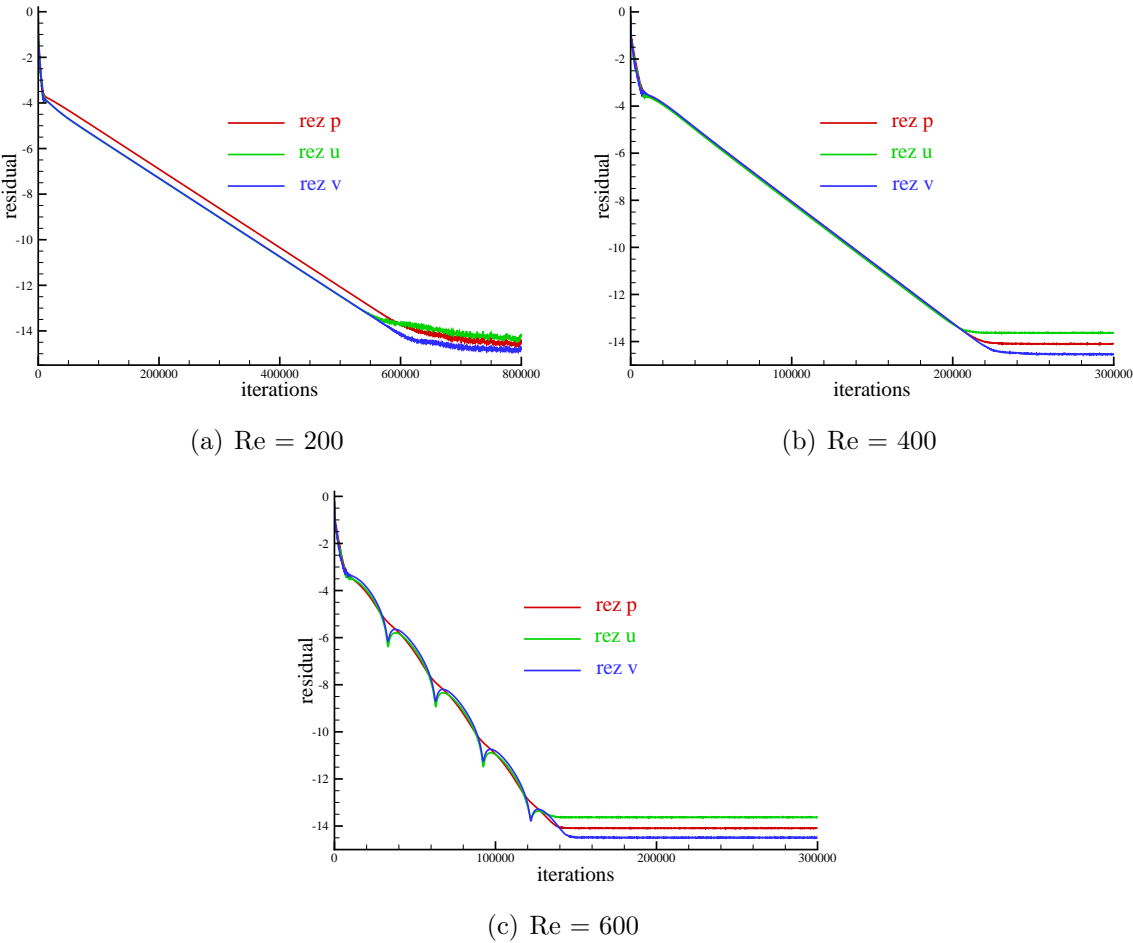


Figure 3.8: The convergence history of Newtonian fluids flow in 2D branching channel with the angle 90 degrees - a)  $Re = 200$  - b)  $Re = 400$  - c)  $Re = 600$

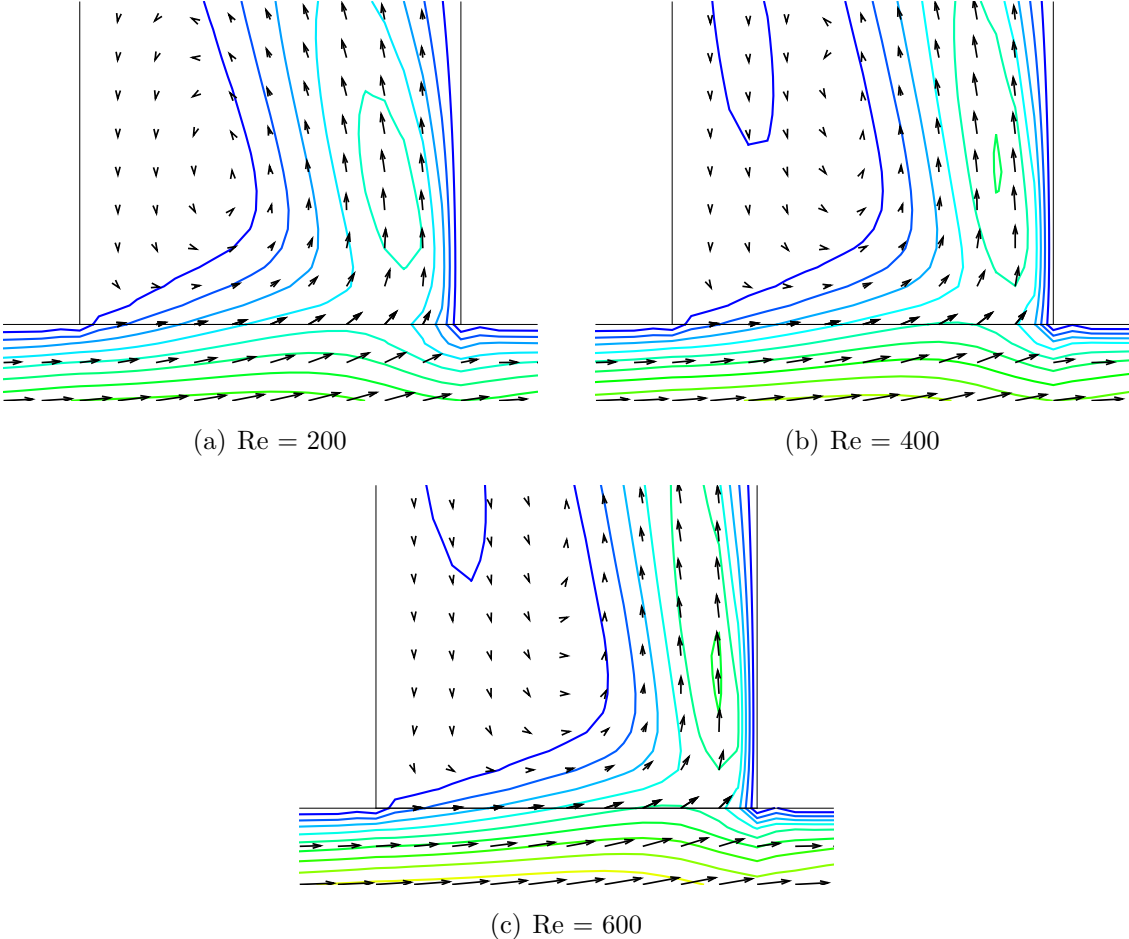


Figure 3.9: The details of separation in the vector form for Newtonian fluids flow in 2D branching channel with the angle 90 degrees - a)  $Re = 200$  - b)  $Re = 400$  - c)  $Re = 600$

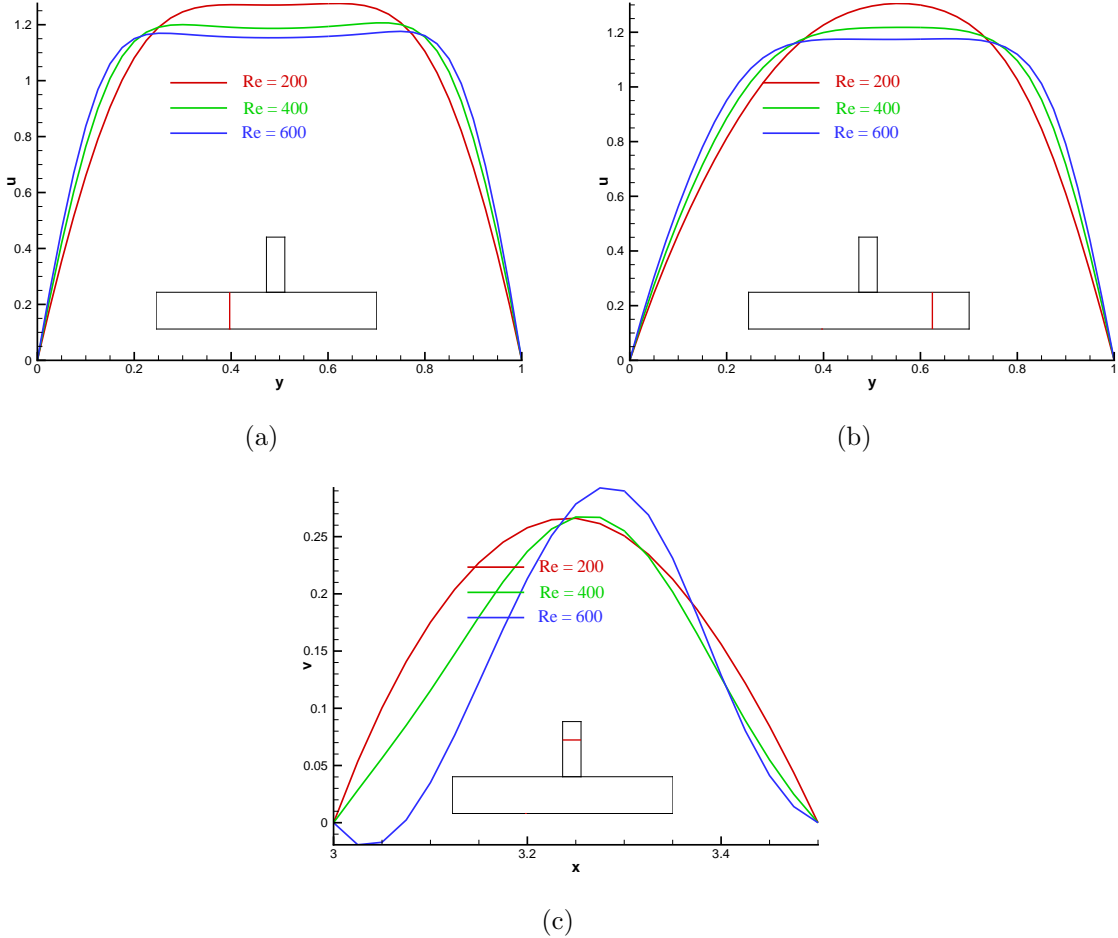


Figure 3.10: Nondimensional velocity profile of velocity component  $u$  as the function of  $y$  in the main channel and the velocity profile of velocity  $v$  as the function of  $x$  in the small branch of 2D branching channel with the angle 90 degrees

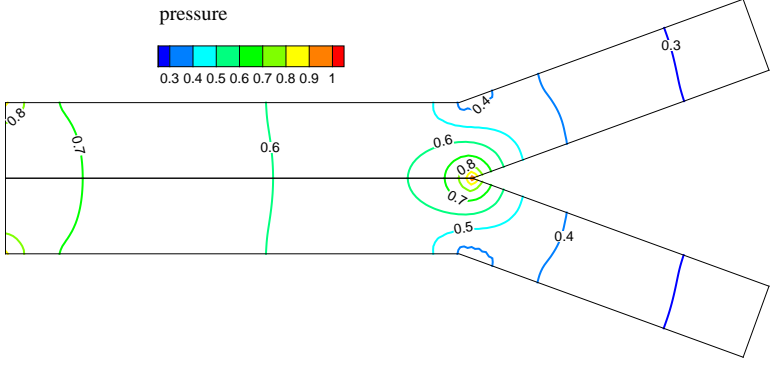
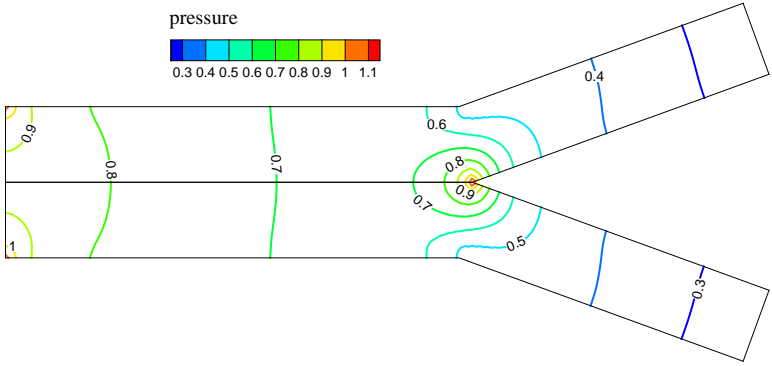
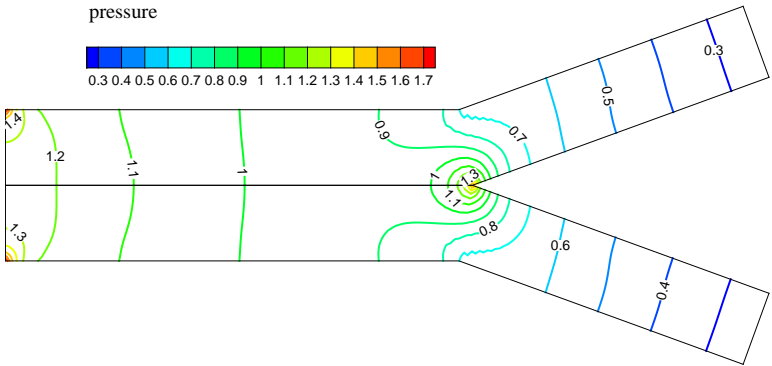
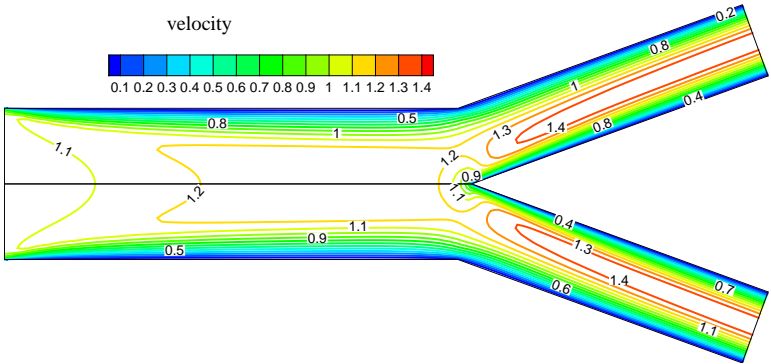
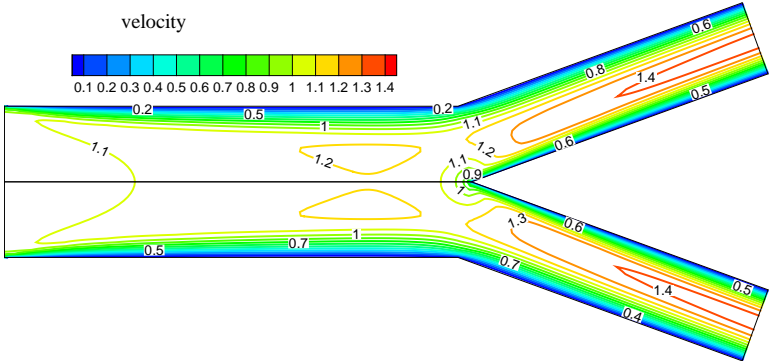


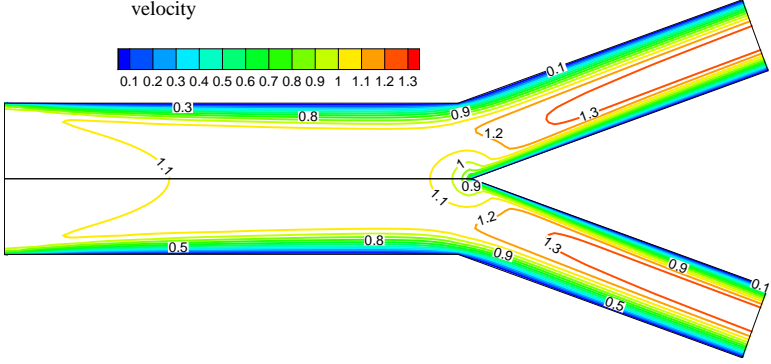
Figure 3.11: Pressure isolines of Newtonian fluids flow in 2D symmetric branching channel with the angle 20 degrees - a)  $Re = 200$  - b)  $Re = 400$  - c)  $Re = 600$



(a)  $Re = 200$



(b)  $Re = 400$



(c)  $Re = 600$

Figure 3.12: Velocity isolines of Newtonian fluids flow in 2D symmetric branching channel with the angle 20 degrees - a)  $Re = 200$  - b)  $Re = 400$  - c)  $Re = 600$

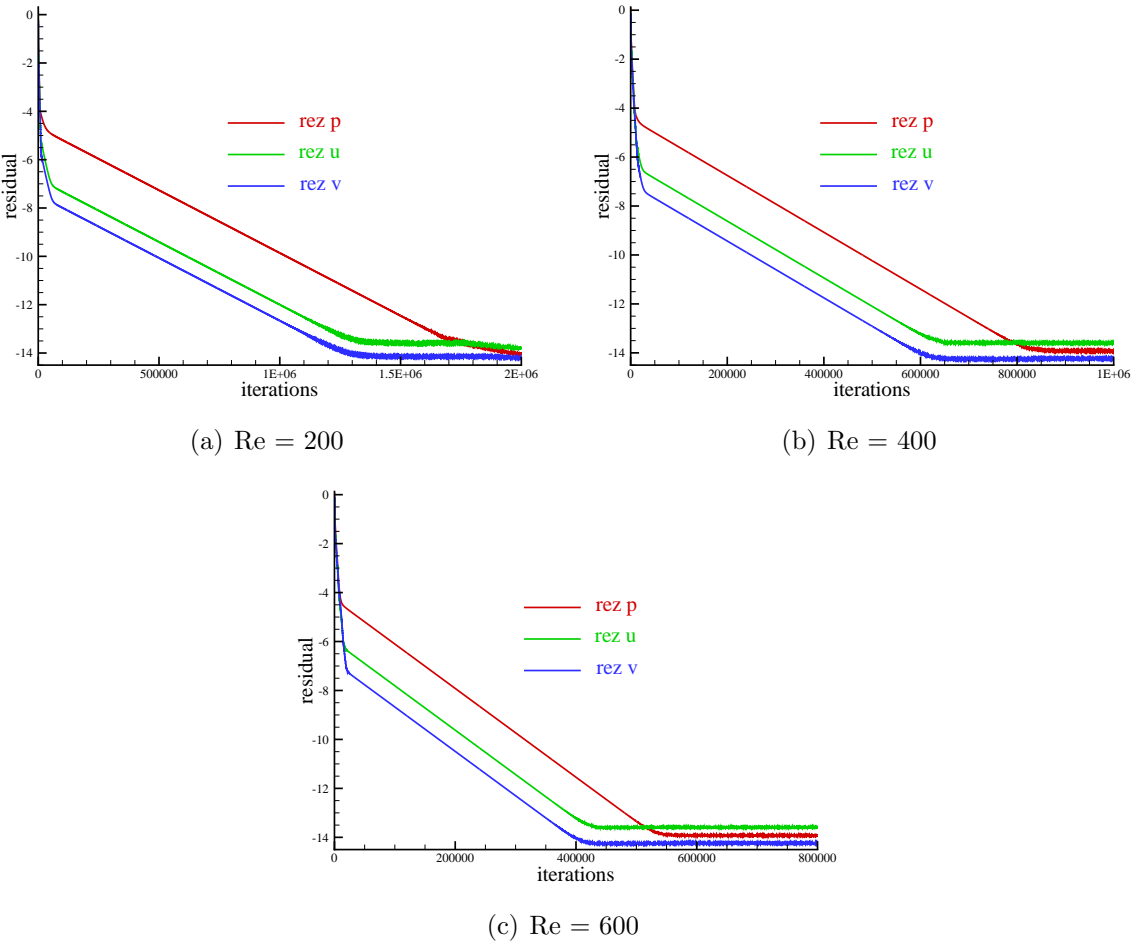


Figure 3.13: The convergence history of Newtonian fluids flow in 2D symmetric branching channel with the angle 20 degrees - a)  $Re = 200$  - b)  $Re = 400$  - c)  $Re = 600$

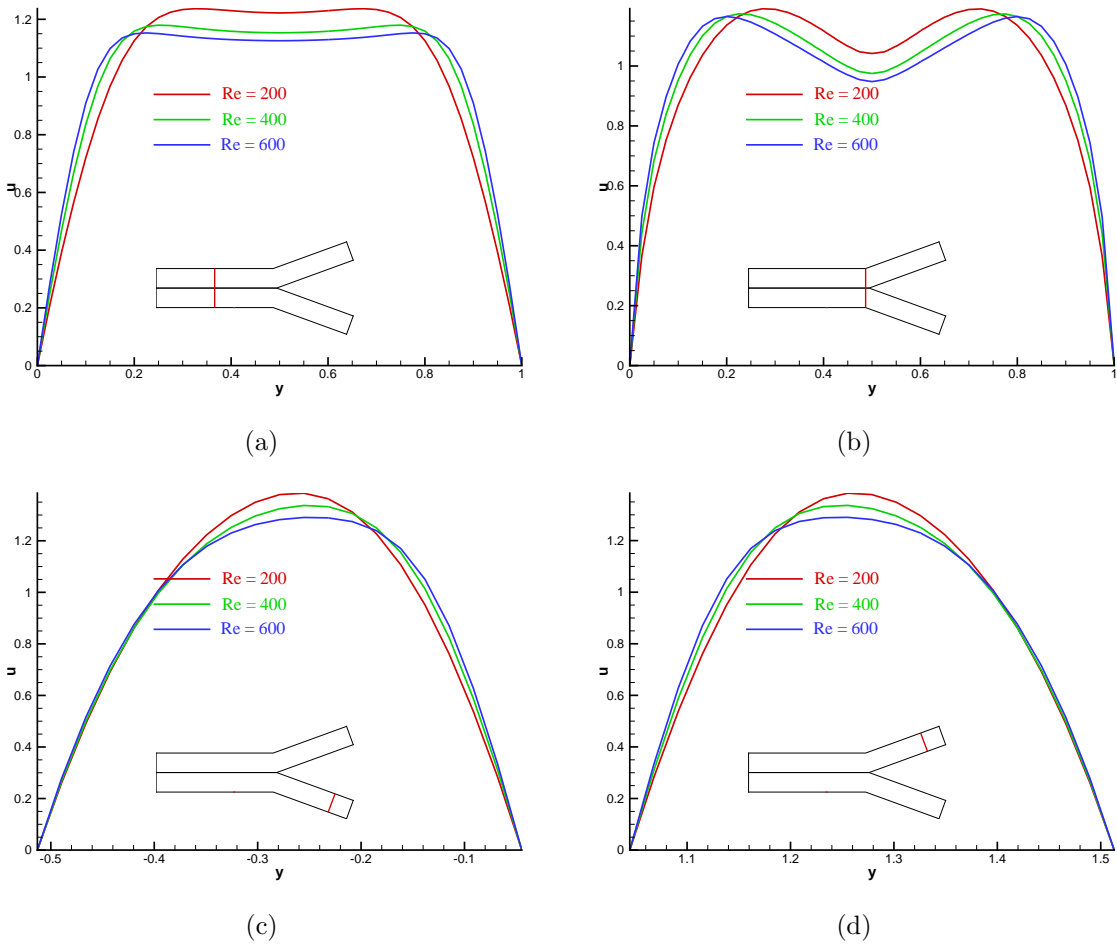
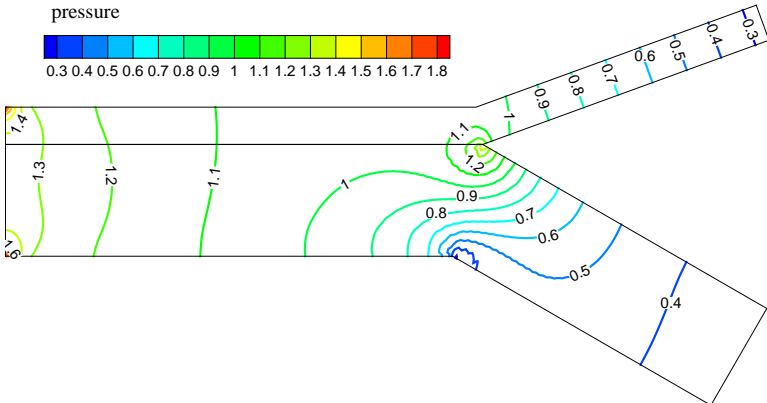
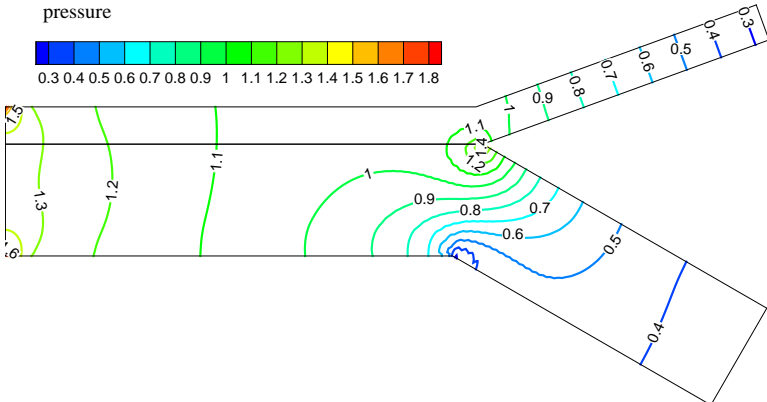


Figure 3.14: Nondimensional velocity profile of velocity component  $u$  as the function of  $y$  in 2D symmetric branching channel with the angle 20 degrees

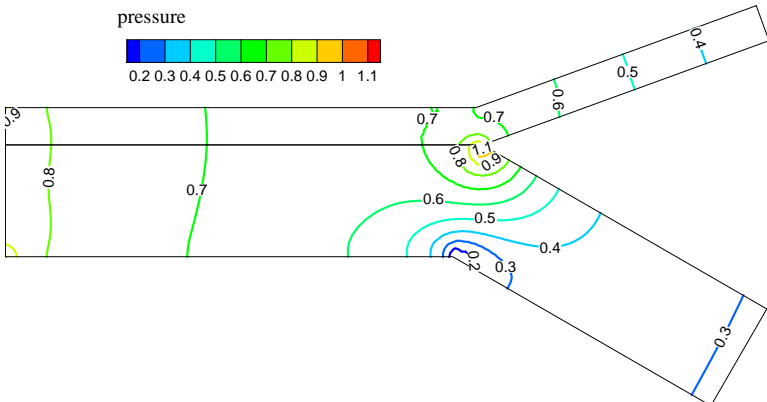




(a)  $Re = 200$

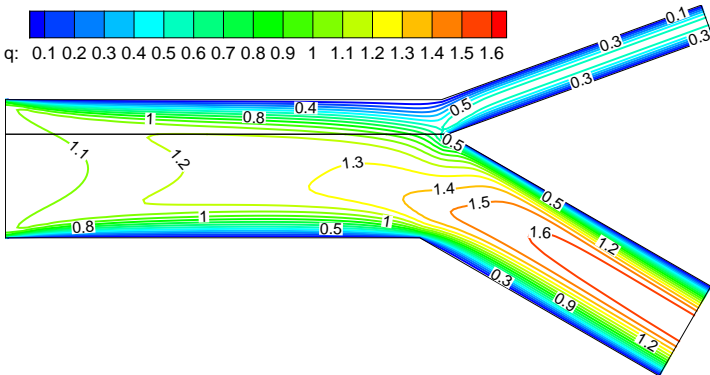


(b)  $Re = 400$

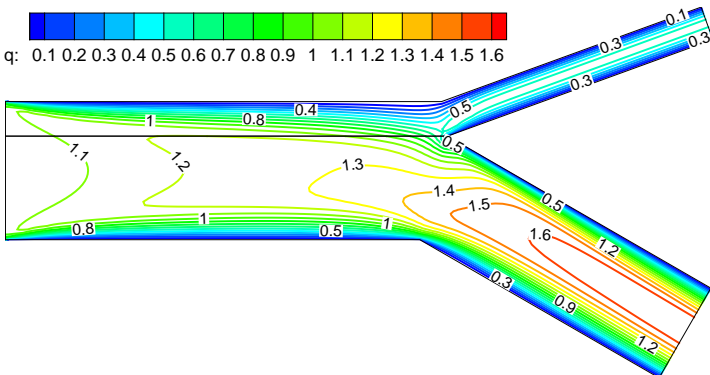


(c)  $Re = 600$

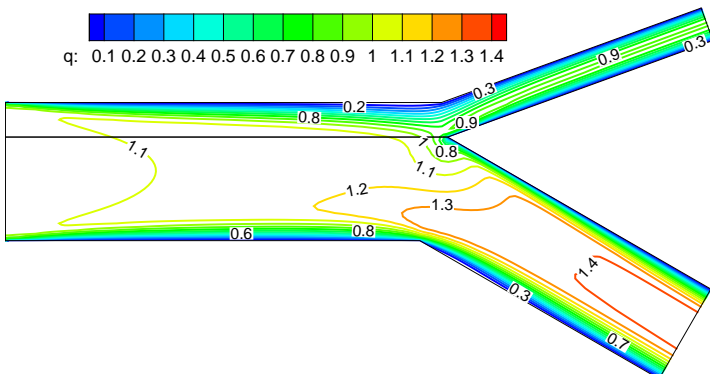
Figure 3.15: Pressure isolines of Newtonian fluids flow in 2D nonsymmetric branching channel with the angles 20 and 30 degrees - a)  $Re = 200$  - b)  $Re = 400$  - c)  $Re = 600$



(a)  $Re = 200$



(b)  $Re = 400$



(c)  $Re = 600$

Figure 3.16: Velocity isolines of Newtonian fluids flow in 2D nonsymmetric branching channel with the angles 20 and 30 degrees - a)  $Re = 200$  - b)  $Re = 400$  - c)  $Re = 600$

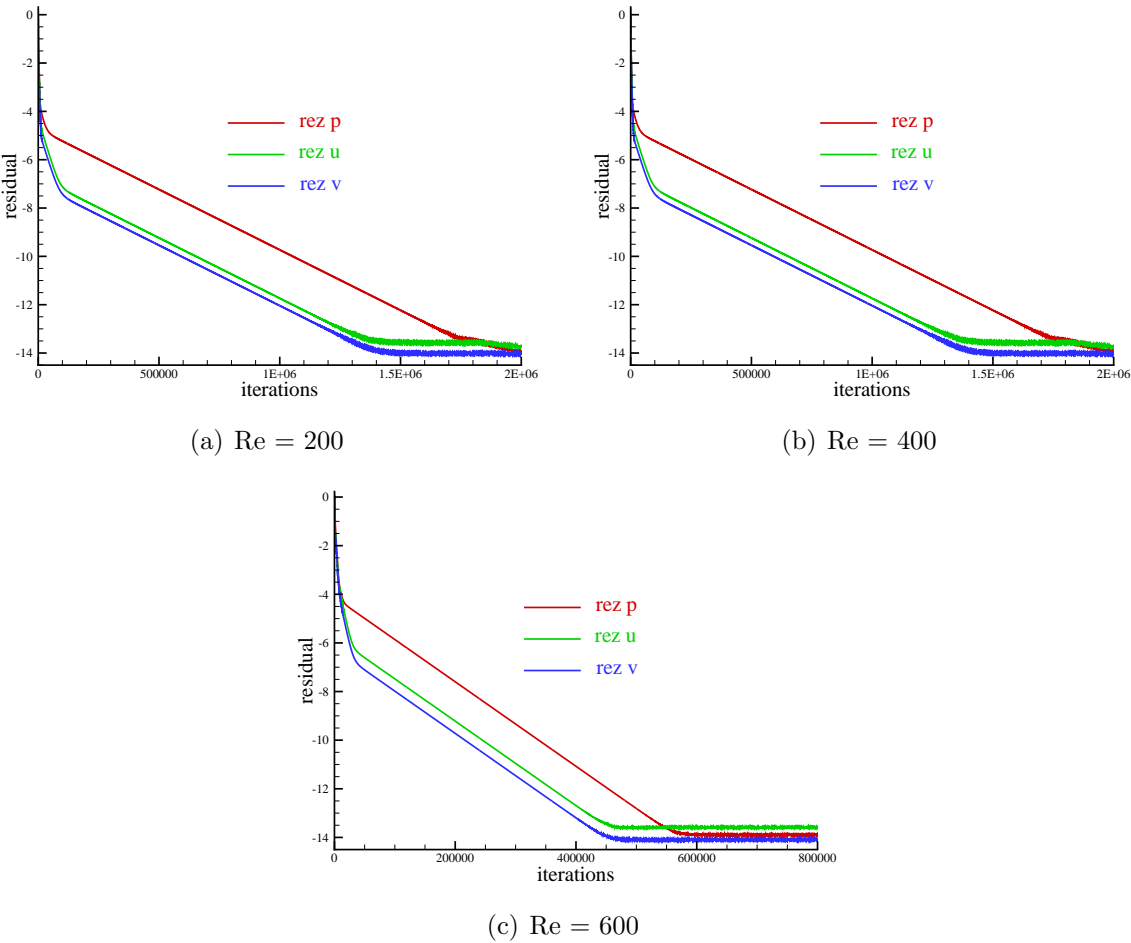


Figure 3.17: The convergence history of Newtonian fluids flow in 2D nonsymmetric branching channel with the angles 20 and 30 degrees - a)  $Re = 200$  - b)  $Re = 400$  - c)  $Re = 600$

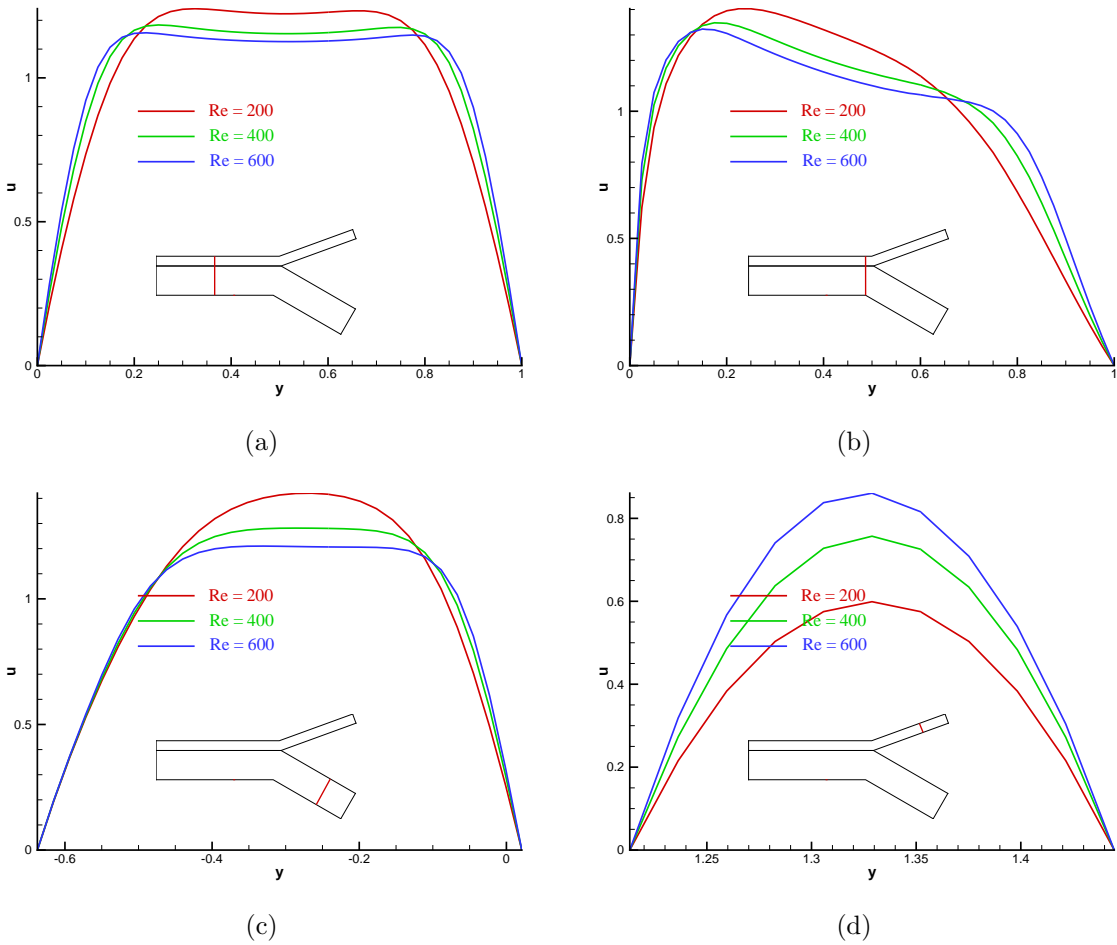


Figure 3.18: Nondimensional velocity profile of velocity component  $u$  as the function of  $y$  in 2D nonsymmetric branching channel with the angles 20 and 30 degrees

## 3.2 Three Dimensional Steady Solutions of Newtonian Fluids

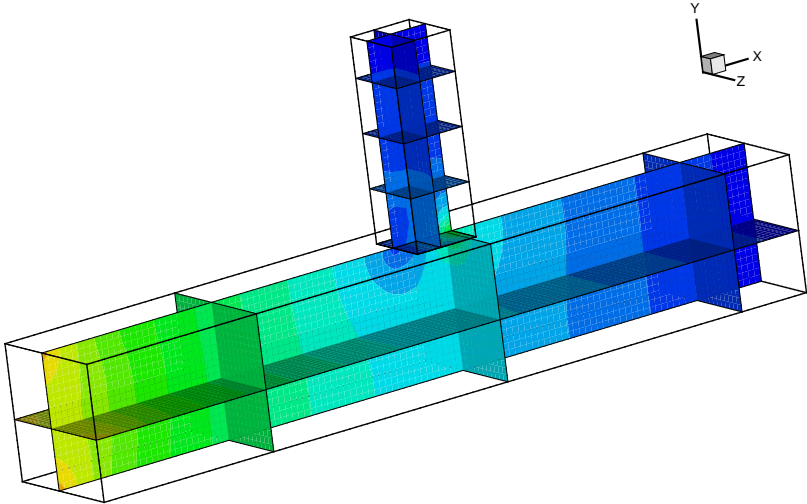
The numerical results of three dimensional incompressible laminar viscous flows for Newtonian fluids are presented and compared. Numerical simulations were performed for three dimensional branching channels with one entrance and two exit parts. The steady boundary conditions are used for the steady state solutions.

The numerical results are shown for two geometries of the domain. Two different values of Reynolds number were used for comparing pressure and velocity isolines for these domains.

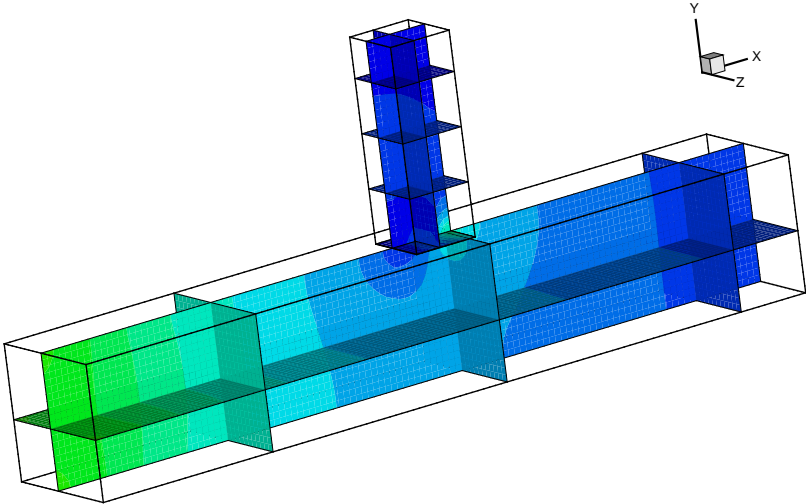
Two shapes of the domain are used. First, the branching channel in the shape T with the angle 90 degrees is considered, second, the symmetric branching channel with the angle 20 degrees is used. Numerical results are compared for two different values of Reynolds number in the form of the pressure isolines (figures 3.21 and 3.28) and in the form of the velocity isolines (figures 3.22 and 3.29). Two values of Reynolds number are tested:  $Re = 200$  and  $Re = 400$ . The figures 3.23 and 3.30 show the cuts through the main channel and the small branch resp. in the form of the velocity isolines. In the small picture the position of the cuts is sketched.

History of the convergence for both tested domains are compared for both values of Reynolds number (figures 3.24, 3.31). In the figures 3.25 and 3.32 the velocity profiles of the velocity component  $u, v$  as the function of the  $y, x$  are presented.

In this section the numerical simulations for two different Reynolds number ( $Re = 200$  and  $Re = 400$ ) and for two different geometries of the domain were compared. It follows the same conclusion as for two dimensional testing (in this case there is not third tested Reynolds number), there are the differences between small Reynolds number ( $Re = 200$ ) and higher Reynolds number ( $Re = 400$ ). The main differences can be seen in the figures 3.21 and 3.28 (the pressure isolines) and 3.24 and 3.31 (the history of the convergence). For the pressure isolines the maximal pressure value is higher for smaller Reynolds number (as for 2D cases) and the convergence of the variables is slower than for higher Reynolds number.

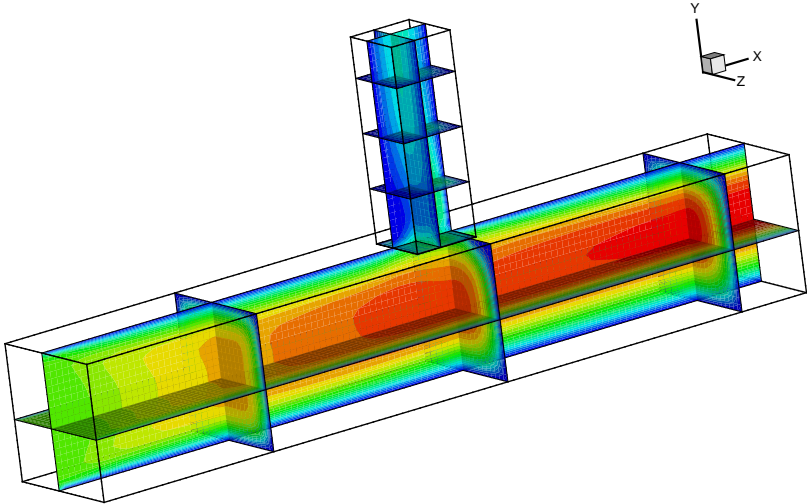


(a)  $Re = 200$

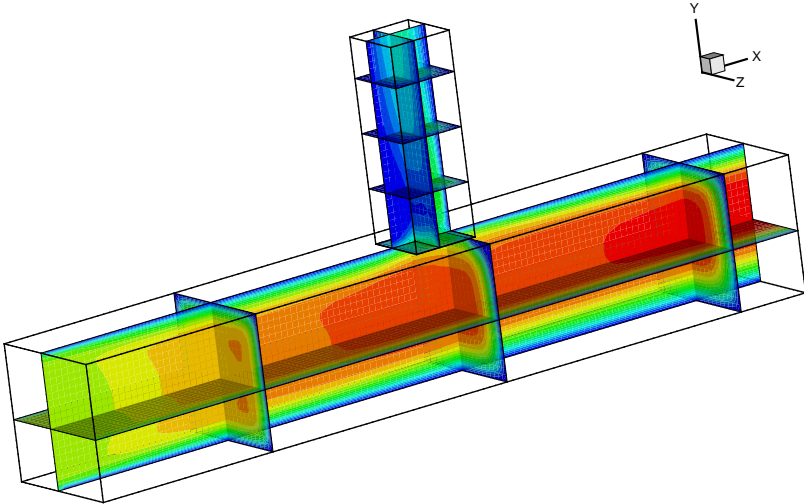


(b)  $Re = 400$

Figure 3.19: Pressure isolines of Newtonian fluids flow in 3D branching channel with the angle 90 degrees - a)  $Re = 200$  - b)  $Re = 400$

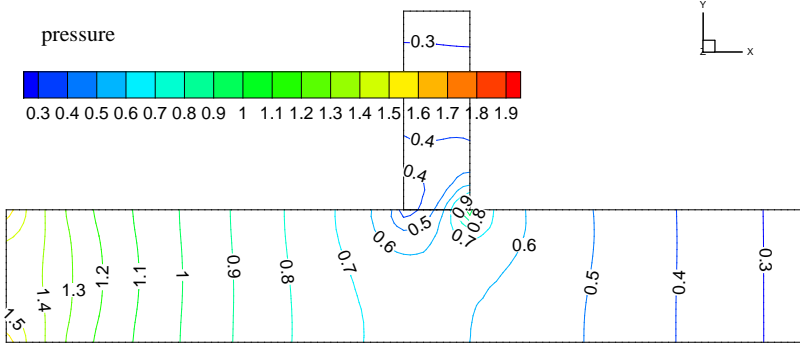


(a)  $Re = 200$

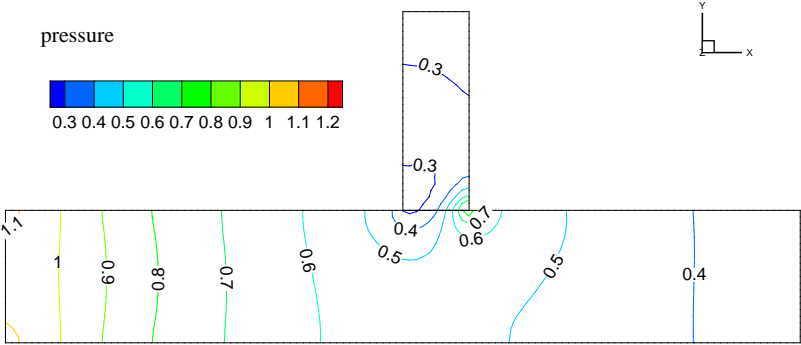


(b)  $Re = 400$

Figure 3.20: Velocity isolines of Newtonian fluids flow in 3D branching channel with the angle 90 degrees - a)  $Re = 200$  - b)  $Re = 400$



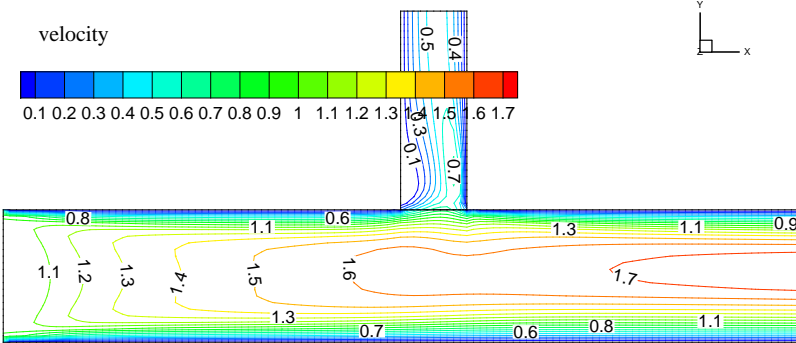
(a)  $Re = 200$



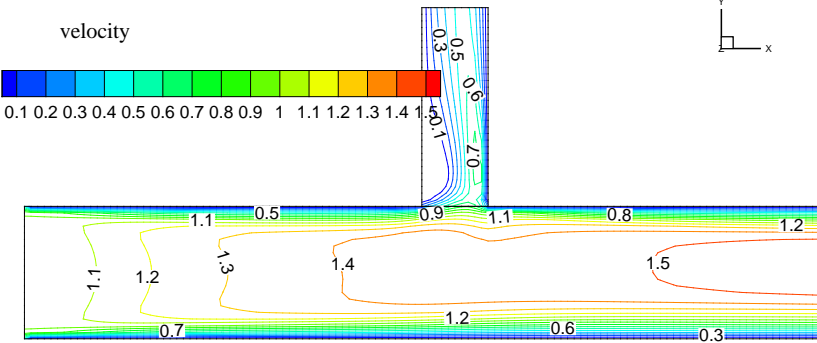
(b)  $Re = 400$

Figure 3.21: Pressure isolines of Newtonian fluids flow in 3D branching channel with the angle 90 degrees - a)  $Re = 200$  - b)  $Re = 400$



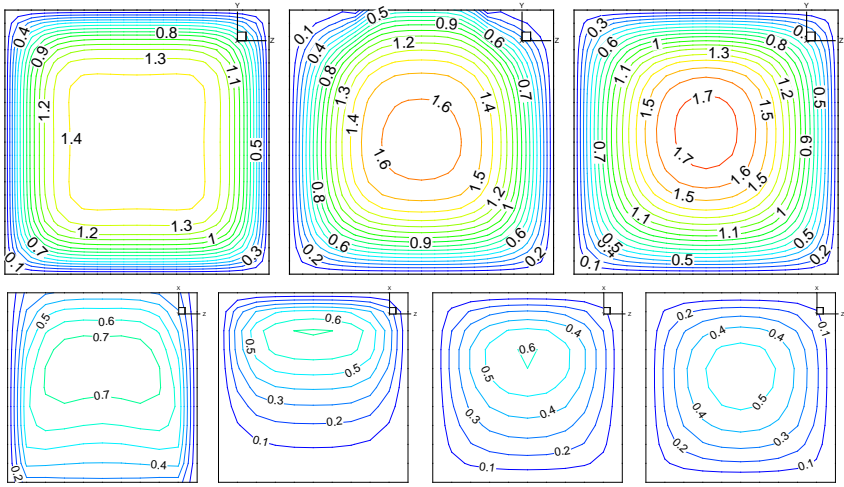


(a)  $Re = 200$

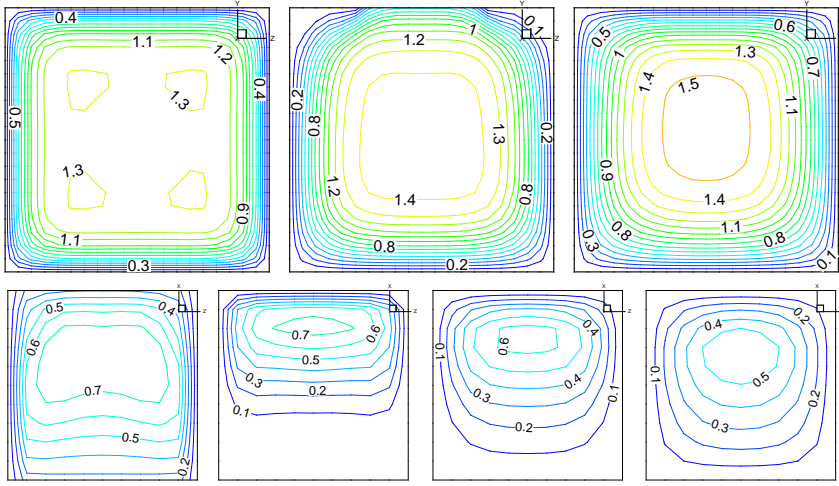


(b)  $Re = 400$

Figure 3.22: Velocity isolines of Newtonian fluids flow in 3D branching channel with the angle 90 degrees - a)  $Re = 200$  - b)  $Re = 400$



(a)  $Re = 200$



(b)  $Re = 400$

Figure 3.23: Cuts through the main channel and through the small branch - a)  $Re = 200$   
- b)  $Re = 400$

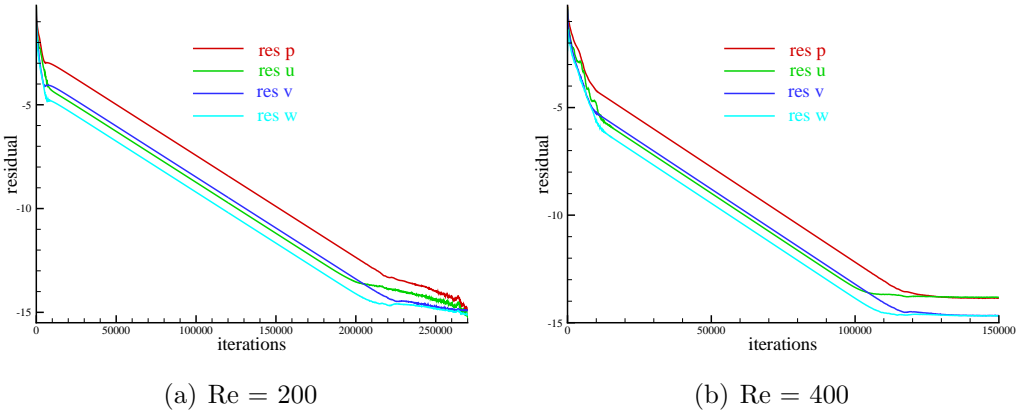


Figure 3.24: History of the convergence - a)  $Re = 200$  - b)  $Re = 400$

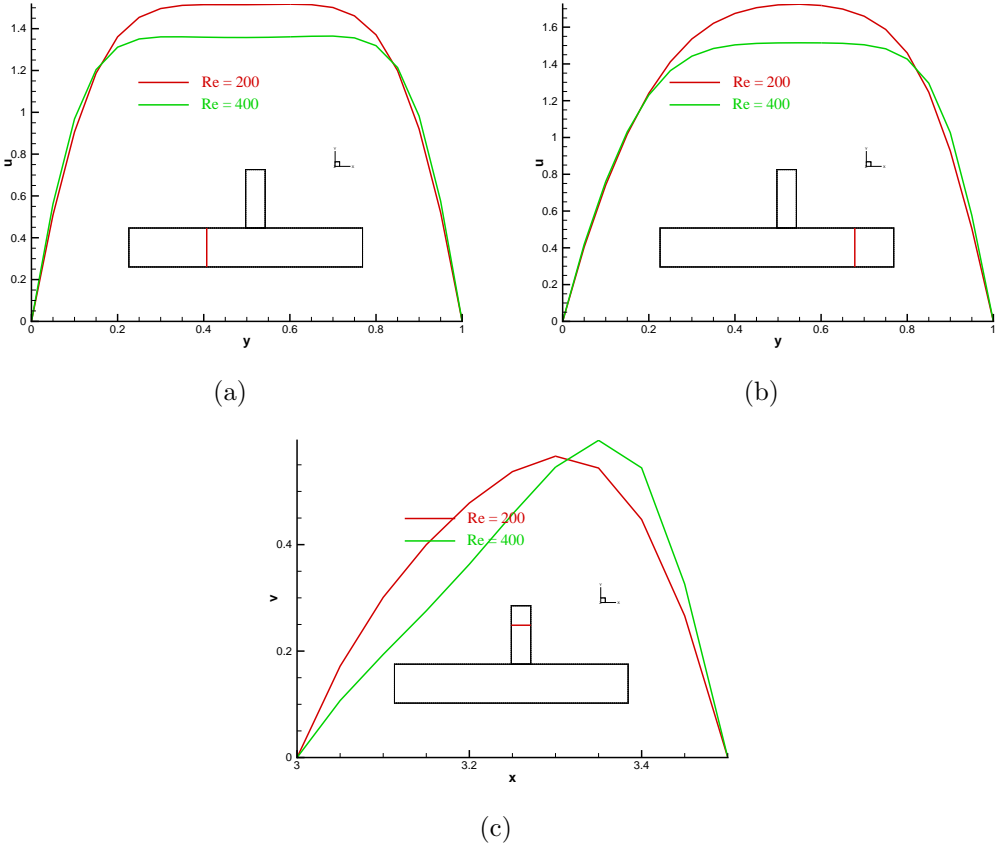
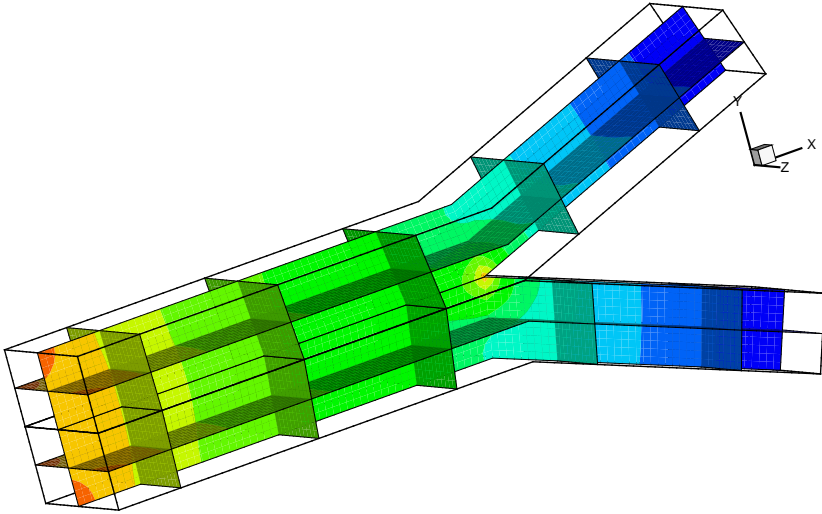
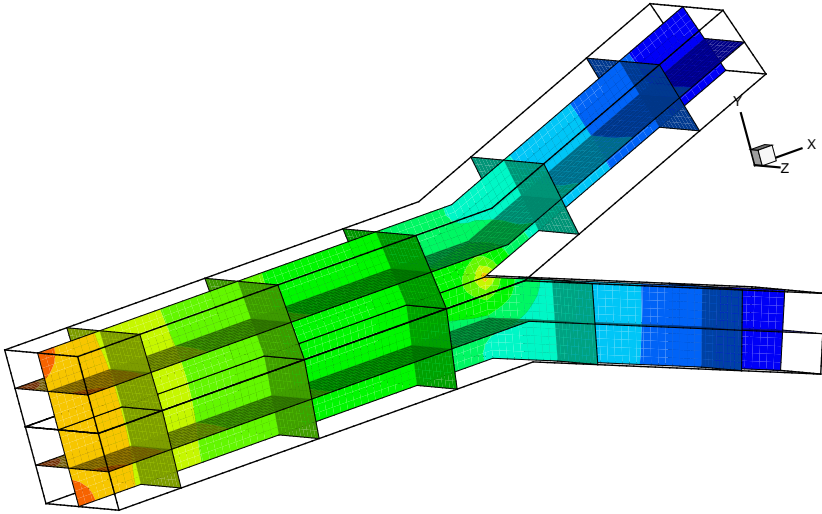


Figure 3.25: Nondimensional velocity profile of velocity component  $u$  as the function of  $y$

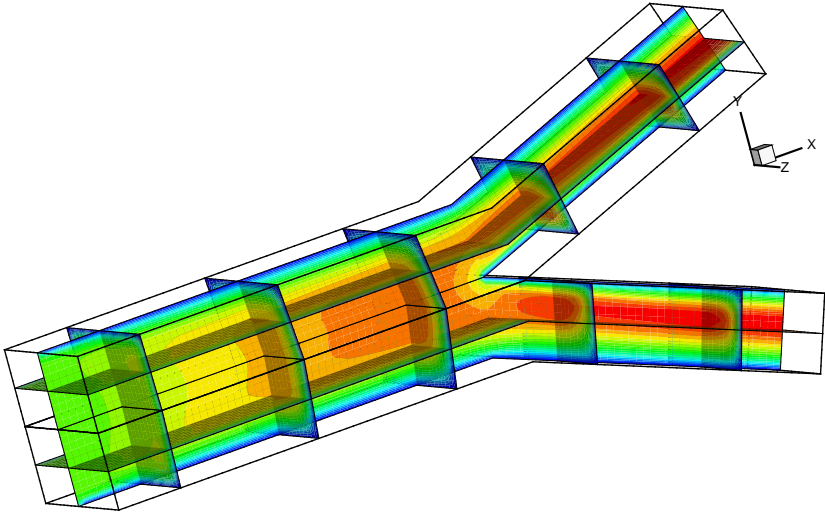


(a)  $Re = 200$

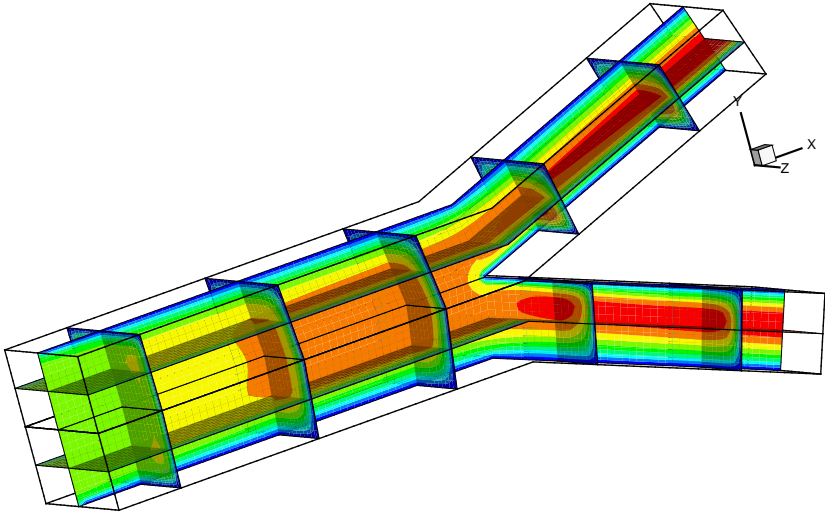


(b)  $Re = 400$

Figure 3.26: Pressure isolines of Newtonian fluids flow in 3D symmetric branching channel with the angle 20 degrees - a)  $Re = 200$  - b)  $Re = 400$

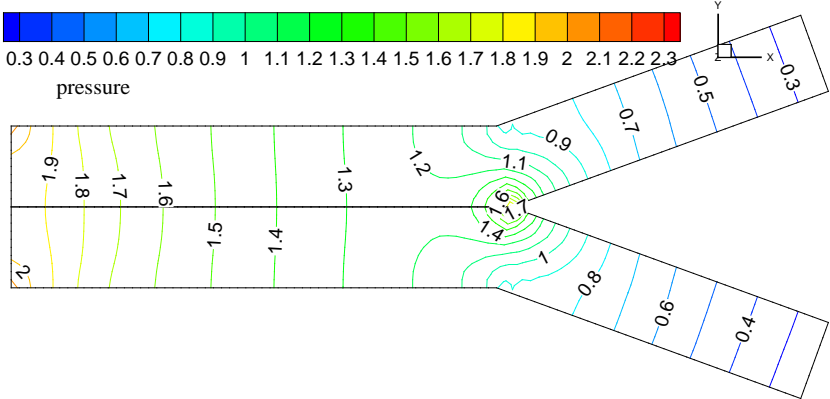


(a)  $Re = 200$

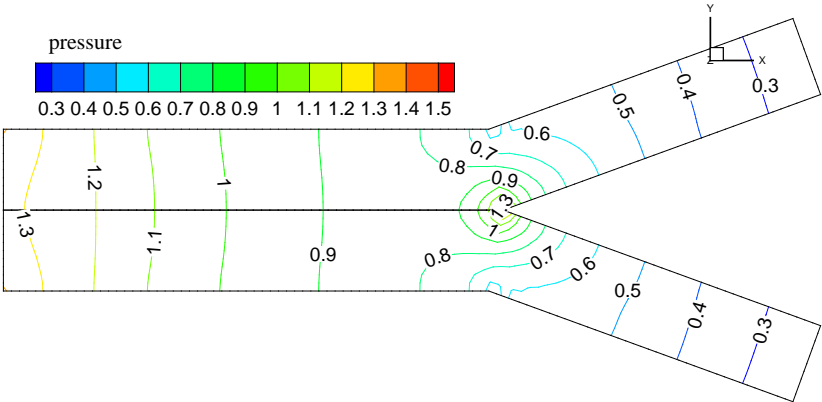


(b)  $Re = 400$

Figure 3.27: Velocity isolines of Newtonian fluids flow in 3D symmetric branching channel with the angle 20 degrees - a)  $Re = 200$  - b)  $Re = 400$

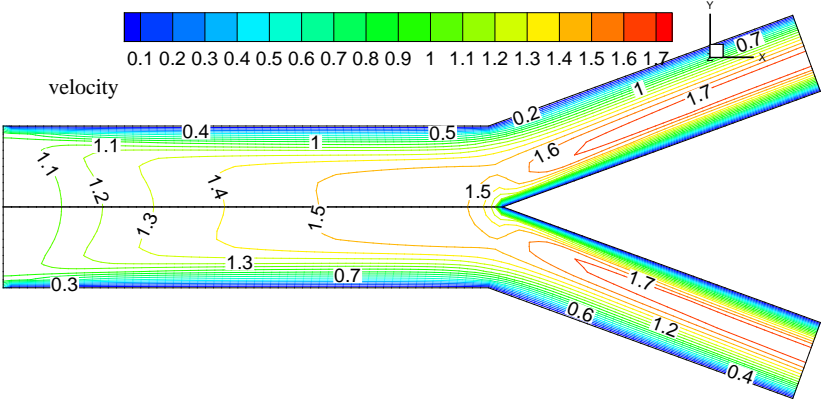


(a)  $Re = 200$

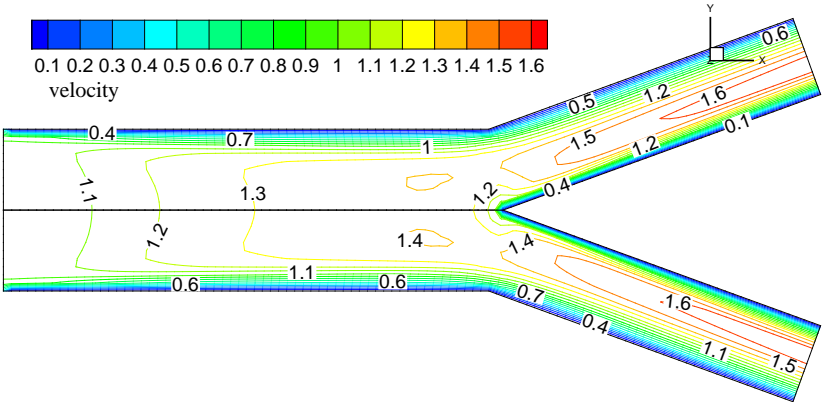


(b)  $Re = 400$

Figure 3.28: Pressure isolines of Newtonian fluids flow in 3D symmetric branching channel with the angle 20 degrees - a)  $Re = 200$  - b)  $Re = 400$

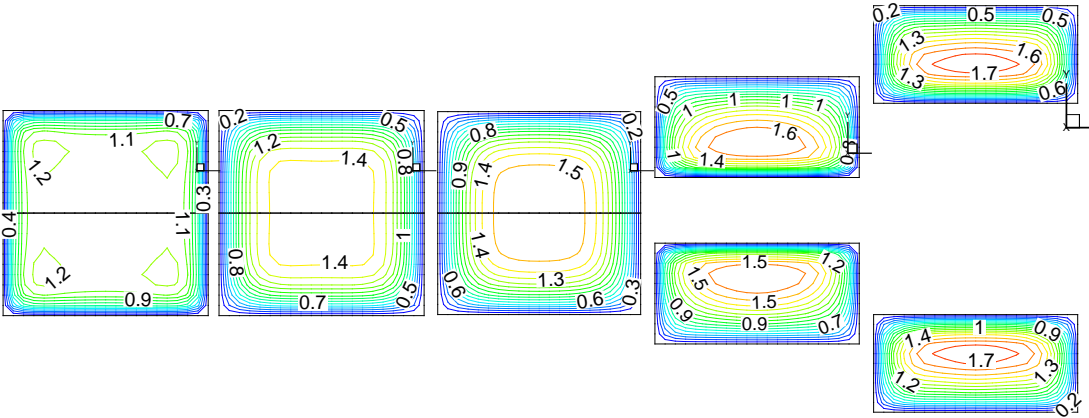


(a)  $Re = 200$

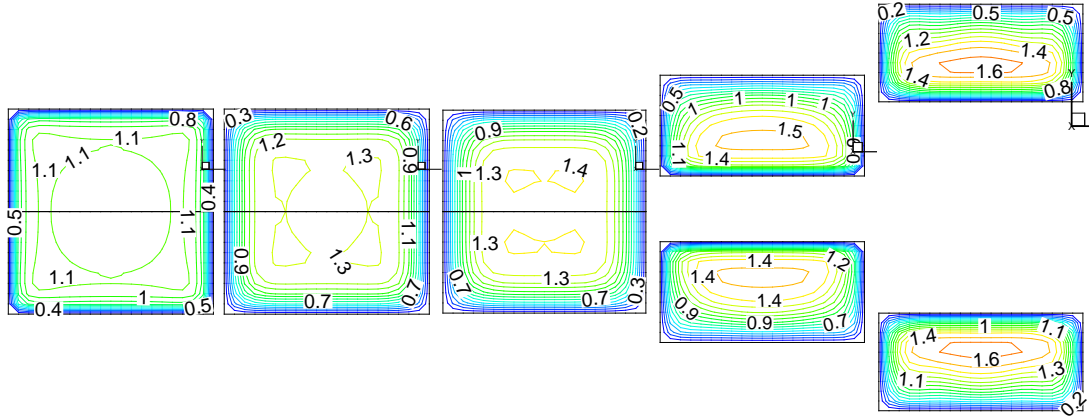


(b)  $Re = 400$

Figure 3.29: Velocity isolines of Newtonian fluids flow in 3D symmetric branching channel with the angle 20 degrees - a)  $Re = 200$  - b)  $Re = 400$



(a)  $Re = 200$



(b)  $Re = 400$

Figure 3.30: Cuts through the main channel and the branches - a)  $Re = 200$  - b)  $Re = 400$



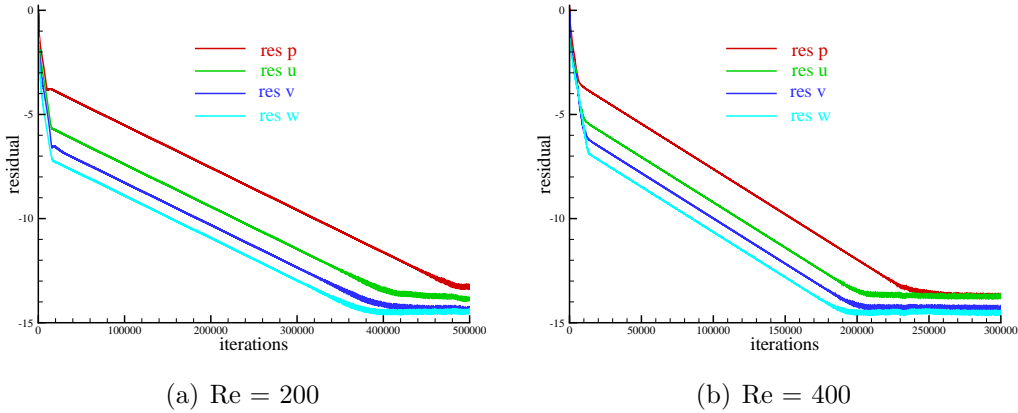


Figure 3.31: History of the convergence - a)  $Re = 200$  - b)  $Re = 400$

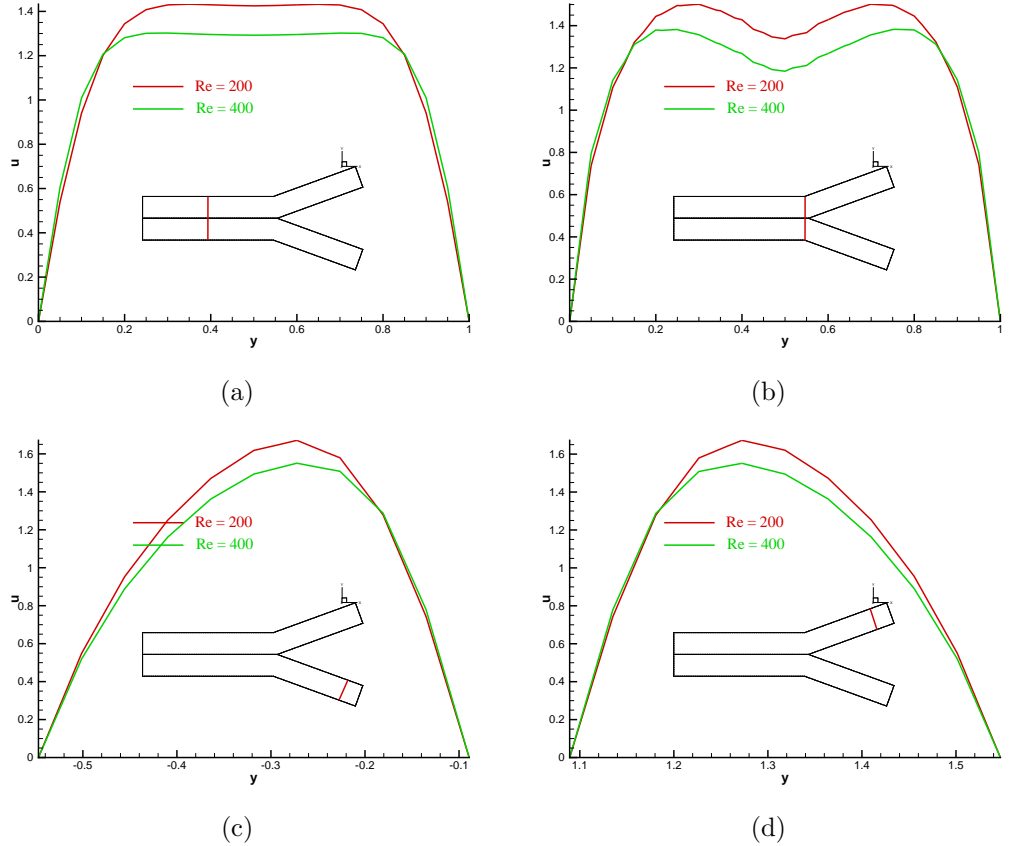


Figure 3.32: Nondimensional velocity profile of velocity component  $u$  as the function of  $y$

### 3.3 Two Dimensional Steady Solutions of Non-Newtonian Fluids

Two dimensional numerical results of incompressible laminar viscous flows for non-Newtonian fluids are presented and compared with numerical solutions of Newtonian fluids. Numerical simulations were performed for two dimensional branching channels with one entrance and two exit parts. The steady boundary conditions are used for the steady state solutions.

First part of this section is concerned on the testing of the three different values of the power-law index  $r$  (eq. (1.42)) ( $r = 0.2$ ,  $r = 0.5$  and  $r = 0.8$ ) for higher Reynolds number ( $Re = 900$ ).

Second part is concerned on the comparing Newtonian fluids flow with the shear thickening non-Newtonian fluids flow for one value of Reynolds number  $Re = 600$ . The power-law index  $r$  are chosen as follows:  $r = 0.5$

As for Newtonian fluids flow (section 3.1), the pressure and the velocity isolines are shown for the tested domain and the tested values of the power-law index  $r$ . The used domain is the branching channel in the shape T with the angle 90 degrees. Histories of the convergence for numerical results are presented.

In the first part of this section it results that with increasing the power-law index  $r$  the pressure value increases. The velocity isolines are similar. Also the convergence of the unknowns is slower with increasing constant  $r$ .

In the last part the same conclusion can be done. The maximal pressure value is higher for non-Newtonian fluids flow ( $r = 0.5$ ) than for Newtonian fluids flow (agree with  $r = 0$ ).

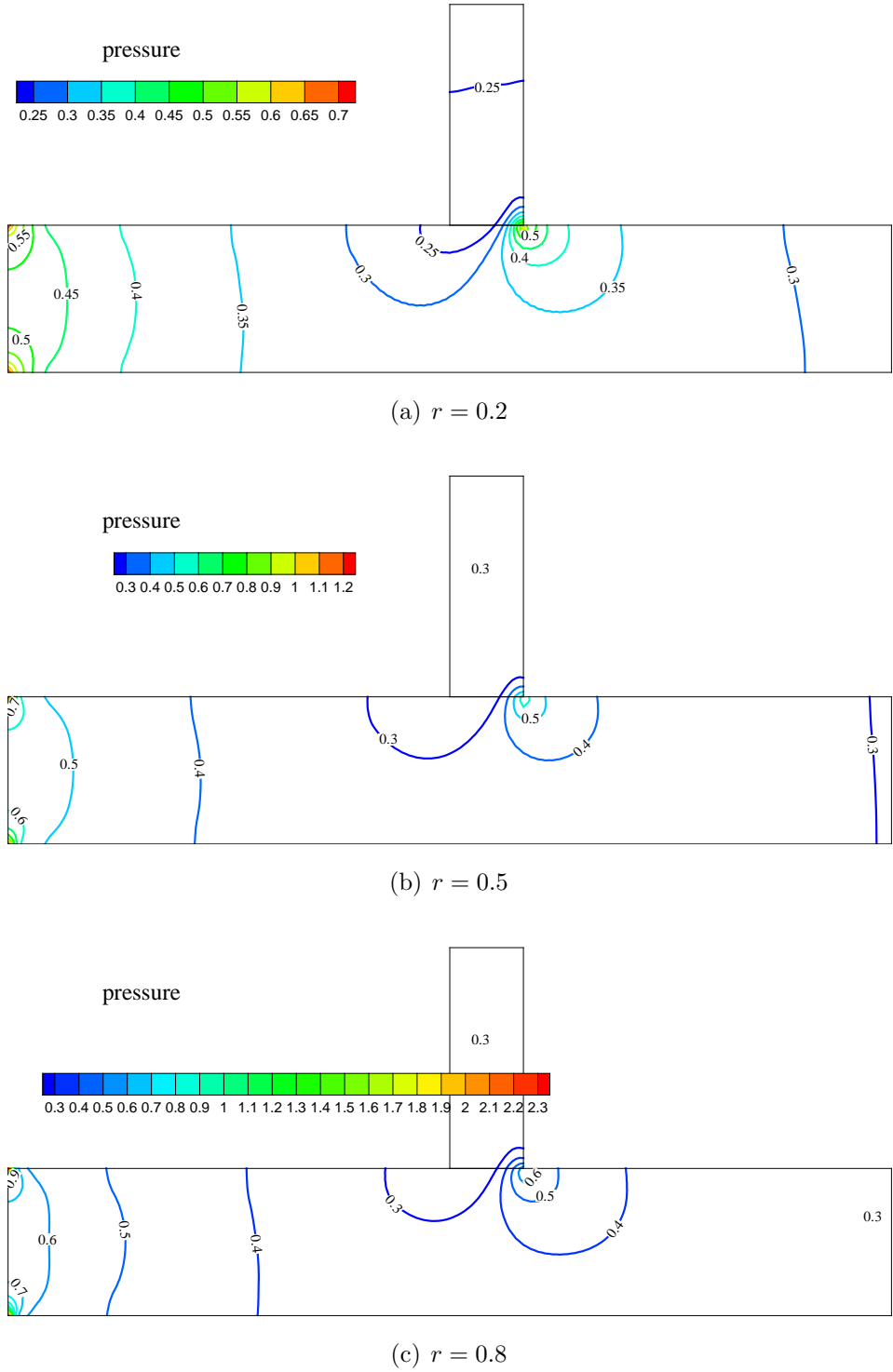


Figure 3.33: Pressure isolines of shear thickening non-Newtonian fluids flow in 2D branching channel for the different values of the power-law index  $r$  - a)  $r = 0.2$  - b)  $r = 0.5$  - c)  $r = 0.8$

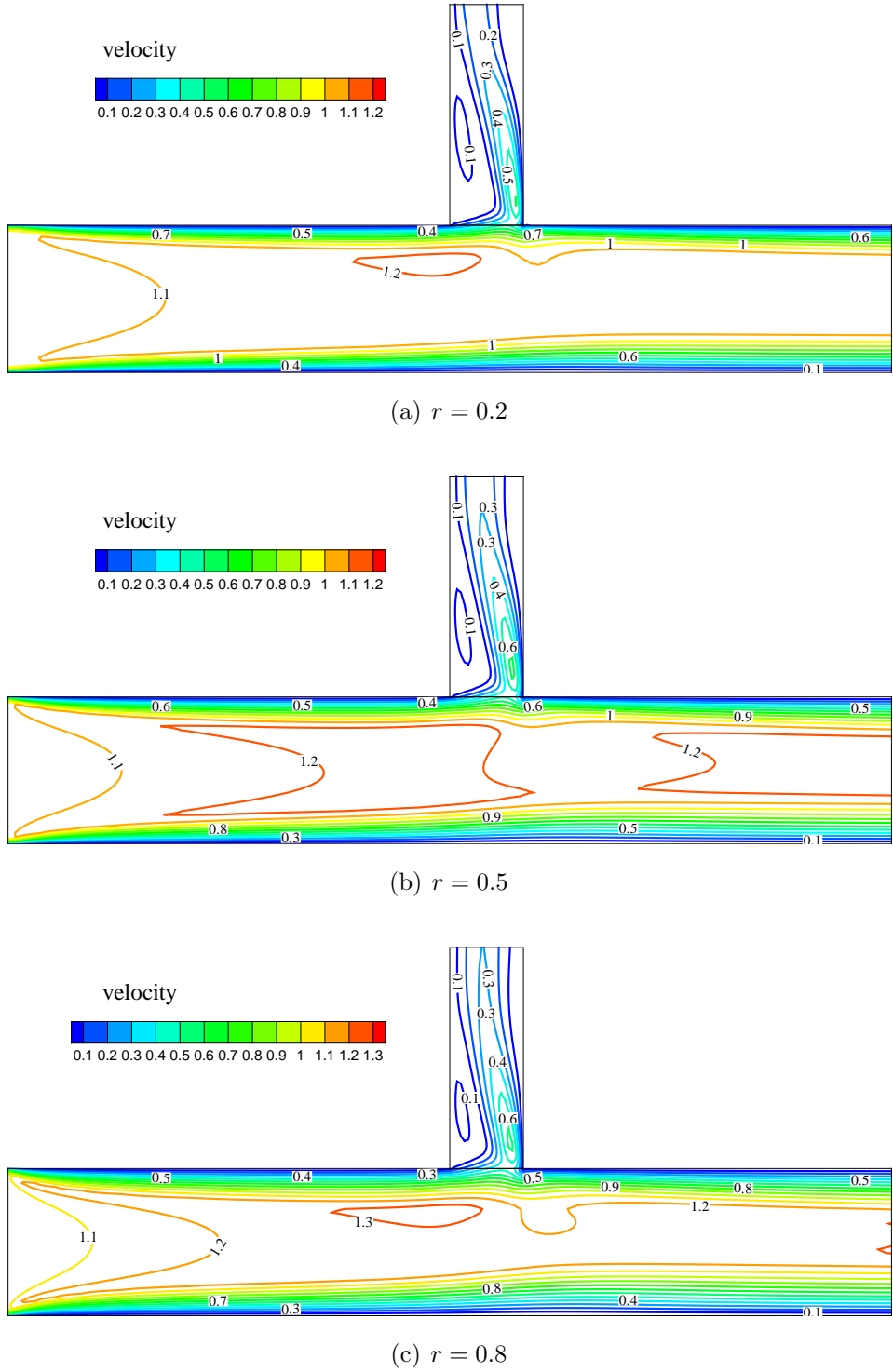


Figure 3.34: Velocity isolines of shear thickening non-Newtonian fluids flow in 2D branching channel for the different values of the power-law index  $r$  - a)  $r = 0.2$  - b)  $r = 0.5$  - c)  $r = 0.8$

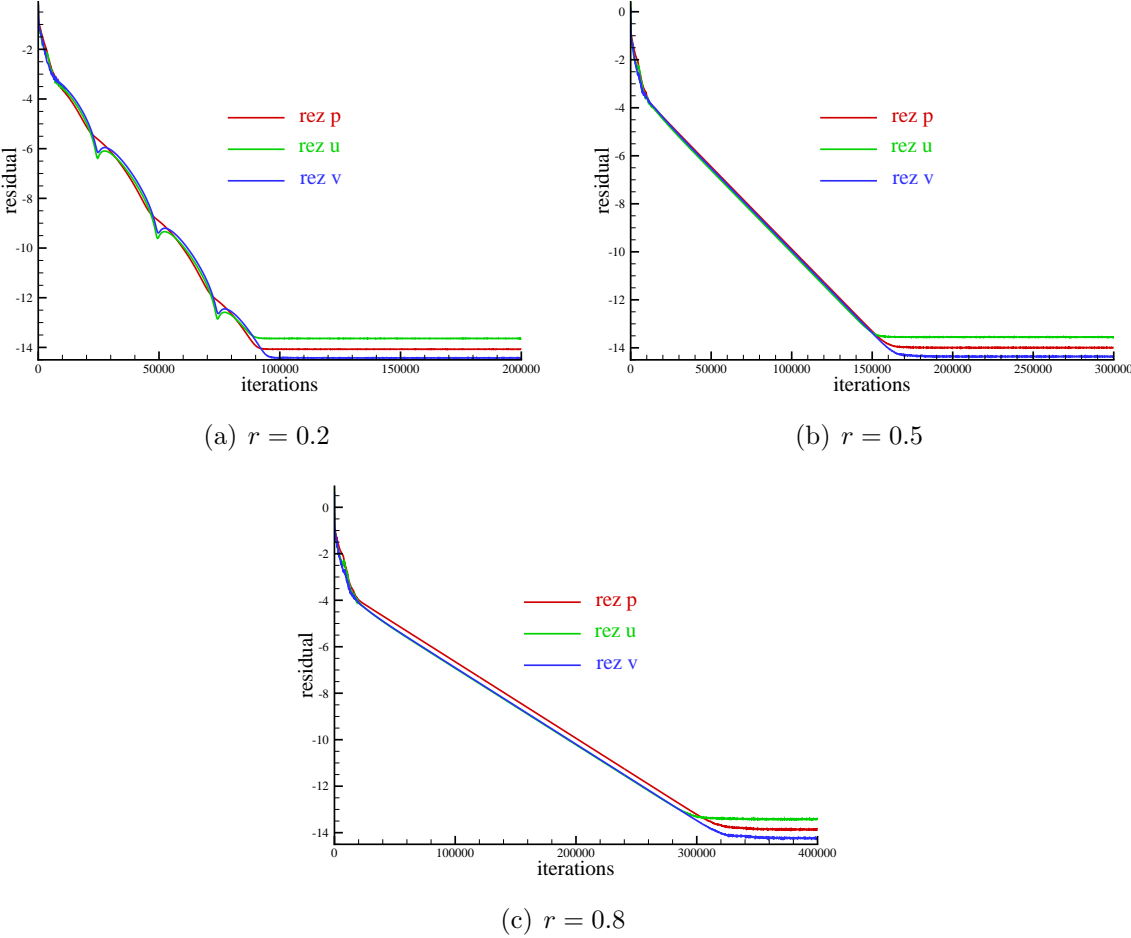


Figure 3.35: History of the convergence of shear thickening non-Newtonian fluids flow in 2D branching channel for the different values of the power-law index  $r$  - a)  $r = 0.2$  - b)  $r = 0.5$  - c)  $r = 0.8$

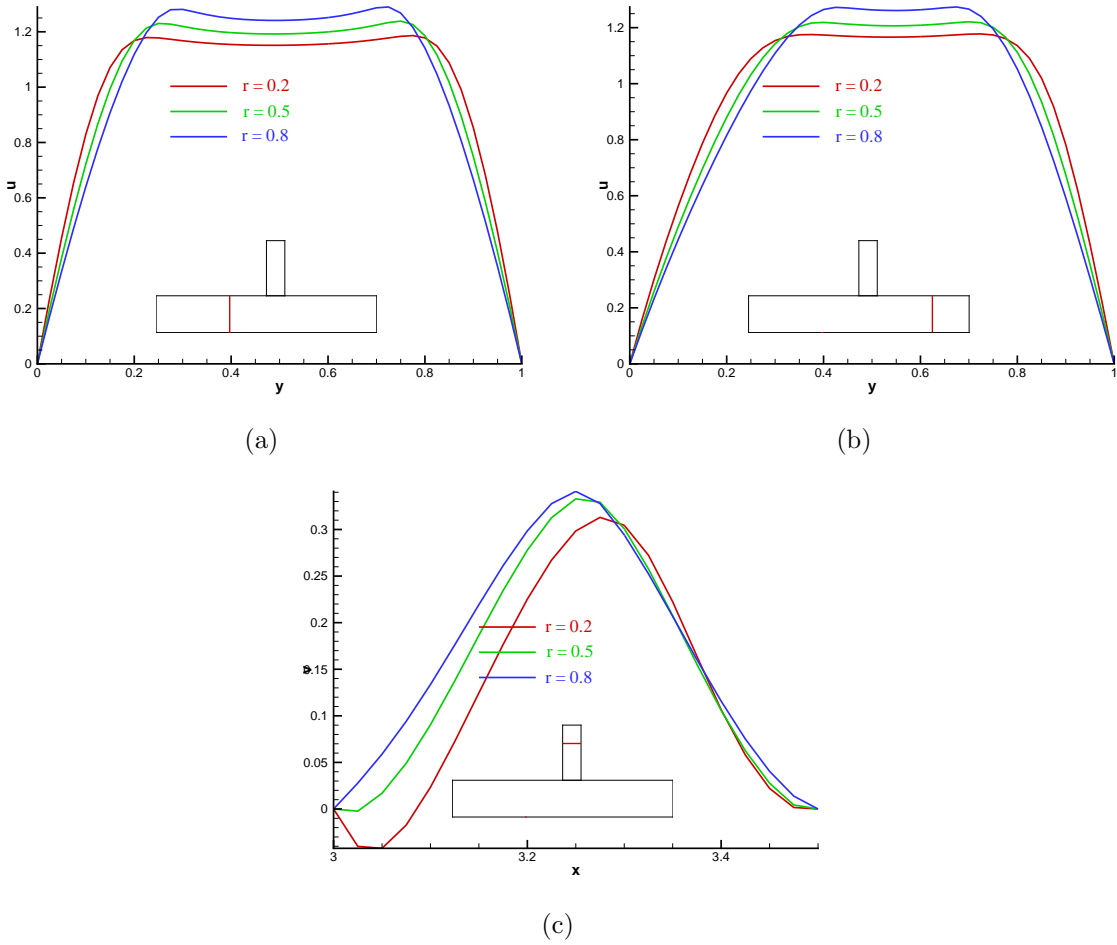
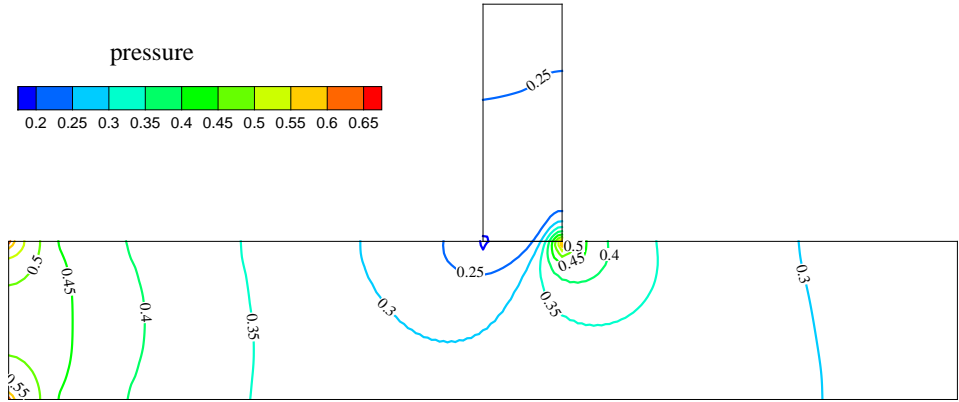
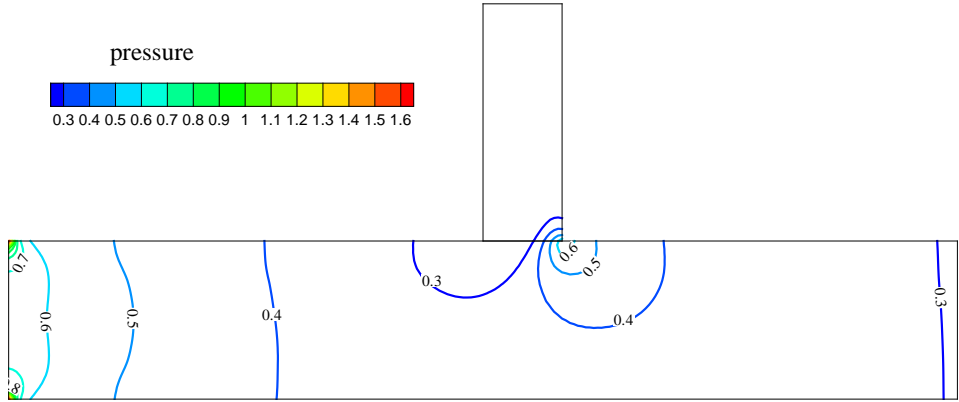


Figure 3.36: Velocity profile of the velocity components  $u, v$  as the functions of  $y, x$

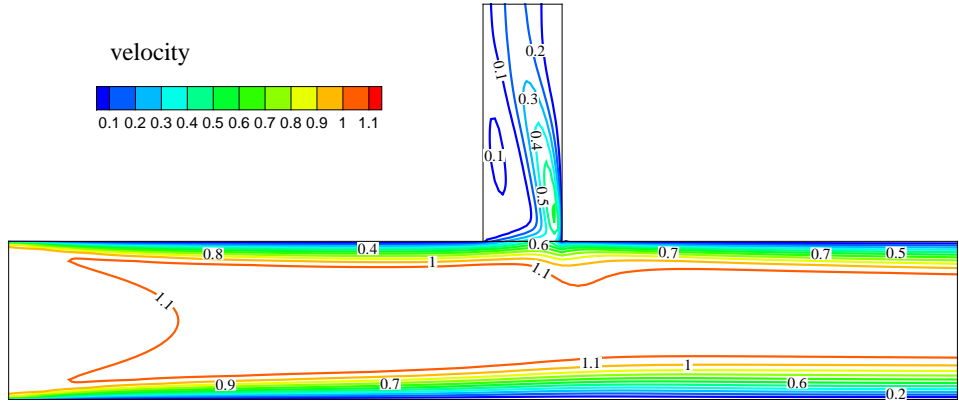


(a) Newtonian

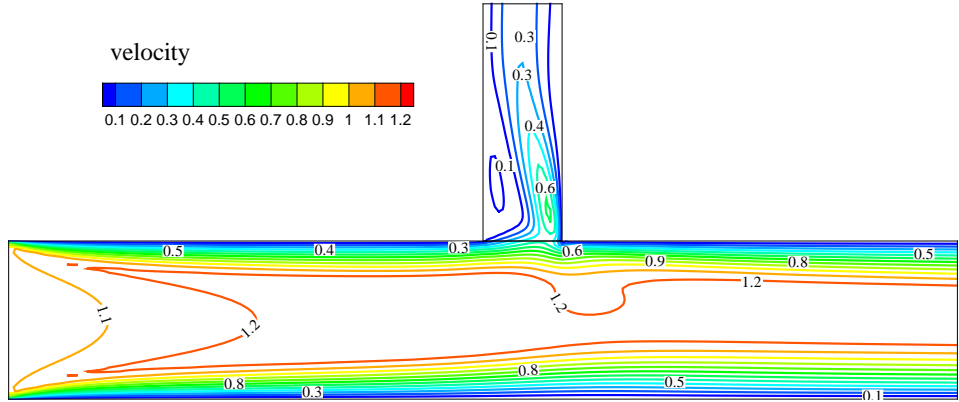


(b) non-Newtonian

Figure 3.37: Pressure isolines of Newtonian fluids flow versus shear thickening non-Newtonian fluids flow with  $Re = 600$  - a) Newtonian - b) non-Newtonian



(a) Newtonian



(b) non-Newtonian

Figure 3.38: Velocity isolines of Newtonian fluids flow versus shear thickening non-Newtonian fluids flow with  $Re = 600$  - a) Newtonian - b) non-Newtonian



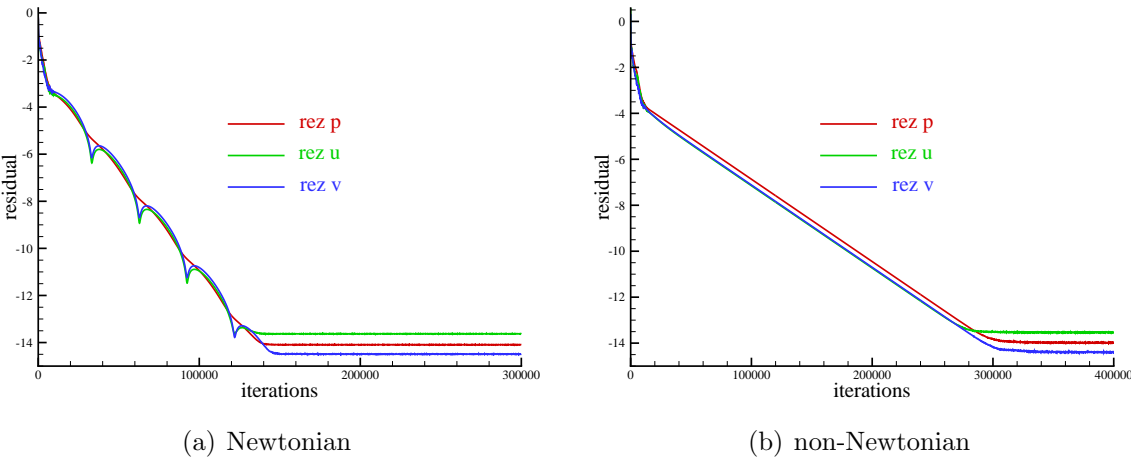


Figure 3.39: History of the convergence of Newtonian fluids flow versus shear thickening non-Newtonian fluids flow with  $Re = 600$  - a) Newtonian - b) non-Newtonian

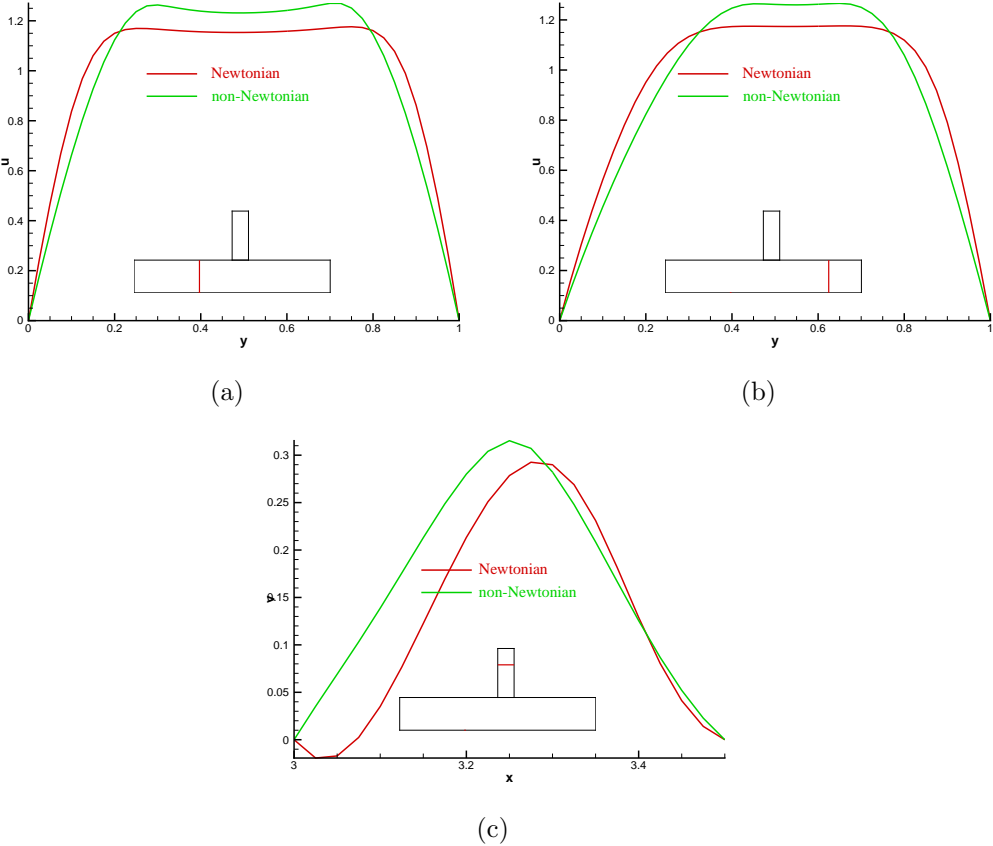


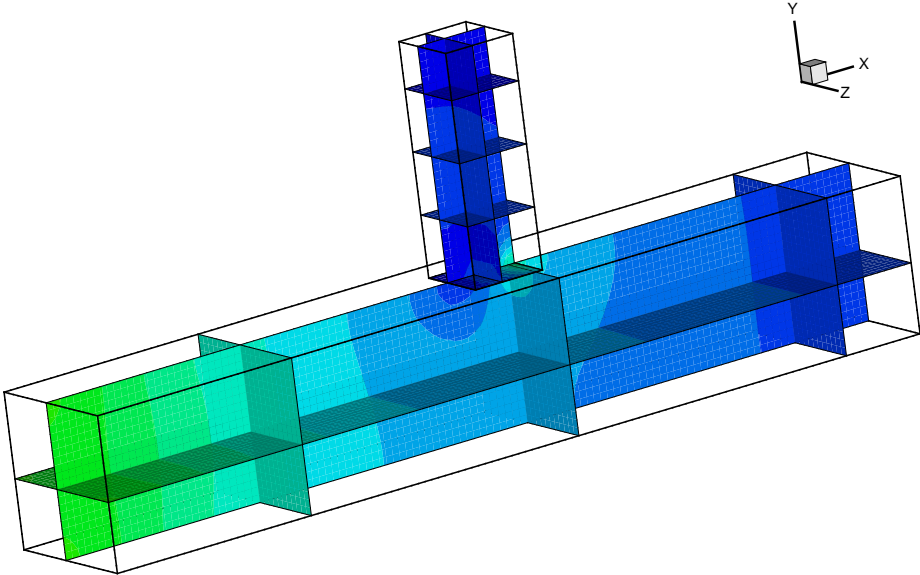
Figure 3.40: Nondimensional velocity profile of velocity component  $u$  as the function of  $y$  for Newtonian fluids flow versus shear thickening non-Newtonian fluids flow with  $Re = 600$

### 3.4 Three Dimensional Steady Solutions of Non-Newtonian Fluids

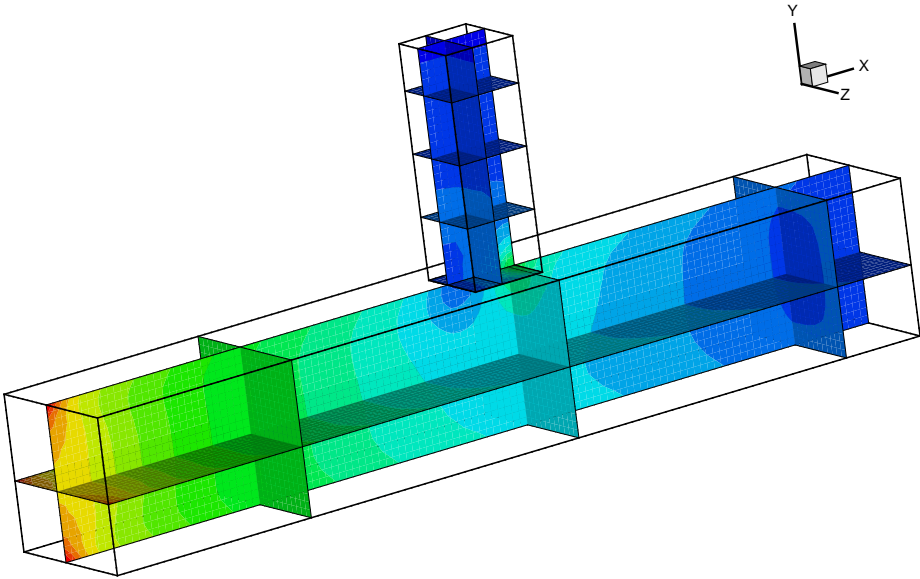
Three dimensional numerical results of incompressible laminar viscous flows for non-Newtonian fluids are presented and compared with numerical solutions of Newtonian fluids. Numerical simulations were performed for three dimensional branching channels with one entrance and two exit parts. The steady boundary conditions are used for the steady state solutions.

This section is concerned on the comparing of the Newtonian and shear thickening non-Newtonian fluids flow. The value of the power-law index  $r$  for non-Newtonian fluids flow is equal to 0.5. Reynolds number for the comparing is chosen as 400.

From the figure 3.43 it results that the maximal pressure value is higher for non-Newtonian fluids flow than for Newtonian fluids flow. Also the maximal velocity value is higher for non-Newtonian than for Newtonian fluids flow. It follows from the characterization of the considered fluids. If constant  $r$  (power-law index) is close to the value 1, the pressure is increasing in the inlet part. The same conclusion were done for two dimensional case. In that section three value of power-law index were tested. And it could be seen that with increasing  $r$  the pressure increased. In this section only one value of power-law index was tested but the same observation can be done.

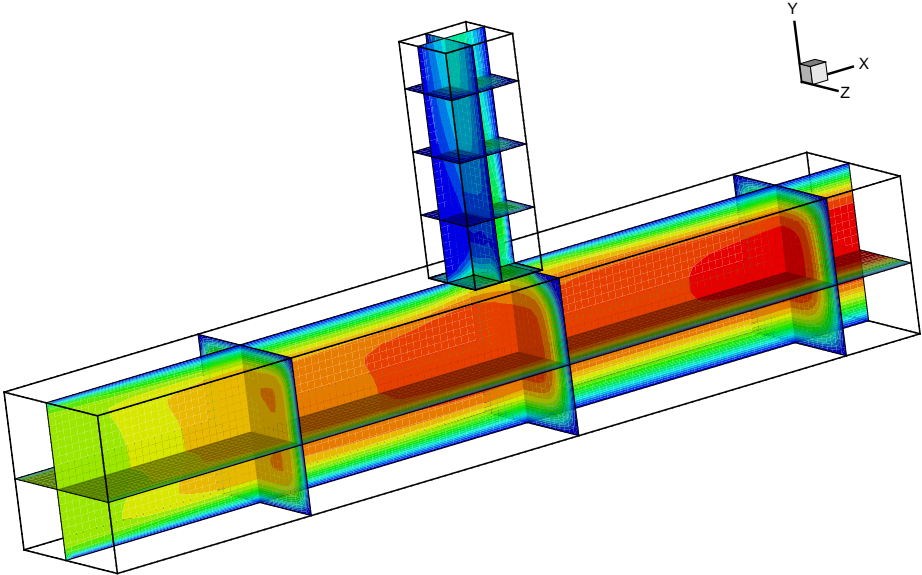


(a) Newtonian

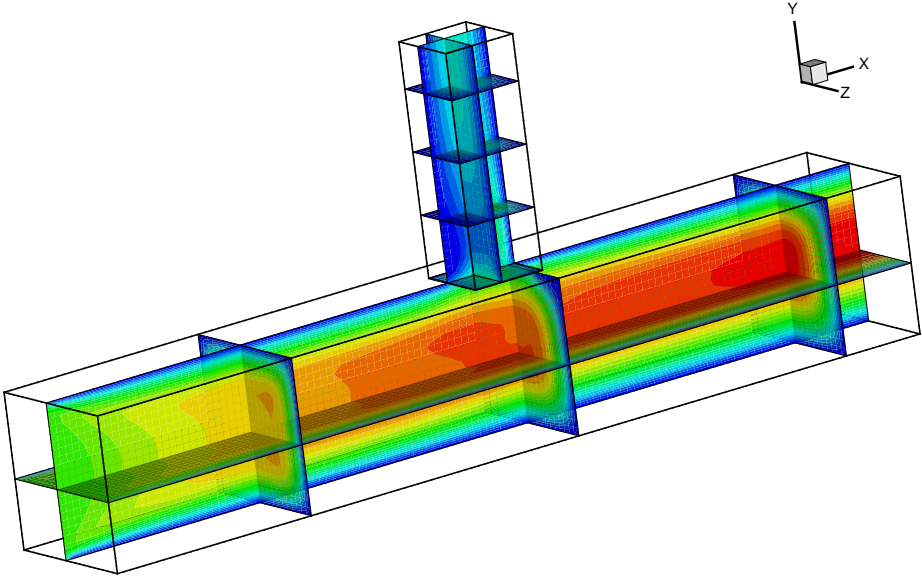


(b) non-Newtonian

Figure 3.41: Pressure isolines of Newtonian fluids flow versus shear thickening non-Newtonian fluids flow with  $Re = 400$  - a) Newtonian - b) non-Newtonian

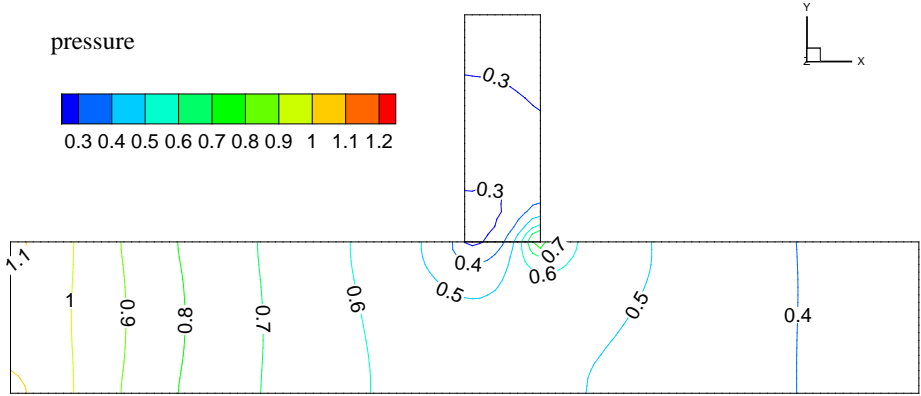


(a) Newtonian

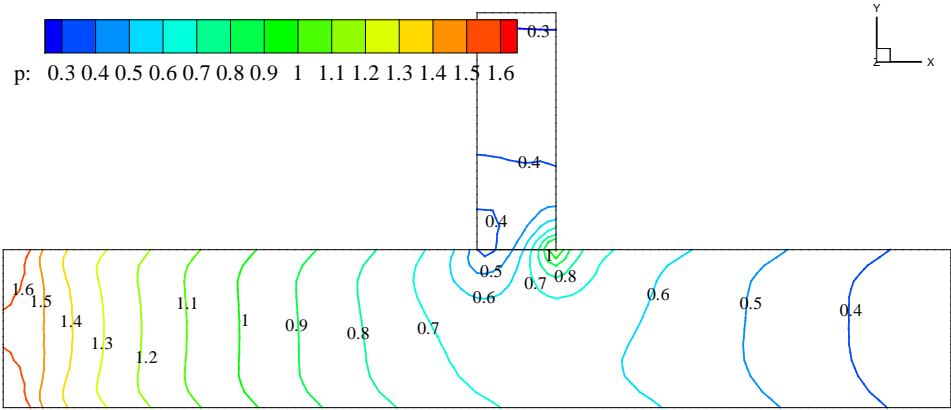


(b) non-Newtonian

Figure 3.42: Velocity isolines of Newtonian fluids flow versus shear thickening non-Newtonian fluids flow with  $Re = 400$  - a) Newtonian - b) non-Newtonian

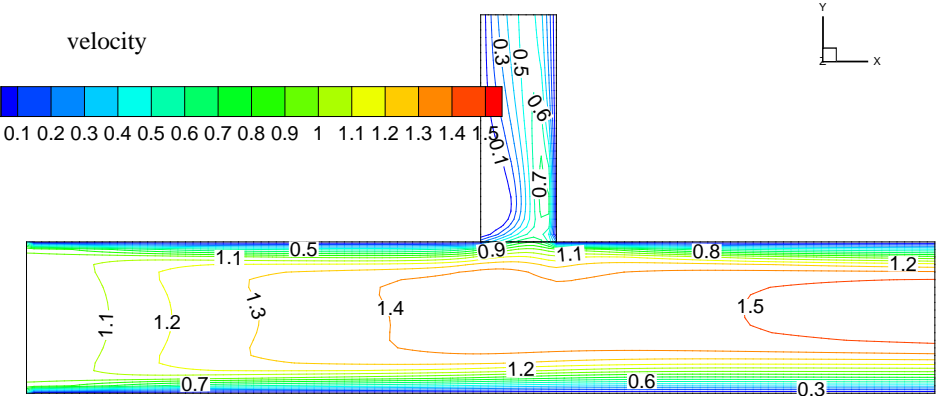


(a) Newtonian

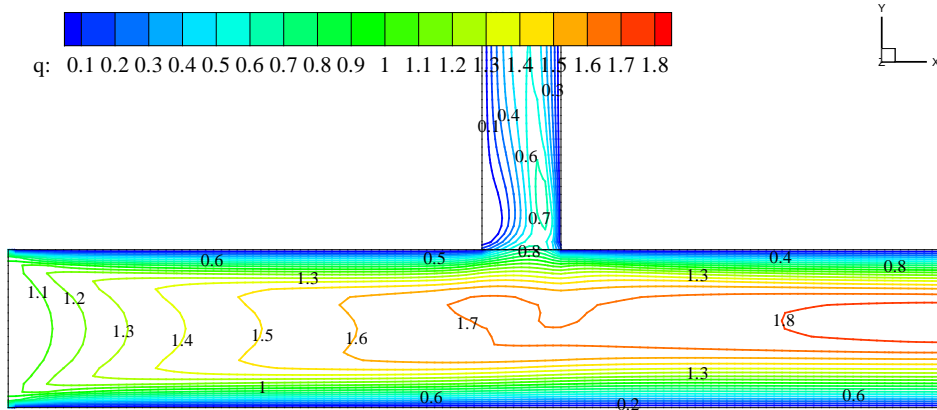


(b) non-Newtonian

Figure 3.43: Pressure isolines of Newtonian fluids flow versus shear thickening non-Newtonian fluids flow with  $Re = 400$  - a) Newtonian - b) non-Newtonian

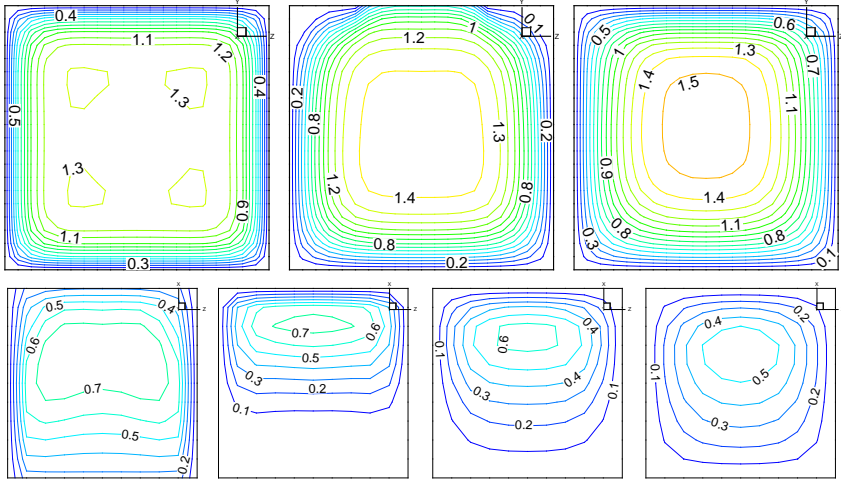


(a) Newtonian

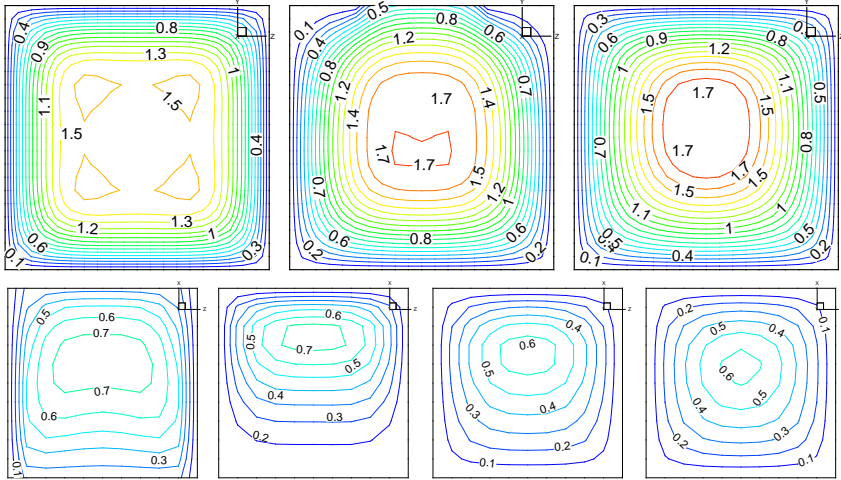


(b) non-Newtonian

Figure 3.44: Velocity isolines of Newtonian fluids flow versus shear thickening non-Newtonian fluids flow with  $Re = 400$  - a) Newtonian - b) non-Newtonian

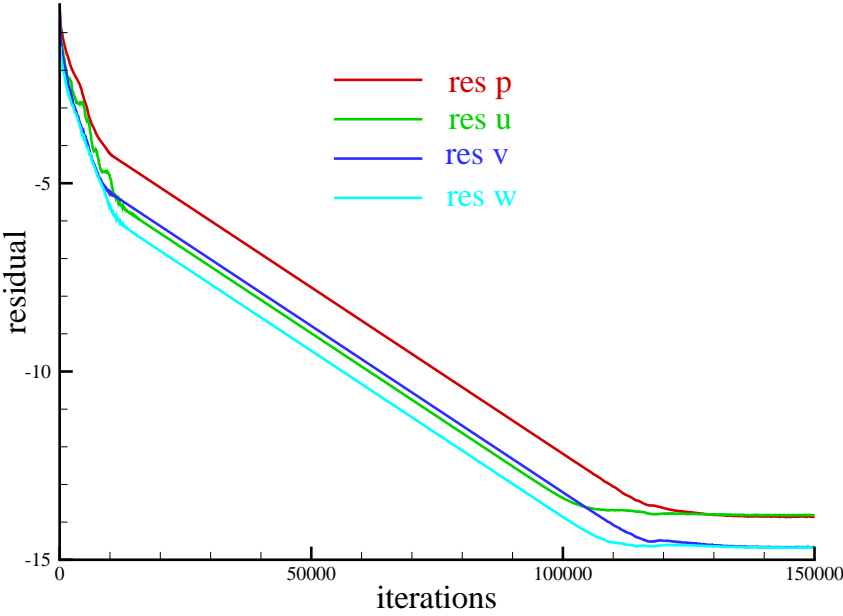


(a) Newtonian

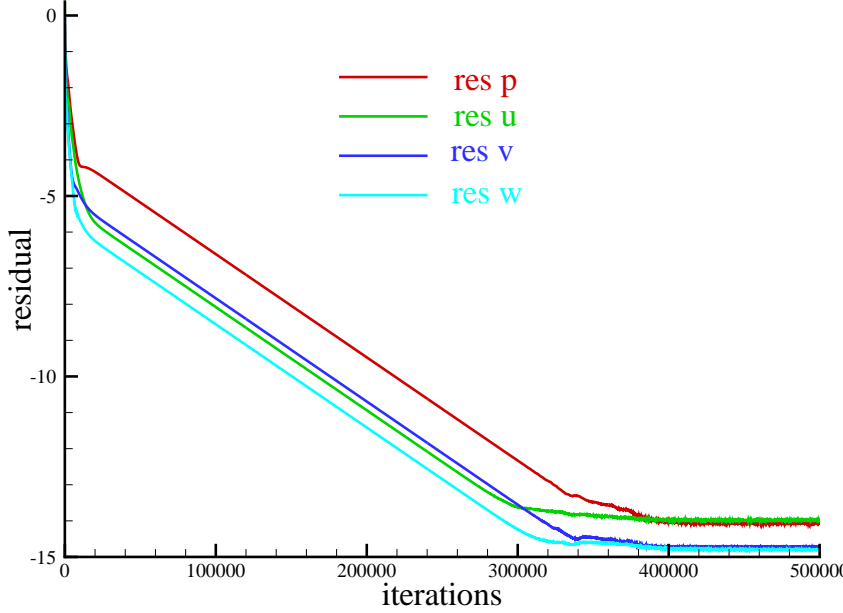


(b) non-Newtonian

Figure 3.45: Cuts through the main channel and through the small branch of Newtonian fluids flow versus shear thickening non-Newtonian fluids flow with  $Re = 400$  - a) Newtonian - b) non-Newtonian



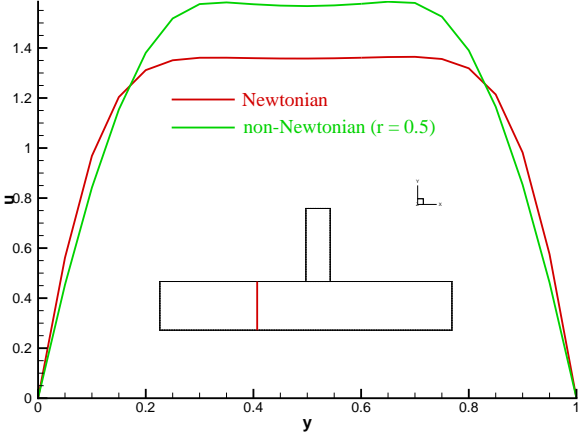
(a) Newtonian



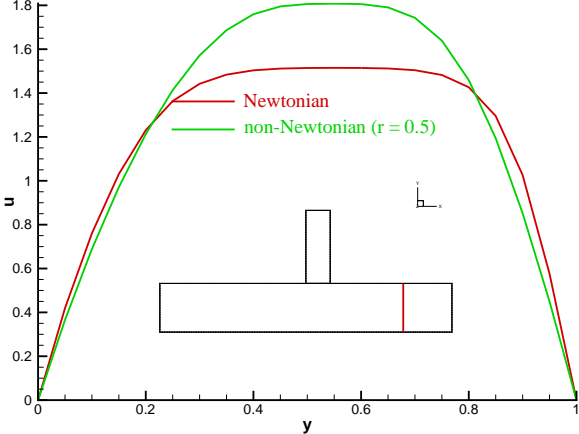
(b) non-Newtonian

Figure 3.46: History of the convergence of Newtonian fluids flow versus shear thickening non-Newtonian fluids flow with  $Re = 400$  - a) Newtonian - b) non-Newtonian

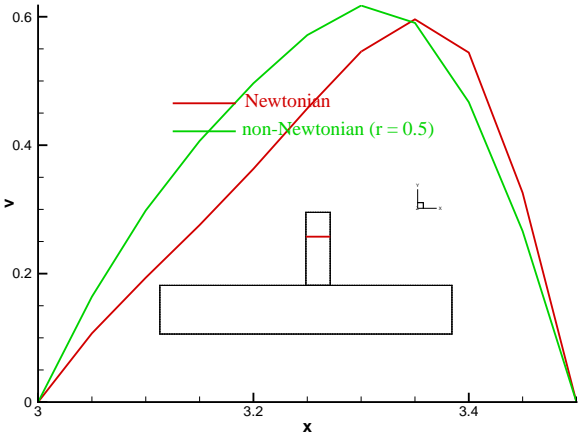




(a)



(b)



(c)

Figure 3.47: Nondimensional velocity profile of the velocity components  $u, v$  as the functions of  $y, x$

### 3.5 Two Dimensional Unsteady Numerical Solutions of Newtonian Fluids

In this section, unsteady numerical results of incompressible laminar viscous flows for Newtonian fluids flow are presented and compared. The unsteady boundary conditions are used for the unsteady simulation. The tested domain is the branching channel in the shape T with the angle 90 degrees.

Two unsteady methods are used for unsteady computations. The artificial compressibility method and the dual-time stepping method are considered.

First part of this section is concerned on the comparing these two methods. Second part is concerned on the testing two parameters in the unsteady numerical simulation: Reynolds number and the frequency by artificial compressibility method.

The pressure outlet value in the small branch is evaluated with respect to formula (2.73)

$$p_{01} = \frac{1}{4} \left( 1 + \frac{1}{2} \sin(\omega t) \right), \quad (3.1)$$

where  $\omega$  is the angular velocity and it's defined as  $\omega = 2\pi f$ , where  $f$  is the frequency.

In the first part for both unsteady methods the frequency  $f$  is equal to 2Hz (using in the nondimensional value) and the artificial compressibility coefficient  $\beta$  is set to the value 10 ( $\beta^2 = 100$ ). In the figure 3.48 the curve of the pressure as the function of the time is plotted with the symbols for positions of five numerical results for the artificial compressibility method - green color and dual-time stepping method - blue color. In the figure 3.49 graphs of the velocity as the function of the time are plotted for both methods. By the blue symbols the positions, where the numerical results are shown, are sketched. These five numerical results are presented in the figure 3.50 for the artificial compressibility method and in the figure 3.51 five numerical results during one period of the pressure function are shown for dual-time stepping method. The results presented are for non-dimensional real-time  $\Delta t = 0.02$ . In the figure 3.52 the history of the decadic logarithm of the  $L^2$  norm of the steady residual in real time for the numerical simulation performed with the use of artificial compressibility method is shown. It reflects the periodic behaviour of the flow in real time by means of periodic residual oscillations. In the figure 3.53 the decadic logarithm of the  $L^2$  norm of the unsteady residual by the dual-time stepping method is presented.

Last part of this section is devoted to the testing of Reynolds number and to the testing of the frequency by the artificial compressibility method.

In the figures 3.54 - 3.57 the testing of Reynolds number is presented. Three values of Reynolds number are used:  $Re = 600$  (figure 3.50),  $Re = 800$ ,  $Re = 1000$ . The artificial compressibility method is used for this testing. The frequency is equal to 2Hz and artificial compressibility coefficient  $\beta$  is equal to 10 ( $\beta^2 = 100$ ). In the figure 3.58 the history of the decadic logarithm of the  $L^2$  norm of the steady residual in real time for the numerical simulation is presented.

In the figures 3.59 - 3.62 the test of the frequency is shown. Three values of frequency are used:  $f = 2\text{Hz}$  (figure 3.50),  $f = 10\text{Hz}$ ,  $f = 20\text{Hz}$ . The artificial compressibility method

is used for this testing. The Reynolds number is equal to 600 and artificial compressibility coefficient  $\beta$  is equal to 10 ( $\beta^2 = 100$ ). In the figure 3.63 the history of the  $L^2$  norm of the steady residual in real time for the numerical simulation is shown.

It results that with increasing frequency the amplitude of the velocity decreases. For the test of Reynolds number it follows that for increasing Reynolds number the amplitude of the velocity is nearly identical.

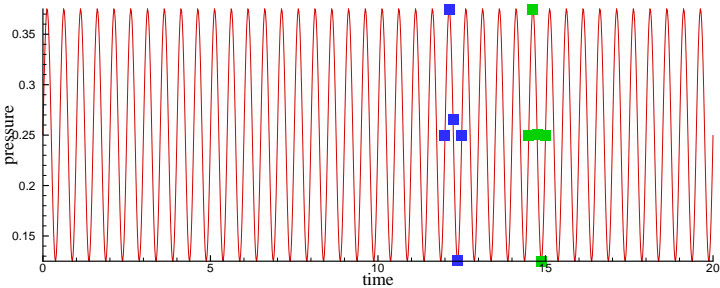
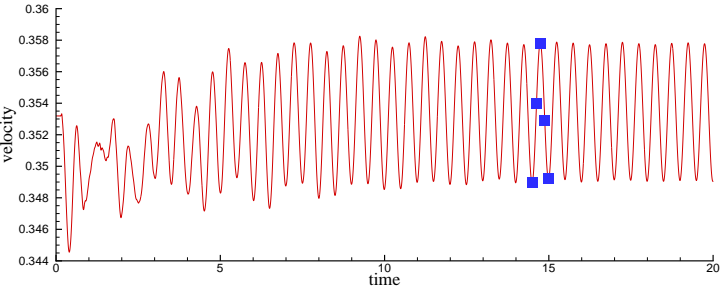
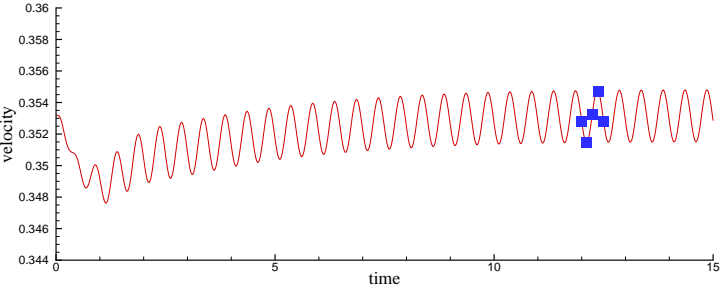


Figure 3.48: The graph of the pressure as the function of the time in the outlet of the domain - artificial compressibility method - green - dual-time stepping method - blue



(a) artificial compressibility method



(b) dual-time stepping method

Figure 3.49: The graph of the velocity as the function of the time in the outlet of the domain - a) artificial compressibility method - b) dual-time stepping method

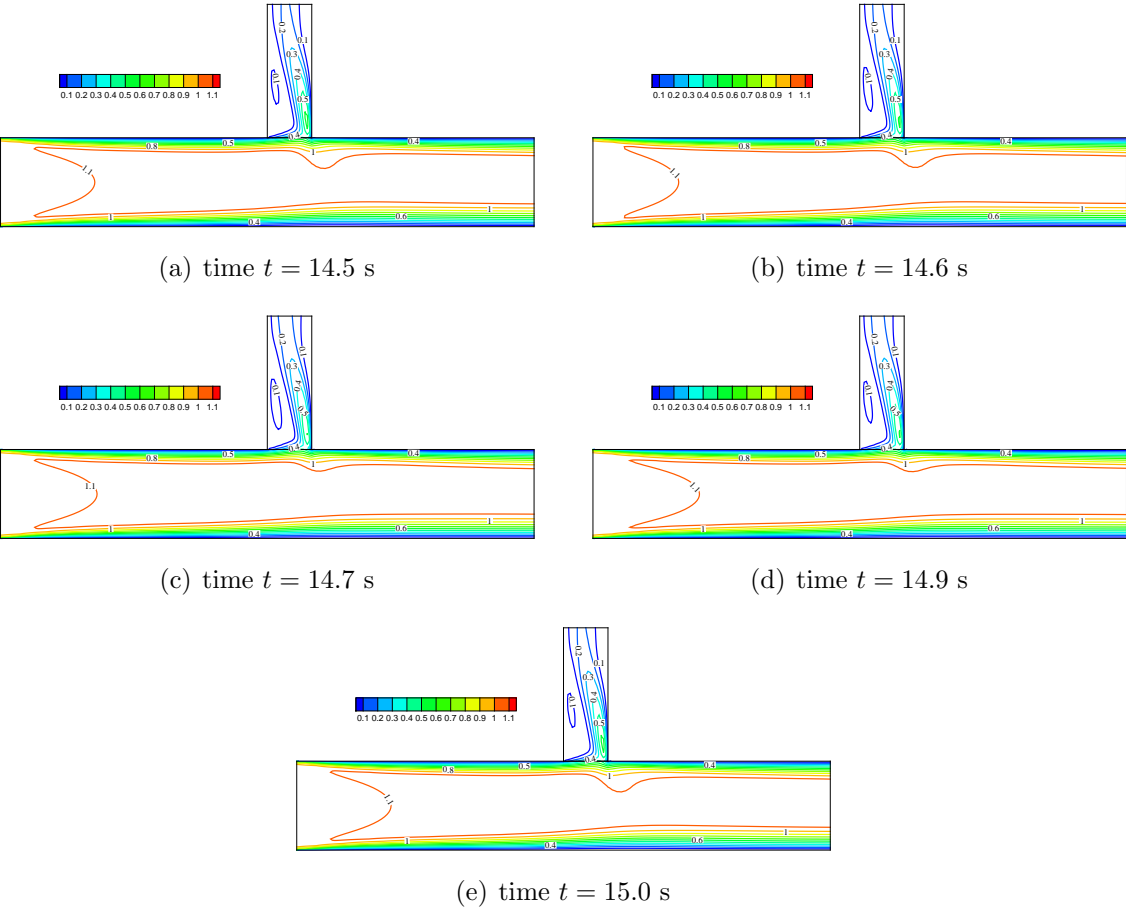


Figure 3.50: Unsteady numerical results during one period by artificial compressibility method - a) time 14.5 s - b) time 14.6 s - c) time 14.7 s - d) time 14.9 s - e) time 15.0 s

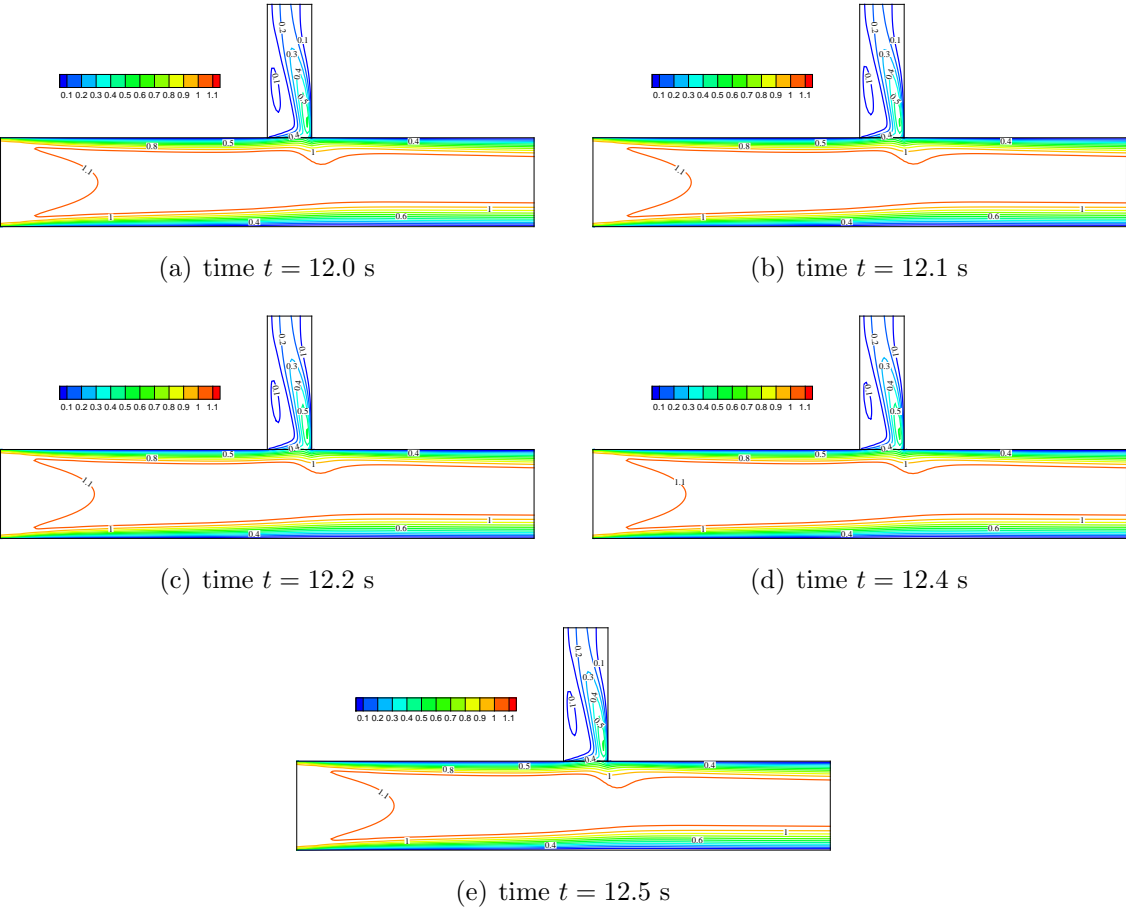


Figure 3.51: Unsteady numerical results during one period by dual-time stepping method - a) time 12.0 s - b) time 12.1 s - c) time 12.2 s - d) time 12.4 s - e) time 12.5 s

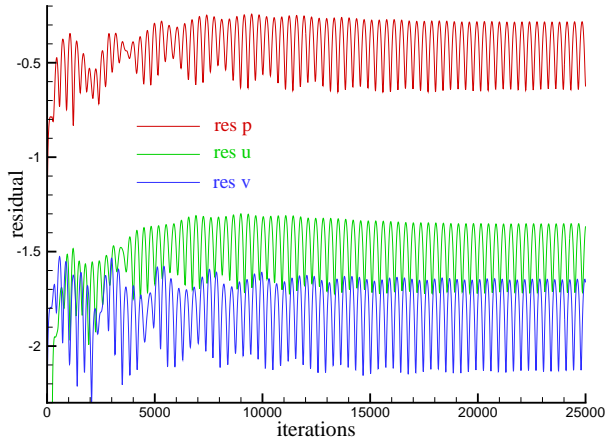


Figure 3.52: Decadic logarithm of the  $L^2$  norm of the steady residual in real time by artificial compressibility method

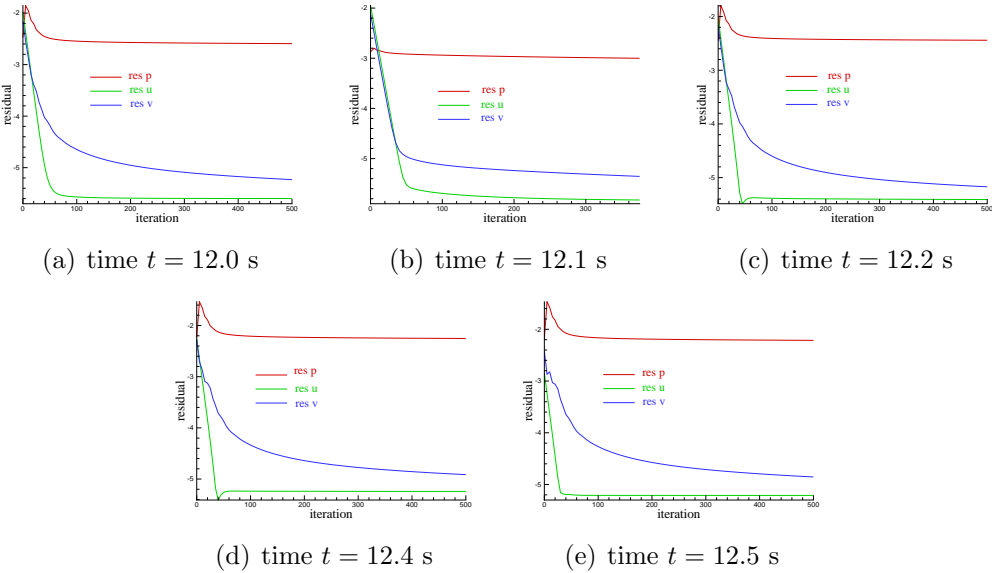


Figure 3.53: Decadic logarithm of the  $L^2$  norm of the unsteady residual during one period by dual-time stepping method - a) time 12.0 s - b) time 12.1 s - c) time 12.2 s - d) time 12.4 s - e) time 12.5 s

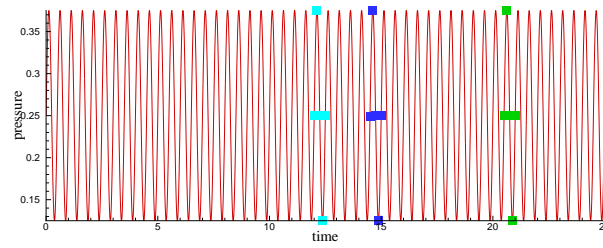
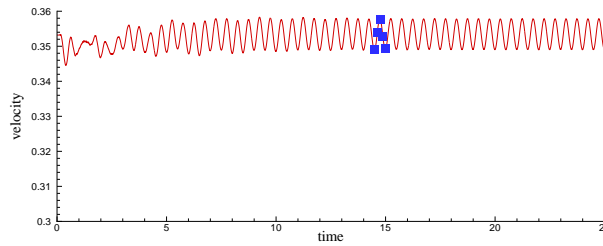
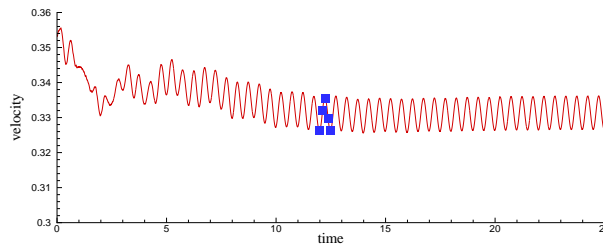


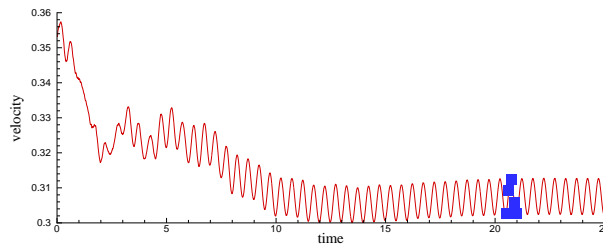
Figure 3.54: The graph of the pressure as the function of the time in the outlet of the domain -  $Re = 600$  - blue,  $Re = 800$  - cyan,  $Re = 1000$  - green



(a)  $Re = 600$



(b)  $Re = 800$



(c)  $Re = 1000$

Figure 3.55: The graph of the velocity as the function of the time in the outlet of the domain - a)  $Re = 600$  - b)  $Re = 800$  - c)  $Re = 1000$

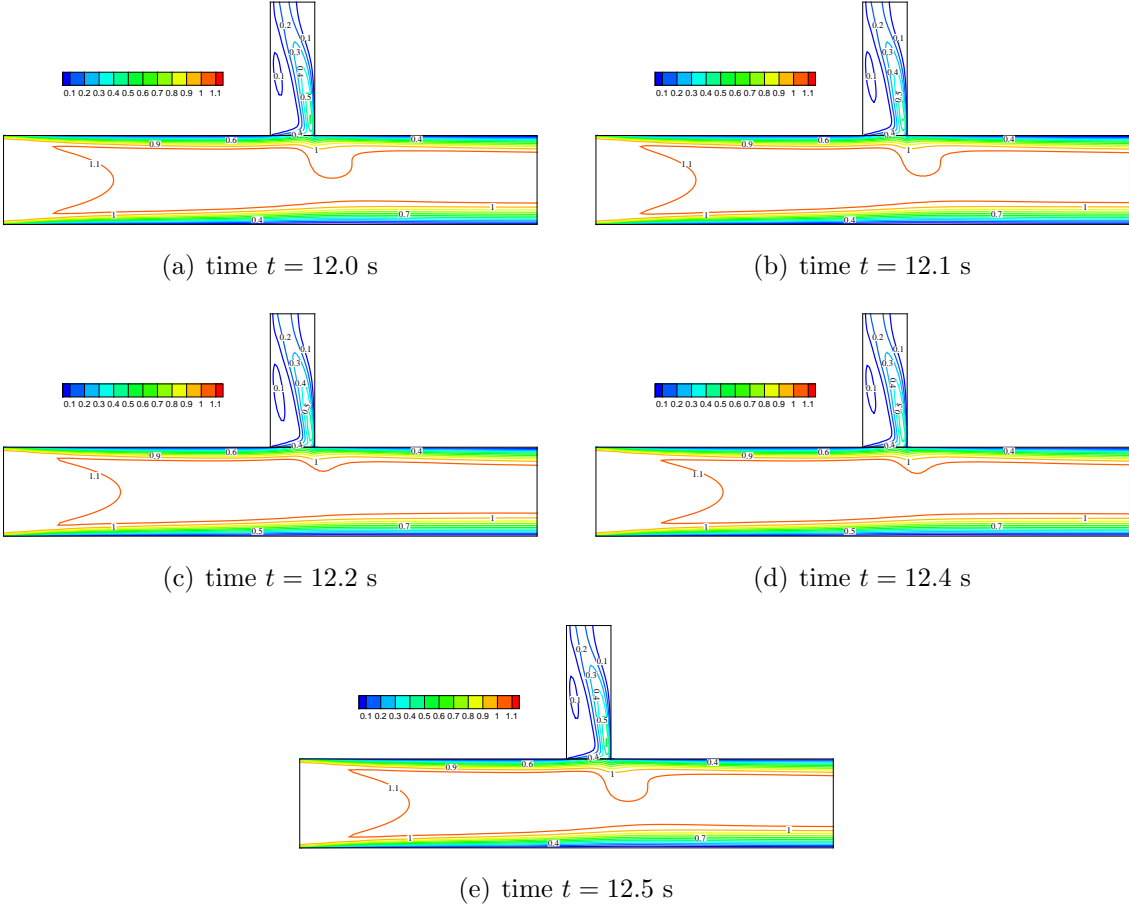


Figure 3.56: Unsteady numerical results during one period by artificial compressibility method with  $Re = 800$  - a) time 12.0 s - b) time 12.1 s - c) time 12.2 s - d) time 12.4 s - e) time 12.5 s



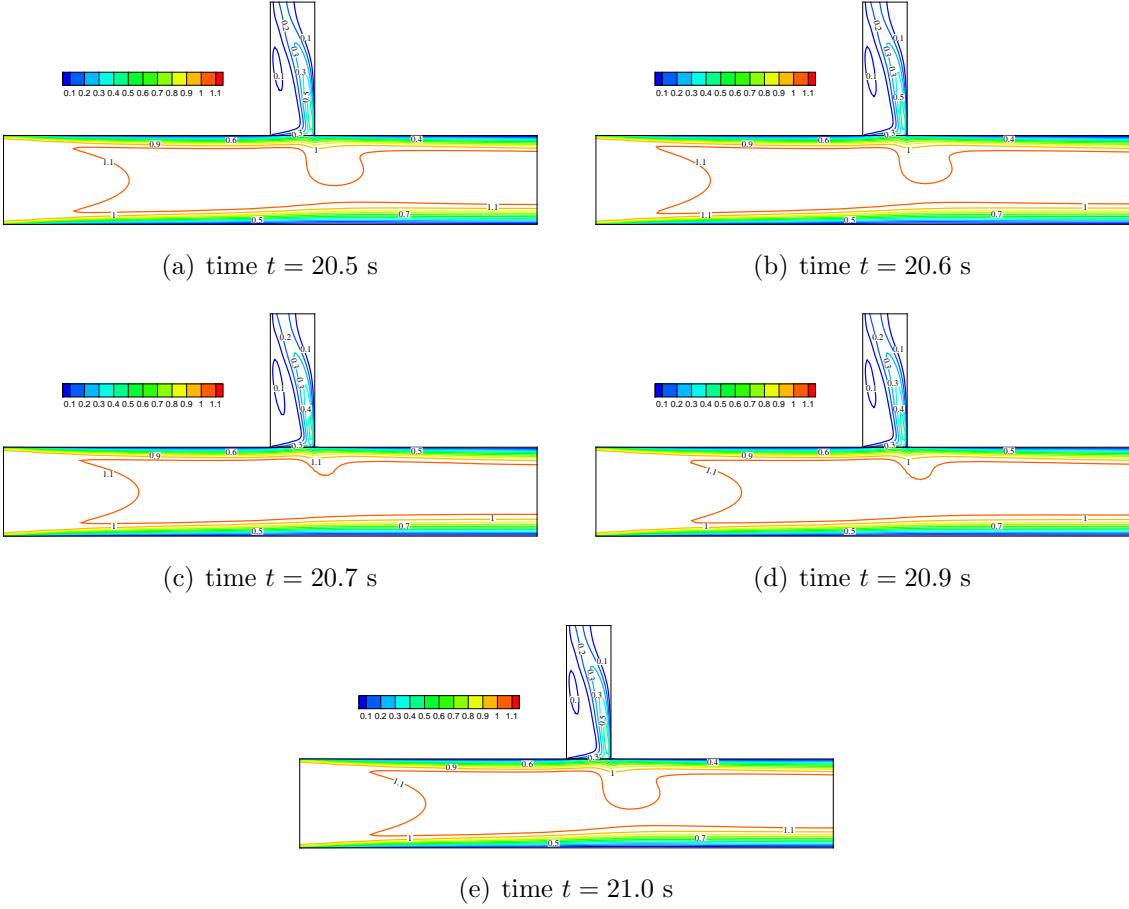


Figure 3.57: Unsteady numerical results during one period by artificial compressibility method - with  $Re = 1000$  - a) time 20.5 s - b) time 20.6 s - c) time 20.7 s - d) time 20.9 s - e) time 21.0 s

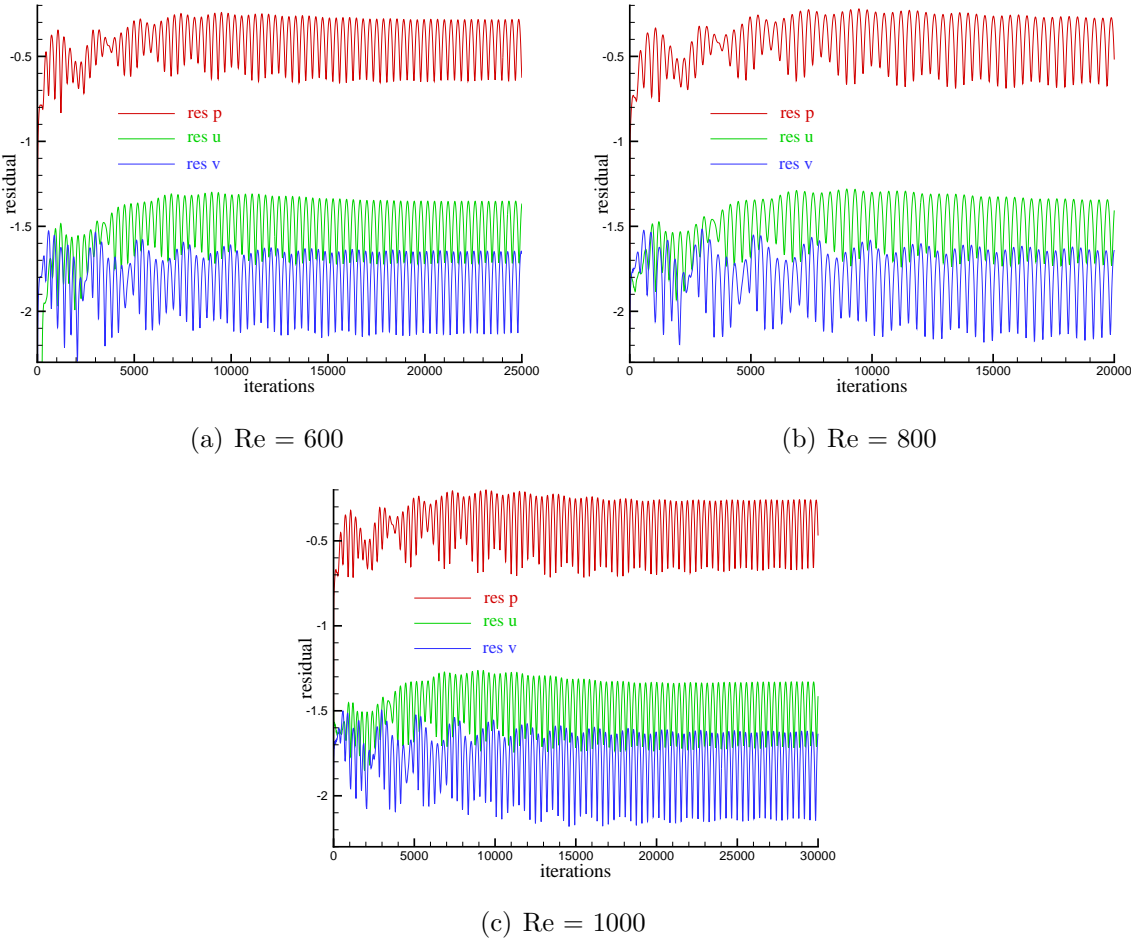


Figure 3.58: Decadic logarithm of the  $L^2$  norm of the steady residual in real time by artificial compressibility method in the branching channel for different Reynolds numbers - a) Re = 600 - b) Re = 800 - c) Re = 1000

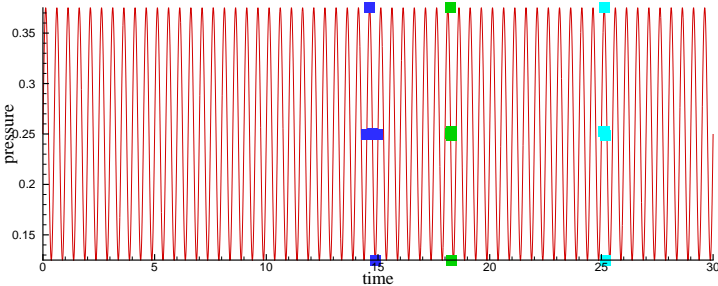
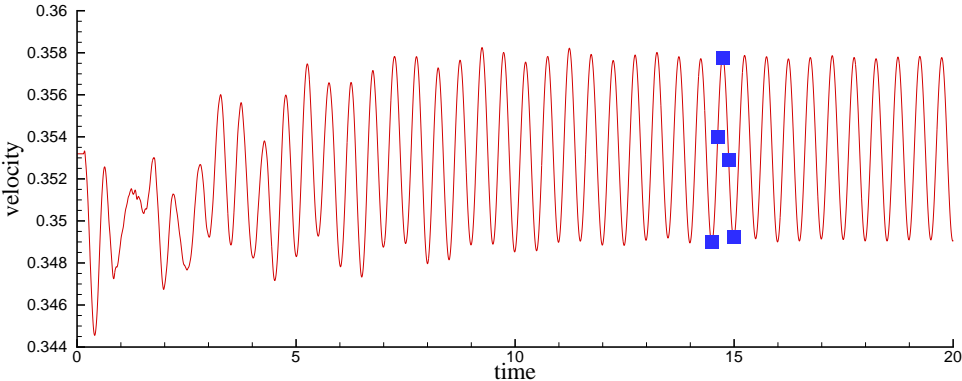
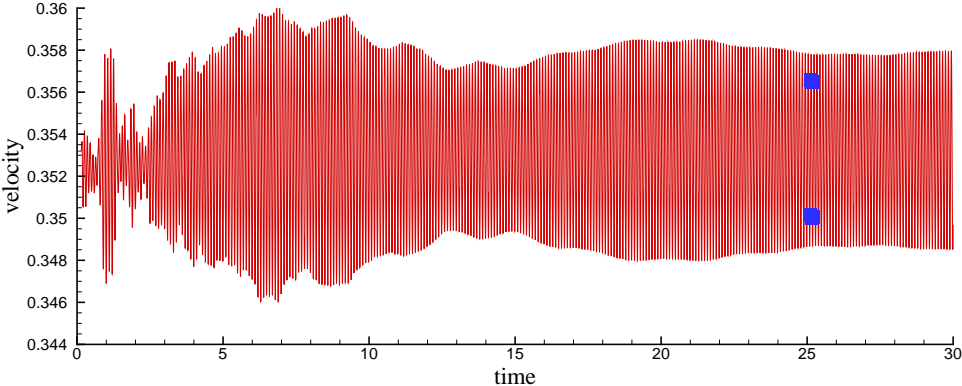


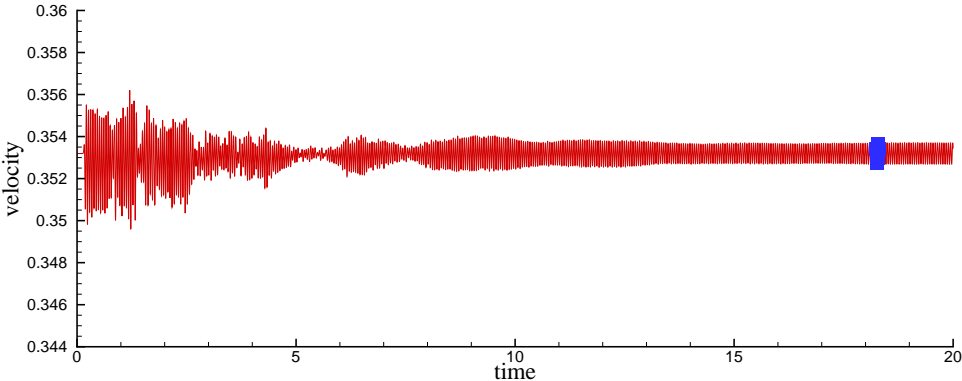
Figure 3.59: The graph of the pressure as the function of the time in the outlet of the domain with different frequency  $f$  -  $f = 2\text{Hz}$  - blue,  $f = 10\text{Hz}$  - cyan,  $f = 20\text{Hz}$  - green



(a) frequency = 2Hz



(b) frequency = 10Hz



(c) frequency = 20Hz

Figure 3.60: The graph of the velocity as the function of the time in the outlet of the domain - a) frequency = 2Hz - b) frequency = 10Hz - c) frequency = 20Hz

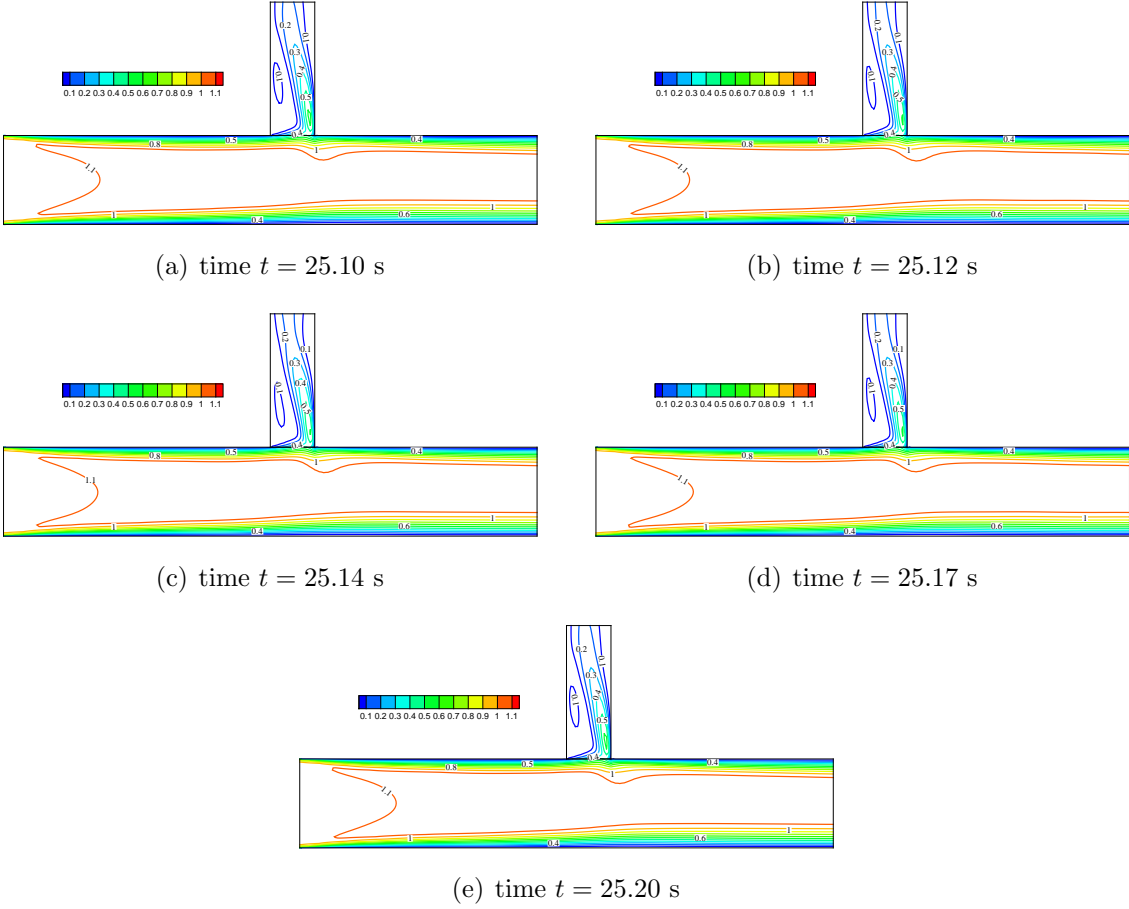


Figure 3.61: Unsteady numerical results during one period by artificial compressibility method with frequency = 10Hz - a) time 25.10 s - b) time 25.12 s - c) time 25.14 s - d) time 25.17 s - e) time 25.20 s

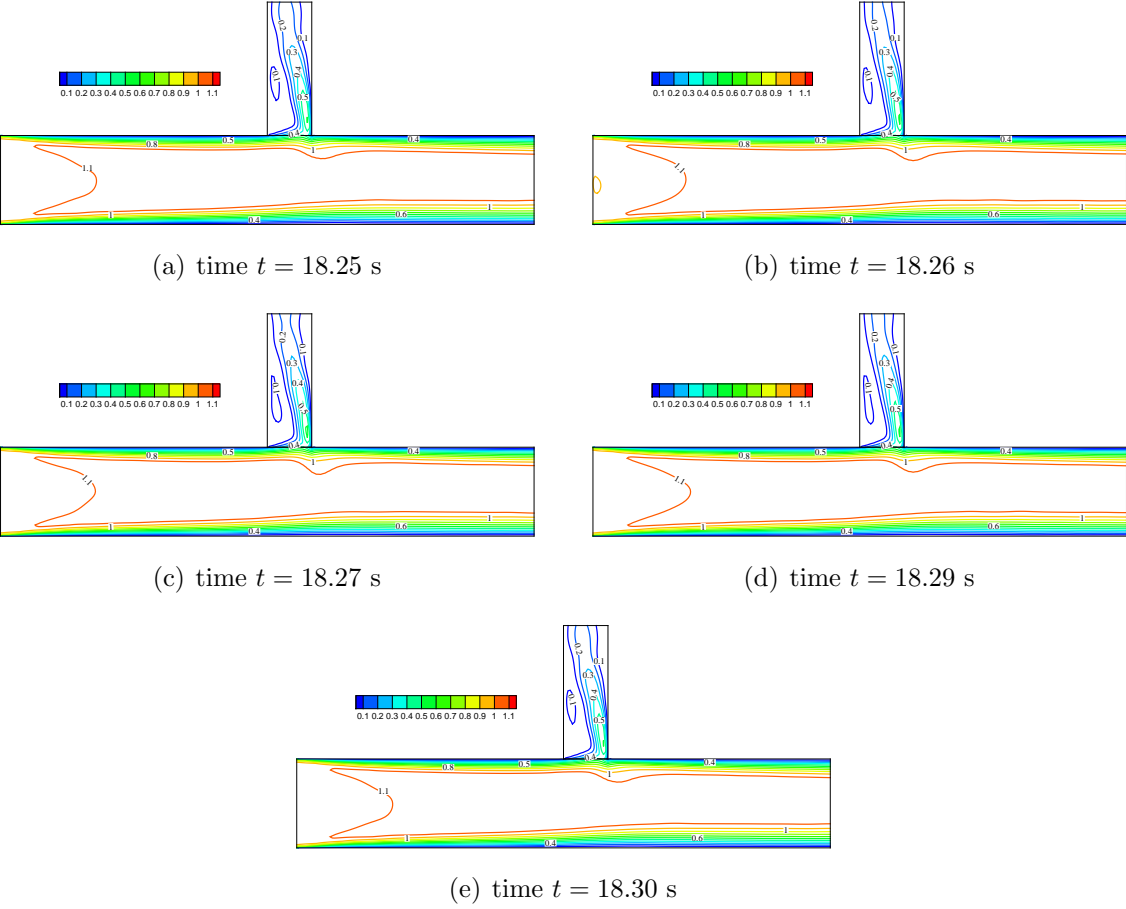
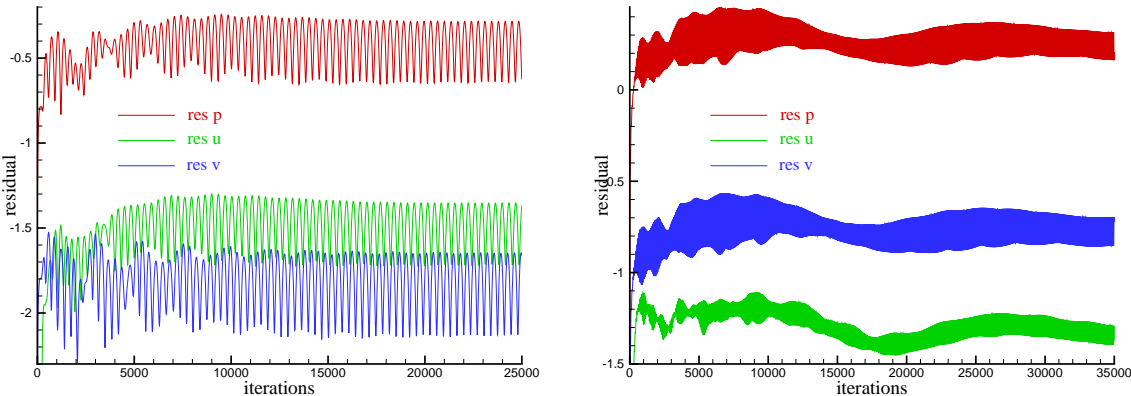
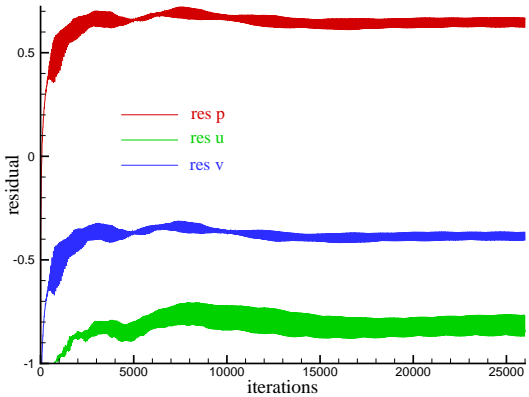


Figure 3.62: Unsteady numerical results during one period by artificial compressibility method with frequency = 20Hz - a) time 18.25 s - b) time 18.26 s - c) time 18.27 s - d) time 18.29 s - e) time 18.30 s



(a)  $f = 2$  Hz

(b)  $f = 10$  Hz



(c)  $f = 20$  Hz

Figure 3.63: Decadic logarithm of the  $L^2$  norm of the steady residual in real time by artificial compressibility method in the branching channel for different frequency - a)  $f = 2$  Hz - b)  $f = 10$  Hz - c)  $f = 20$  Hz

### 3.6 Two Dimensional Steady Solutions of Newtonian Fluids - Test of the Meshes

In this section the numerical solution of Newtonian fluids flow in three types of the meshes are tested. The using type of the domain is the branching channel in the shape T with the angle 90 degrees. First mesh is with the step of the mesh  $h = 0.05$  (2700 cells), second mesh is with the step  $h_1 = \frac{h}{2} = 0.025$  (10800 cells) and the last mesh is with the step  $h_2 = \frac{h}{4} = 0.0125$  (43200 cells).

Reynolds number for this computations is set to be 400. The numerical solutions are compared for these three meshes in the form of the pressure isolines (figure 3.65) and the velocity isolines (figure 3.66). The history of the convergence for all tested cases are presented (figure 3.64).

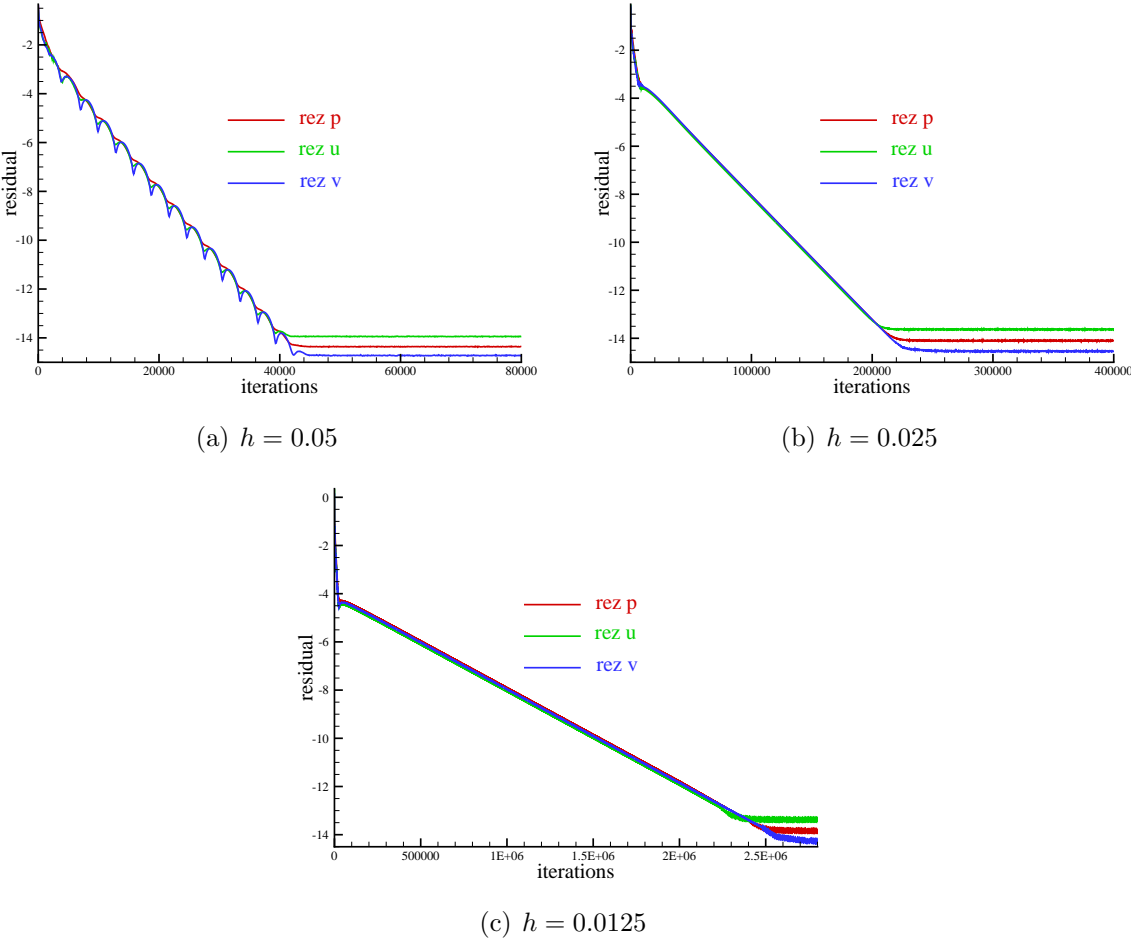
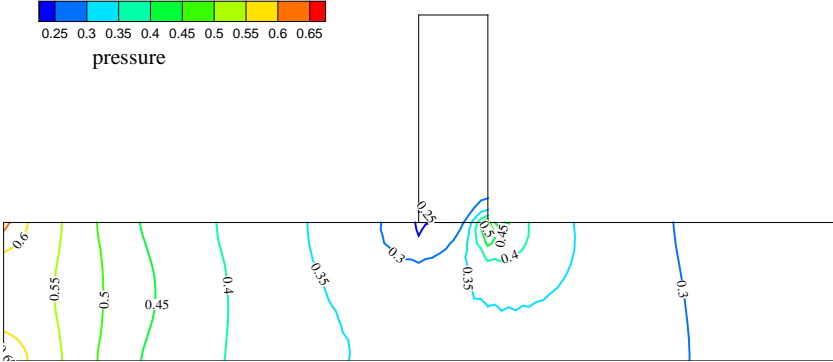
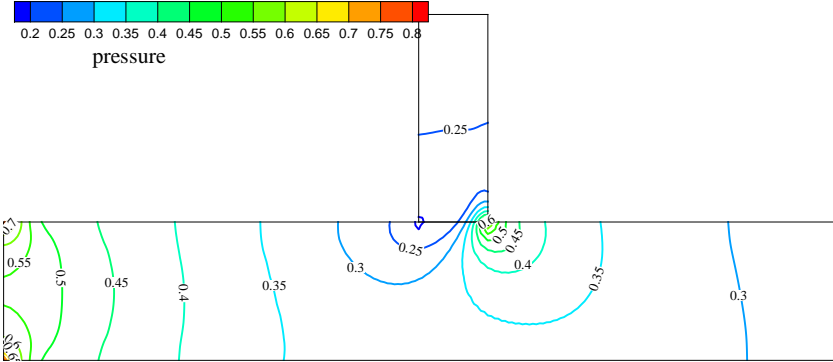


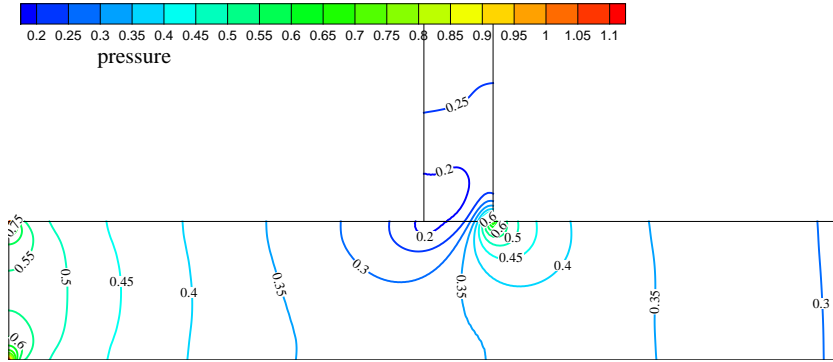
Figure 3.64: The convergence history of Newtonian fluids flow in the branching channel with the angle 90 degrees - a)  $h = 0.05$  - b)  $h = 0.025$  - c)  $h = 0.0125$



(a)  $h = 0.05$



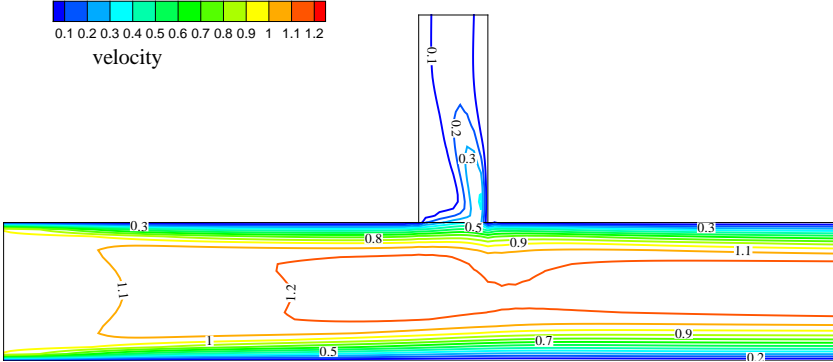
(b)  $h = 0.025$



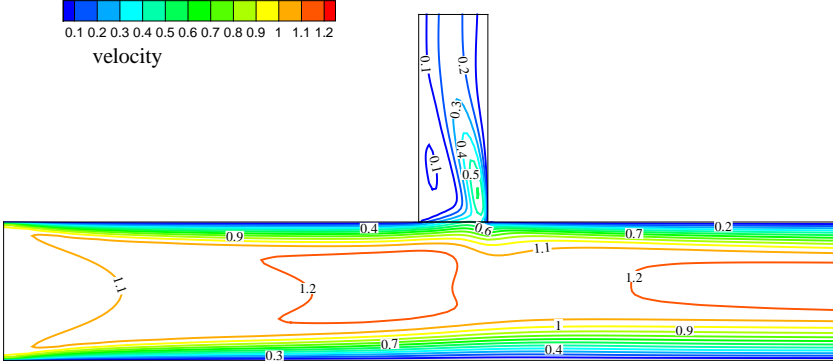
(c)  $h = 0.0125$

Figure 3.65: Pressure isolines of Newtonian fluids flow in the branching channel with the angle 90 degrees - a)  $h = 0.05$  - b)  $h = 0.025$  - c)  $h = 0.0125$

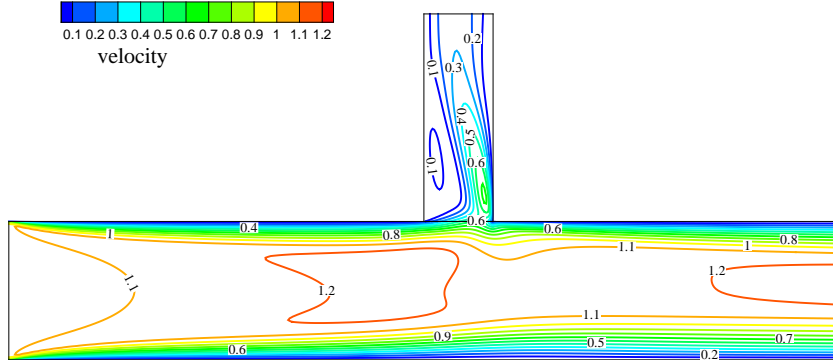




(a)  $h = 0.05$



(b)  $h = 0.025$



(c)  $h = 0.0125$

Figure 3.66: Velocity isolines of Newtonian fluids flow in the branching channel with the angle 90 degrees - a)  $h = 0.05$  - b)  $h = 0.025$  - c)  $h = 0.0125$

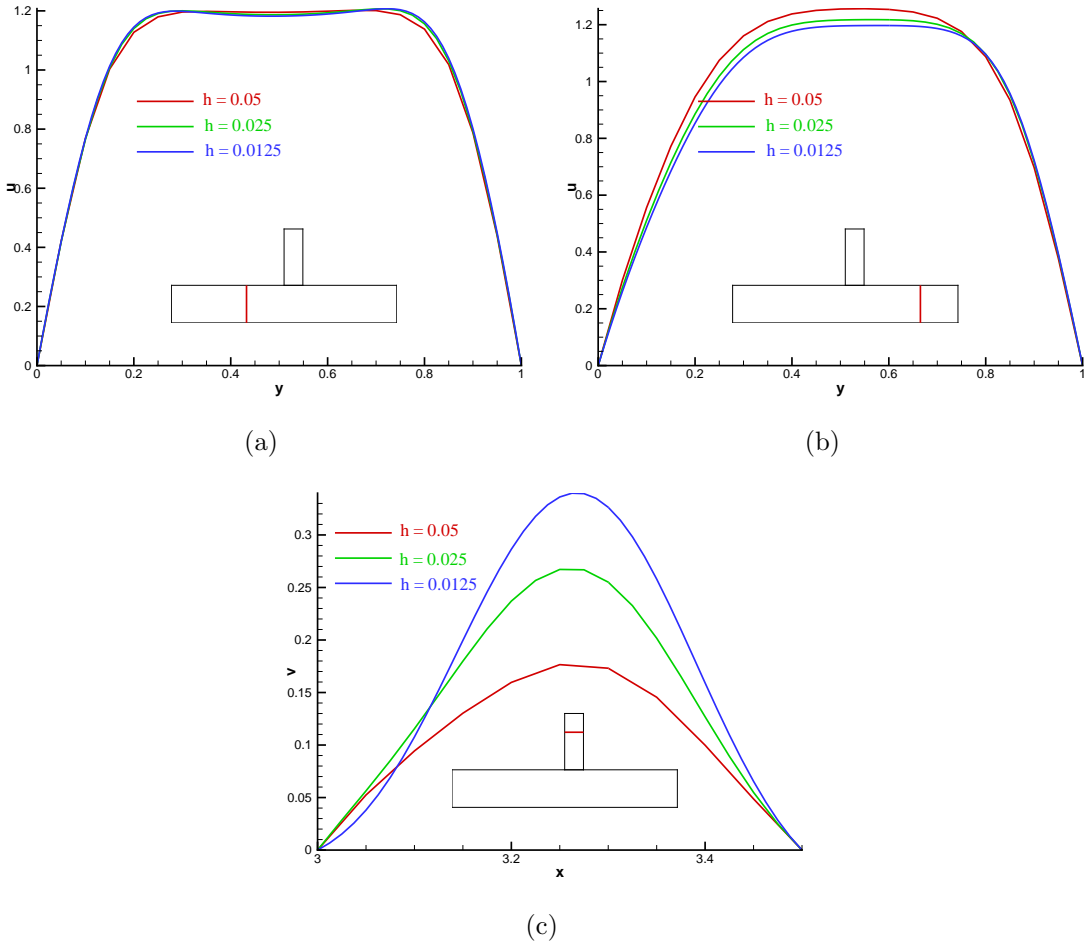


Figure 3.67: Nondimensional velocity profiles of the velocity components  $u, v$  as the functions of  $y, x$

# Conclusions

A finite volume solver of two and three dimensional incompressible laminar viscous flows for simulation of Newtonian and non-Newtonian shear thickening fluid flows in the branching channel with one entrance and two exit parts was developed and implemented. The method was applied for several different types of channel configurations. For generalized Newtonian fluids flow case the simple power-law model was used.

The numerical modelling were computed for several different values of power-law index  $r$ . First value  $r = 0$  was used for the case of Newtonian fluids. The values  $r = 0.2$ ,  $r = 0.5$  and  $r = 0.8$  were used for the numerical computations of non-Newtonian shear thickening fluids flow.

Explicit Runge-Kutta numerical method for solving steady state flows for two dimensional case are presented together with detailed description of time step restriction and simulations convergence condition. This method in conjunction with the artificial compressibility method was used for numerical modelling of two and three dimensional branching channels. The numerical results are compared with the same characteristic parameters, e.g. Reynolds number using constant viscosity of Newtonian fluids, initial boundary conditions. The convergence history confirms the robustness of the method used. For steady state numerical modelling the steady state boundary conditions were used.

Two approaches were considered for numerical simulation of unsteady governing equations with the unsteady boundary conditions. First, the artificial compressibility approach with the periodic pulsation of the outlet pressure value was used in this work. And second, the dual time stepping method was used for the unsteady numerical computation.

The future steps are to continue in the unsteady numerical computations for three dimensional branching channel and to develop and implement semiimplicit numerical scheme for unsteady numerical modelling.

# Bibliography

- [1] R. Chhabra, J. Richardson, Non-Newtonian Flow in the Process Industries, Biddles Ltd, Guildford and King's Lynn, Great Britain, 1999.
- [2] A. Robertson, A. Sequeira, M. Kameneva, Hemorheology, Birkhäuser Verlag Basel, Switzerland, 2008.
- [3] A. Robertson, Review of Relevant Continuum Mechanics, Birkhäuser Verlag Basel, Switzerland, 2008.
- [4] M. Avram, M. Avram, C. Illiescu, A. Bragaru, Flow of non-Newtonian fluids, IEEE.
- [5] R. Bird, W. Stewart, E. Lightfoot, Transport Phenomena, John Wiley and Sons, 2002.
- [6] M. Brdička, L. Samek, B. Sopko, Mechanika Kontinua (in czech), Academia, AV ČR, 2000.
- [7] F. Maršík, Termodynamika Kontinua (in czech), Academia, AV ČR, 1999.
- [8] R. Honzátko, Numerical simulations of incompressible flows with dynamical and aeroelastic effects, Ph.D. thesis, Czech Technical University (2007).
- [9] R. Bird, R. Armstrong, O. Hassager, Dynamics of Polymeric Liquids, Volume 1, Fluid Dynamics, John Wiley and Sons, 1987.
- [10] R. Keslerová, K. Kozel, Numerical simulation of 2D and 3D incompressible laminar flows, in: C. P. Department of Mathematics, Faculty of Civil Engineering (Ed.), Seminar of Applied Mathematics, Prague, Czech Republic, 2005.
- [11] R. Dvořák, K. Kozel, Mathematical Modelling in Aerodynamics (in czech), CTU, 1996.
- [12] M. Feisteuer, J. Felcman, I. Straškraba, Mathematical and Computational Methods for Compressible Flow, Clarendon Press Oxford, 2003.
- [13] R. LeVeque, Finite-Volume Methods for Hyperbolic Problems, Cambridge University Press, 2004.
- [14] R. Eymard, T. Gallouët, R. Herbin, Finite Volume Method, LATP Marseille, 2006.

- [15] R. Bird, R. Armstrong, O. Hassager, C. Curtiss, Dynamics of Polymeric Liquids, Volume 2, Kinetic Theory, John Wiley and Sons, 1987.
- [16] R. Keslerová, K. Kozel, V. Prokop, Numerical simulation of Newtonian and non-Newtonian fluids, in: P. Institute of Thermomechanics, AS CR (Ed.), Topical Problems of Fluid Mechanics 2007, Prague, Czech Republic, 2007.
- [17] K. Morton, P. Crumpton, J. Mackenzie, Cell vertex methods for inviscid and viscous flows, *Journal of Computers Fluids* 22 (1993) 91–102.
- [18] R. Keslerová, K. Kozel, Numerical simulations of incompressible laminar flow for Newtonian and non-Newtonian fluids, in: S.-V. Berlin (Ed.), Numerical Mathematics and Advanced Applications, ENUMATH 2007, Berlin, Germany, 2008.
- [19] A. Chorin, A numerical method for solving incompressible viscous flow problem, *Journal of Computational Physics* 135 (1997) 118–125.
- [20] P. Louda, Numerické řešení dvourozměrného a třírozměrného turbulentního impaktního proudění, Ph.D. thesis, Czech Technical University (2002).
- [21] A. Jameson, W. Schmidt, E. Turkel, Numerical solution of the Euler equations by finite volume methods using Runge-Kutta time-stepping schemes, in: D. of Aeronautics, S. Astronautics (Eds.), AIAA 14th Fluid and Plasma Dynamic Conference, Palo Alto, California, 1981.
- [22] R. Keslerová, K. Kozel, Numerical solution of incompressible laminar flow, in: B. U. o. T. Department of Fluid Mechanics, Economics (Eds.), CMFF'06, Budapest, Hungary, 2006.
- [23] R. Swanson, E. Turkel, Multistage schemes with multigrid for Euler and Navier-Stokes equations, NASA Technical Paper 3631.
- [24] K. Kozel, Fůrst, Numerické metody řešení problémů proudění I, CTU Prague, 2001.
- [25] K. Kozel, J. Fůrst, J. Fořt, P. Louda, Numerické metody řešení problémů proudění III, CTU Prague, 2004.
- [26] A. Gaitonde, A dual-time method for two dimensional unsteady incompressible flow calculations, *International Journal for Numerical Methods in Engineering* 41 (1998) 1153–1166.
- [27] P. Louda, Numerical solution of steady and unsteady viscous incompressible flows, Habilitation Thesis, Czech Technical University (2008).
- [28] C. de Jouët, O. Laget, J.-M. Le Gouez, H. Viviand, A dual time stepping method for fluid-structure interaction problems, *Computers and Fluids* (2002) 509–537.